

2011

## Immobilized Cytochrome P450 2C9 (CYP2C9): Applications for Metabolite Generation, Monitoring Protein-Protein Interactions, and Improving In-vivo Predictions Using Enhanced In-vitro Models

Lance A. Wollenberg  
*West Virginia University*

Follow this and additional works at: <https://researchrepository.wvu.edu/etd>

---

### Recommended Citation

Wollenberg, Lance A., "Immobilized Cytochrome P450 2C9 (CYP2C9): Applications for Metabolite Generation, Monitoring Protein-Protein Interactions, and Improving In-vivo Predictions Using Enhanced In-vitro Models" (2011). *Graduate Theses, Dissertations, and Problem Reports*. 3473.  
<https://researchrepository.wvu.edu/etd/3473>

This Dissertation is protected by copyright and/or related rights. It has been brought to you by the The Research Repository @ WVU with permission from the rights-holder(s). You are free to use this Dissertation in any way that is permitted by the copyright and related rights legislation that applies to your use. For other uses you must obtain permission from the rights-holder(s) directly, unless additional rights are indicated by a Creative Commons license in the record and/ or on the work itself. This Dissertation has been accepted for inclusion in WVU Graduate Theses, Dissertations, and Problem Reports collection by an authorized administrator of The Research Repository @ WVU. For more information, please contact [researchrepository@mail.wvu.edu](mailto:researchrepository@mail.wvu.edu).

**Immobilized Cytochrome P450 2C9 (CYP2C9): Applications for Metabolite Generation,  
Monitoring Protein-Protein Interactions, and Improving *In-vivo* Predictions Using  
Enhanced *In-vitro* Models**

**Lance A. Wollenberg**

Dissertation submitted to the  
School of Pharmacy at West Virginia University  
In partial fulfillment of the requirements for the degree

**Doctor of Philosophy  
Pharmaceutical and Pharmacological Sciences**

**Peter M. Gannett, Ph.D., Chair  
Grazyna Szklarz, Ph.D.  
Patrick Callery, Ph.D.  
Nianqiang Wu, Ph.D.  
Robert Griffith, Ph.D.**

**Program in Basic Pharmaceutical Sciences  
Morgantown, West Virginia 2011**

**Keywords: Cytochrome P450 Enzymes, Drug Metabolism, Surface Plasmon Resonance,  
Immobilized P450 Enzyme, Nanostructure Array, Protein-Protein Interactions**

## Abstract

### Development of Au-Immobilized P450 Platform for Exploring the Effect of Oligomer Formation on P450-Mediated Metabolism for *In Vitro* to *In Vivo* Drug Metabolism Predictions

**Lance A. Wollenberg**

Cytochrome P450 (P450) enzymes are a family of oxoferroreductase enzymes containing a heme moiety and are well known to be involved in the metabolism of a wide variety of endogenous and xenobiotic materials. It is estimated that roughly 75% of all pharmaceutical compounds are metabolized by these enzymes. Traditional reconstituted *in-vitro* incubation studies using recombinant P450 enzymes are often used to predict *in-vivo* kinetic parameters of a drug early in development. However, in many cases, these reconstituted incubations are prone to aggregation which has been shown to affect the catalytic activity of an enzyme. Moreover, the presence of other isoforms of P450 enzymes present in a metabolic incubation, as is the case with microsomal systems, may affect the catalytic activity of an enzyme through isoform-specific protein-protein interactions. Both of these effects may result in inaccurate prediction of *in-vivo* drug metabolism using *in-vitro* experiments.

Here we described the development of immobilized P450 constructs designed to elucidate the effects of aggregation and protein-protein interactions between P450 isoforms on catalytic activities. The **long term objective of this project** is to develop a system to control the oligomeric state of Cytochrome P450 enzymes to accurately elucidate discrepancies between *in vitro* reconstituted systems and actual *in vivo* drug metabolism for the precise prediction of metabolic activity. This approach will serve as a system to better draw correlations between *in-vivo* and *in-vitro* drug metabolism data. The **central hypothesis** is that Cytochrome P450 enzymes catalytic activity can be altered by protein-protein interactions occurring between Cytochrome P450 enzymes involved in drug metabolism, and is dependent on varying states of protein aggregation.

This dissertation explains the details of the construction and characterization of a nanostructure device designed to control the state of aggregation of a P450 enzyme. Moreover, applications of immobilized P450 enzyme constructs will also be used for monitoring protein-protein interaction and metabolite production with the use of immobilized-P450 bioreactor constructs. This work provides insight into the effect on catalytic activity caused by both P450 aggregation as well as isoform-specific protein-protein interactions and provides insight in the production of biosynthetically produced drug metabolites.

## Acknowledgements

I would like to take this opportunity to thank my advisor, Dr. Peter Gannett, for his guidance as a graduate mentor. Dr. Gannett has provided me with countless hours of mentoring, and his dedication to myself as well as other members in the laboratory has been unparalleled. Additionally, I would like to thank the members of my committee including Dr. Patrick Callery, Dr. Robert Griffith and Dr. Grazyna Szklarz for all of their fruitful discussions. Moreover, I would like to thank my STEM Fellowship co-advisor and committee member, Dr. Nianqiang Wu, for his dedication to my dissertation project and his willingness to teach myself and members of this lab exciting techniques outside of the traditional pharmacy field.

I would also like to thank members of the Gannett laboratory, including Dr. Jarod Kabulski, who helped provide a foundation of scientific knowledge necessary for success in graduate school. I would also like to thank all past and current members of the Gannett laboratory, including John Jett, Brian Train, Vorasit Vongsuittlers, Robyn Ayscue, Katherine Hickey and Chris Bostick, for their assistance on projects and issues, as well as their warm and friendly attitudes which made attending work on a daily basis a pleasure.

I would also like to commend the support staff for the School of Pharmacy for all of their assistance, with special recognition going out to Penny Dailey and Donna Mathess. Without their hard work and dedication in providing the laboratory with supplies, none of the experiments described in this dissertation would even be possible. I cannot thank them enough for everything they have done.

Finally I would like to thank my mother, Carol, my father Mark, and my sister Emily, for their dedication to my success throughout my graduate career. Thanks for all of your love and support.

## Table of Contents

### Chapter 1 – Introduction

1.1. Cytochrome P450 History.....	2
1.2. P450 Nomenclature.....	3
1.3. P450-CPR Redox Complex Structure.....	4
1.4. P450 Catalytic Cycle.....	5
1.5. Shunt Pathways of P450 Enzymes.....	7
1.6. P450 Substrates and Subsequent Reactions.....	8
1.7. The Role of Cytochrome P450 in the Clearance of Xenobiotics.....	9
1.8. Formation of Reactive Metabolites.....	10
1.9. In-vitro Model Systems of Cytochrome P450 Activity.....	11
1.10. Drug-drug Interactions.....	13
1.11. Kinetic Evaluation of P450 Enzymes.....	14
1.12. Aggregation in In-vitro P450 Incubations.....	18
1.13. Flexibility of P450 Enzymes.....	18
1.13. Techniques to Reduce P450 Aggregation In-vitro.....	18
1.13.1. Enzyme Mutation.....	19
1.13.2. Detergent.....	20
1.13.3. Nanodisc.....	21
1.13.4. Immobilization of P450 Enzymes.....	22
1.14. Protein-protein Interaction Between P450 Isoforms.....	23
1.15. Self-assembled Monolayers.....	23
1.15.1. Thiol-gold Based SAMs.....	24
1.15.2. Silane-silicon Dioxide Based SAMs.....	25
1.16. Characterization of Gold-immobilized Constructs.....	26
1.16.1. Contact Angle Goniometry.....	27
1.16.2. X-ray Photoelectron Spectroscopy.....	28
1.16.3. Surface Plasmon Resonance.....	29
1.16.4. Atomic Force Microscopy.....	32
1.16.5. Self-Assembled Monolayer Desorption Ionization-Mass Spectrometry.....	34
1.17. Project Aims.....	35

### Chapter 2 – Applications of Immobilized CYP2C9 for Use in Bioreactor Constructs to Biosynthetically Generate Drug Metabolites

2.1. Introduction.....	40
2.2. Materials and Methods.....	43
2.2.1. General.....	43
2.2.2. Materials.....	44
2.2.3. PMMA Chip Fabrication.....	44
2.2.4. PMMA Plug-flow Bioreactor Fabrication.....	44
2.2.5. PMMA-CYP2C9 Chip Preparation.....	46

2.2.6. PMMA-AcBzTacn-CYP2C9 Chip Fabrication.....	46
2.2.7. Gold-OT/MUA-CYP2C9 Chip Fabrication.....	47
2.2.8. PMMA-CYP2C9 and Au-OT/MUA-CYP2C9 Chip Metabolic Incubation.....	47
2.2.9. Fabrication of PMMA-CYP2C9 Bioreactor EDC-NHS Construct (Dynamic Application).....	48
2.2.10. Fabrication of PMMA-CYP2C9 Bioreactor EDC-NHS Construct (Static Application).....	48
2.2.11. Fabrication of PMMA-CYP2C9 Bioreactor AcBzTacn Construct.....	49
2.2.12. Metabolite generation of PMMA-CYP2C9 Bioreactor.....	49
2.2.13. Chromatographic Detection of Diclofenac.....	51
2.2.14. Immobilization of CYP2C9 Enzyme on a Gold Electrode.....	51
2.2.15. Electrocatalytic Metabolism of Warfarin.....	52
2.2.16. Reconstituted CYP2C9 Incubation with Warfarin.....	53
2.2.17. Chromatographic Analysis of Warfarin.....	53
2.3. Results.....	54
2.3.1. Introduction.....	54
2.3.2. Variation of 2C9 Immobilization Concentration.....	54
2.3.3. CYP2C9 Attachment Time.....	56
2.3.4. CYP2C9 Attachment Type.....	57
2.3.5. Metabolite Production of Completed Plug-flow Bioreactor.....	59
2.3.6. Electrochemical Batch Bioreactor Generated Warfarin Metabolites.....	61
2.4. Discussion.....	63
2.4.1. PMMA Based Plug-Flow Bioreactor.....	63
2.4.2. Electrochemical Batch Bioreactor.....	71
2.4.3. Conclusion.....	72

### **Chapter 3 – Nanostructure Device Designed to Control Aggregation between CYP2C9 Enzymes**

3.1. Introduction.....	75
3.2. Materials and Methods.....	79
3.2.1. General.....	79
3.2.2. Materials.....	79
3.2.3. SPR Film Fabrication.....	80
3.2.4. X-ray Photoelectron Spectroscopy Analysis.....	81
3.2.5. Gold-thiol Self-assembled Monolayer Fabrication.....	81
3.2.6. Silicon Dioxide-silane Self-assembled Monolayer Fabrication.....	82
3.2.7. SPR Binding Analysis.....	82
3.2.8. Quantitation of CYP2C9 Surface Coverage.....	82
3.2.9. Adsorbed Enzyme Constructs.....	83
3.2.10. Preparation of Adsorbed CYP2C9 Constructs for Metabolic Incubation.....	83
3.2.11. Nano-array Fabrication.....	84
3.2.12. Nano-array Imaging.....	85

3.2.13. Metabolic Incubation of the Nano-array.....	85
3.2.14. Chromatographic Detection of 4'hydroxydiclofenac.....	86
3.3. Results.....	86
3.3.1. Biocatalysis of Diclofenac by Adsorbed CYP2C9.....	86
3.3.2. SPR Measurement of CYP2C9 Adsorption.....	88
3.3.3. XPS Characterization of CYP2C9 Adsorption.....	91
3.3.4. AFM Imaging of the Nano-array.....	94
3.3.5. SEM Imaging of Nano-array.....	95
3.3.6. XPS Characterization of Nano-array Fabrication.....	96
3.3.7. Metabolic Activity of the Completed Nano-array.....	99
3.4. Discussion.....	100

#### **Chapter 4 – Gold-Immobilized CYP2C9 as a Platform to Characterize Protein-Protein Interactions Occuring in P450 Enzymes**

4.1. Introduction.....	109
4.2. Materials and Methods.....	112
4.2.1. General.....	112
4.2.2. Materials.....	113
4.2.3. SPR Substrate Fabrication.....	113
4.2.4. Gold-thiol Self-assembled Monolayer Fabrication (SPR Sensor).....	114
4.2.5. SPR Immobilization.....	114
4.2.6. Binding of Immobilized CYP2C9 with CYP2D6.....	115
4.2.7. Gold-OT/MUA-CYP2C9 Chip Fabrication.....	116
4.2.8. Metabolic Incubation of CYP2C9 Chips with Flurbiprofen.....	117
4.2.9. Chromatographic Detection of 4'hydroxyflurbiprofen.....	117
4.3. Results.....	118
4.3.1. SPR Based Real-time Immobilization of CYP2C9 to OT:MUA.....	118
4.3.2. Binding of CYP2D6 to Immobilized CYP2C9.....	119
4.3.3. SPR Model Fitting.....	122
4.3.4. Metabolism of Flurbiprofen with Immobilized CYP2C9.....	123
4.3.5. Effect of Increasing Concentrations of CYP2D6 on the Metabolism of Flurbiprofen by Immobilized CYP2C9.....	125
4.4. Discussion.....	126

#### **Chapter 5 – Summary and Future Directions**

5.1. Summary and Future Directions.....	133
5.1.1. Summary.....	133
5.1.2. Future Directions.....	137
5.2. Conclusion.....	138

## Chapter 6 – Bibliography

6.1. Bibliography.....	140
------------------------	-----

## Chapter 7 – Back Matter

7.1. Curriculum Vitae.....	160
----------------------------	-----

### Index to Figures

#### Chapter 1 – Introduction

<b>Figure 1.1.</b> Crystal structure of CYP2C9 (1R9O.pdb) (ribbon diagram). Prosthetic heme group (stick diagram) is shown at the center of the protein. Figure was rendered with Pymol (www.pymol.com).....	3
<b>Figure 1.2.</b> Crystal structure of CPR (1AMO.pdb) (ribbon diagram). Prosthetic FMN (left) and FMN (right) groups (stick diagram) are shown. Protein is presented as a dimer. Figure was rendered with Pymol (www.pymol.com).....	5
<b>Scheme 1.1.</b> Oxidation of NADPH to NADP+. Electrons from reaction are shuttled from NADPH through CPR to the heme-center of the P450 enzyme).....	6
<b>Scheme 1.2.</b> Catalytic cycle of a Cytochrome P450 enzyme).....	7
<b>Table 1.1.</b> Major substrate classification of known Cytochrome P450 isoforms. ).....	9
<b>Figure 1.3.</b> Contribution of each individual isoform to P450 mediated clearance).....	10
<b>Figure 1.4.</b> Generic plot representing Michaelis-Menten kinetics commonly observed in P450 biotransformation.....	16
<b>Figure 1.5.</b> Generic plot representing inhibition in Michaelis-Menten kinetics (grey dashed line).....	17
<b>Scheme 1.3.</b> Formation of a thiol-based SAM on a gold film.....	24
<b>Scheme 1.4.</b> Formation of a silane-based SAM on a silicon dioxide wafer.....	26
<b>Figure 1.6.</b> Diagram outlining the obtainment of ( $\theta_Y$ ) by using contact angle goniometry.....	27
<b>Figure 1.7.</b> Diagram of X-ray Photoelectron Spectroscopy.....	29
<b>Figure 1.8.</b> Diagram of Surface Plasmon Resonance Spectroscopy.....	31
<b>Figure 1.9.</b> Diagram of the key parts of an atomic force microscopy (AFM) experiment.....	33
<b>Figure 1.10.</b> Diagram of SAM dissolution and crystallization in SAMDI matrix.....	35

#### Chapter 2 – Applications of Immobilized CYP2C9 for Use in Bioreactor Constructs to Biosynthetically Generate Drug Metabolites

<b>Figure 2.1.</b> Milling schematic for the plug and flow bioreactor channel. Listed dimensions are given in millimeters (mm).....	45
<b>Figure 2.2.</b> Setup corresponding to continuous flow PMMA-based bioreactor.....	50
<b>Figure 2.3.</b> UV mediated cleavage of ester moieties present within the PMMA polymer. Subsequent EDC/NHS activation allows for the covalent linkage of CYP2C9 to the polymer surface.....	55



<b>Figure 2.4.</b>	Metabolic formations from PMMA chips prepared with different concentrations (50, 100, 200, 400 nM) of CYP2C9 applied to EDC/NHS activated PMMA chips (grey). Solution incubation (black) contains 0.5 pmol CYP2C9 and dilaurophosphatidyl choline (black). All incubations contain CPR and NADPH.....	<b>56</b>
<b>Figure 2.5.</b>	Incubation study optimizing CYP2C9 attachment time (2, 4, 6, 8, and 24 h) to an EDC/NHS activated PMMA chips. ....	<b>57</b>
<b>Figure 2.6.</b>	Comparison of metabolite production based on his-tag directed coordination (AcBzTacn) and covalent coupling (EDC/NHS) on gold-OT:MUA(3:1) self-assembled monolayer (bricked) or PMMA (grey). Incubations were conducted for 24h.....	<b>59</b>
<b>Figure 2.7.</b>	Time course analysis of metabolite production by a CYP2C9 immobilized plug and flow PMMA bioreactor. His-tag directed coordination with Acbztaen (circles) is compared to plug and flow channels fabricated using EDC/NHS covalent immobilization. Further comparison of EDC/NHS immobilization techniques is shown by continuous injection (10 mL, continuously injected at 500 $\mu$ L per hour for 20 h total) of CYP2C9 (100nM) (squares) and static injection (2 mL, injected immediately, for 20 h) (triangles) of CYP2C9 (500 nM).....	<b>61</b>
<b>Figure 2.8.</b>	Time course analysis of metabolite production by a CYP2C9 immobilized plug and flow PMMA bioreactor. His-tag directed coordination with Acbztaen (circles) is compared to plug and flow channels fabricated using EDC/NHS covalent immobilization. Further comparison of EDC/NHS immobilization techniques is shown by continuous injection (10 mL, continuously injected at 500 $\mu$ L per hour for 20 h total) of CYP2C9 (100 nM) (squares) and static injection (2 mL, injected immediately, for 20 h) (triangles) of CYP2C9 (500 nM).....	<b>63</b>

### Chapter 3 – Nanostructure Device Designed to Control Aggregation between CYP2C9 Enzymes

<b>Figure 3.1.</b>	Effect of SAM composition on metabolic activity of CYP2C9. Solution mixtures contained CYP2C9, CPR, diclofenac and phospholipid. Chip immobilized mixture were comprised of gold chips with the indicated SAM, bound (OT and EG3) or bonded ((3:1) OT:MUA) CYP2C9, diclofenac, CPR and NADPH.....	<b>88</b>
<b>Figure 3.2.</b>	SPR sensorgram comparing interaction of CYP2C9 with self-assembled monolayers produced from A.) Gold-thiol self-assembled monolayers (octanethiol) (black) and (11-Mercaptoundecyl)tri(ethylene glycol) (gray) and B.) Silane-silicon dioxide self-assembled monolayers (n-octyltrimethoxysilane (black) and 2-[methoxy(polyethyleneoxy)propyl]trimethoxy silane (gray)). Sensorgram curves represents an average of 3 separate experiments.....	<b>90</b>
<b>Table 3.1.</b>	Observed $\Delta$ RU and Calculated Protein Coverage on Various SAMs.....	<b>91</b>
<b>Figure 3.3.</b>	X-ray photoelectron spectra comparing N1s core level scans of CYP2C9 adsorbed to self-assembled monolayers comprised of A) octanethiol (black) and (11-Mercaptoundecyl)tri(ethylene glycol) (gray) on gold and B) N-	

octyltrimethoxysilane (black) and 2-methoxy(polyethyleneoxy)propyl] trimethoxysilane (gray) on silicon dioxide. Each spectrum is the sum of 15 scans.....	93
<b>Table 3.2.</b> XPS Bond energies (N1s).....	94
<b>Figure 3.4.</b> Atomic force images of the nanowell array structure.....	95
<b>Figure 3.5.</b> (A) Low magnification scanning electron micrograph (SEM) of the nanowell array. (B) High magnification SEM image of the nanowell array.....	96
<b>Table 3.3.</b> XPS Peak Bond Energies (C1s).....	97
<b>Figure 3.6.</b> XPS spectra of the A) C1s core level spectra and B) N1s core level spectra obtained during fabrication of the nanowell chip bearing OT and 2-[methoxy(polyethyleneoxy)propyl]trimethoxysilane and CYP2C9. Successive spectra (from bottom) in each panel are of the step-by-step fabrication of the nanowell array and are 1) the bare array, 2) (1) + OT SAM, 3) (2) + 2-[methoxy(polyethyleneoxy)propyl]-trimethoxysilane, 4) (3) + CYP2C9.....	98
<b>Table 3.4.</b> CYP2C9-Nanowell Metabolite Production from Diclofenac.....	99

#### **Chapter 4 – Gold-Immobilized CYP2C9 as a Platform to Characterize Protein-Protein Interactions Occuring in P450 Enzymes**

<b>Figure 4.1.</b> Real time immobilization of CYP2C9 using SPR. The active flow cell (FC2) containing CYP2C9 was treated with CYP2C9 before ethanolamine to promote covalent bonding of CYP2C9 to the SAM. Negative control experiment used to generate the blank flow cell is treated with ethanolamine before CYP2C9 to block covalent binding of CYP2C9 to the surface.....	119
<b>Figure 4.2.</b> SPR data obtained from a solution of CYP2D6 interacting with immobilized CYP2C9 (see Figure 1 for set-up). Concentrations, from lower trace upward, of CYP2D6 are 0 nM, 5 nM, 10 nM, 50 nM, 100 nM and 500 nM. Sensorgrams are presented as a subtracted response, where the response in the active flow cell (FC2) is subtracted from the blank flow cell (FC1). Sensorgram corresponding to 0 nM is used to correct the sensorgrams for changes in refractive index associated to the sample buffer.....	122
<b>Figure 4.3.</b> Residual plot of kinetic fit models. An example of a poorly fit model is shown (gray squares), as well kinetic model which is well fit to the data (black triangles). The horizontal line at the y-axis origin (Model Fit) represents the computer generated model response to which SPR binding curves are fit.....	123
<b>Figure 4.4.</b> Effect of B <sub>5</sub> composition on metabolic activity of CYP2C9. All chip incubations contained CYP2C9, CPR, and flurbiprofen. Chip immobilized mixture were comprised of gold chips with the indicated SAM, bound (OT and EG3) or bonded ((3:1) OT:MUA) CYP2C9, flurbiprofen, CPR and NADPH.....	124
<b>Figure 4.5.</b> Effect of solution CYP2D6 on the metabolism of flurbiprofen by CYP2C9. Chip incubations contained CYP2C9, CPR, cytochrome B <sub>5</sub> and flurbiprofen. Incubations containing solution CYP2D6 contain (0.75 nM (0.3:1)), (1.25 nM (0.5:1)), (2.5 nM (1:1)) and (5 nM (2:1)), respectively.....	126

# **Chapter 1**

## **Introduction**

## Chapter 1 - Introduction

### 1.1. Cytochrome P450 History

The earliest evidence that suggested the occurrence of P450 catalyzed reactions was described early as the 1940's, when researchers found liver homogenates capable of metabolizing the azo dye, 4-dimethylaminoazobenzene<sup>1</sup>. Nearly 20 years later, a protein was identified in liver microsomes with bound carbon monoxide after being reduced with dithionite<sup>2</sup>. By measuring the spectrum of the reduced form of this protein, a peak at 450 nm was observed, which lead the researchers to coin the term "P450". In 1968, it was found that a redox partner, a reductase, facilitated P450 mediated  $\omega$ -hydroxylation of fatty acids<sup>3</sup> eventually giving rise to the current model of the P450 redox complex. Eventually, human P450 enzymes were purified from human livers,<sup>4</sup> though yields of these purified proteins were quite low. Finally, technological breakthroughs, primarily the expression of P450 enzymes in *Escherichia coli*, produced a remarkable increase in expression in bacterial cells<sup>5</sup>. This allowed scientists to generating high resolution crystal structures of P450 enzymes,<sup>6</sup> necessary to fully explain structure-function relationships, thus further elucidating the role of these enzymes in the metabolism of xenobiotics. For this work, an important example is the crystal structure of CYP2C9, an enzyme which is utilized in much of the work presented here and is shown in Figure 1.1.

For Educational Use Only



**Figure 1.1.** Crystal structure of CYP2C9 (1R9O.pdb) (ribbon diagram). Prosthetic heme group (stick diagram) is shown at the center of the protein. Figure was rendered with Pymol ([www.pymol.com](http://www.pymol.com)).

## 1.2. P450 Nomenclature

During early P450 enzyme based research had yet to clarify the depth and variability of P450 enzymes and, as such, the naming and genetic characterization was not standardized. In an attempt to better organize the nomenclature of P450 enzymes<sup>7,8</sup>, a universal system was suggested which would abbreviate all P450 enzymes, CYP enzymes. A number was chosen to denote the gene family, which shares approximately 40% genetic sequence identity. Next, a letter is used to denote the sub-family, a population of enzymes which shares approximately 65% of

the genetic sequence identity. Each individual gene is labeled with a second numeral. For an example of this we will use the CYP2C9 gene, which belongs to the 2 family, the C subfamily and finally is labeled with 9 to denote the individual gene. Mutants of CYP enzymes containing one or a few mutations in amino acid sequence are denoted with a \* followed by a number. For example the CYP2C9\*3 gene, is a mutation representing a single nucleotide polymorphism which produces an alteration in amino acid sequence e.g. (Ile359→Leu359) for CYP2C9\*1→CYP2C9\*3.<sup>9</sup>

### **1.3. P450-CPR Redox Complex Structure**

P450 enzymes are primarily located in hepatic tissue and have been well characterized to exist as membrane associated proteins, either alone or as complexes. Generally these membrane bound complexes are found within hepatocytes, on the smooth endoplasmic reticulum. The active redox complex consists of a single membrane-bound P450 enzyme, which is bound to the membrane by amino terminal transmembrane helix and a single membrane-bound Cytochrome P450 Reductase (CPR) enzyme<sup>5,10,11</sup>. These two proteins interact through a binding site on the surface of the P450 enzyme. Once bound, CPR can transfer electrons from nicotinamide adenine dinucleotide phosphate (reduced form) (NADPH) through bound flavin adenine dinucleotide (FAD) and flavin mononucleotide (FMN) moieties, shown in figure 1.2, to the heme iron at the center of the P450 enzyme<sup>12</sup>. Generally this complex is capable of shuttling two electrons to the heme center, however shuttling of a second electron may also be catalyzed by a third enzyme, cytochrome b<sub>5</sub><sup>13</sup> when present.

For Educational Use Only

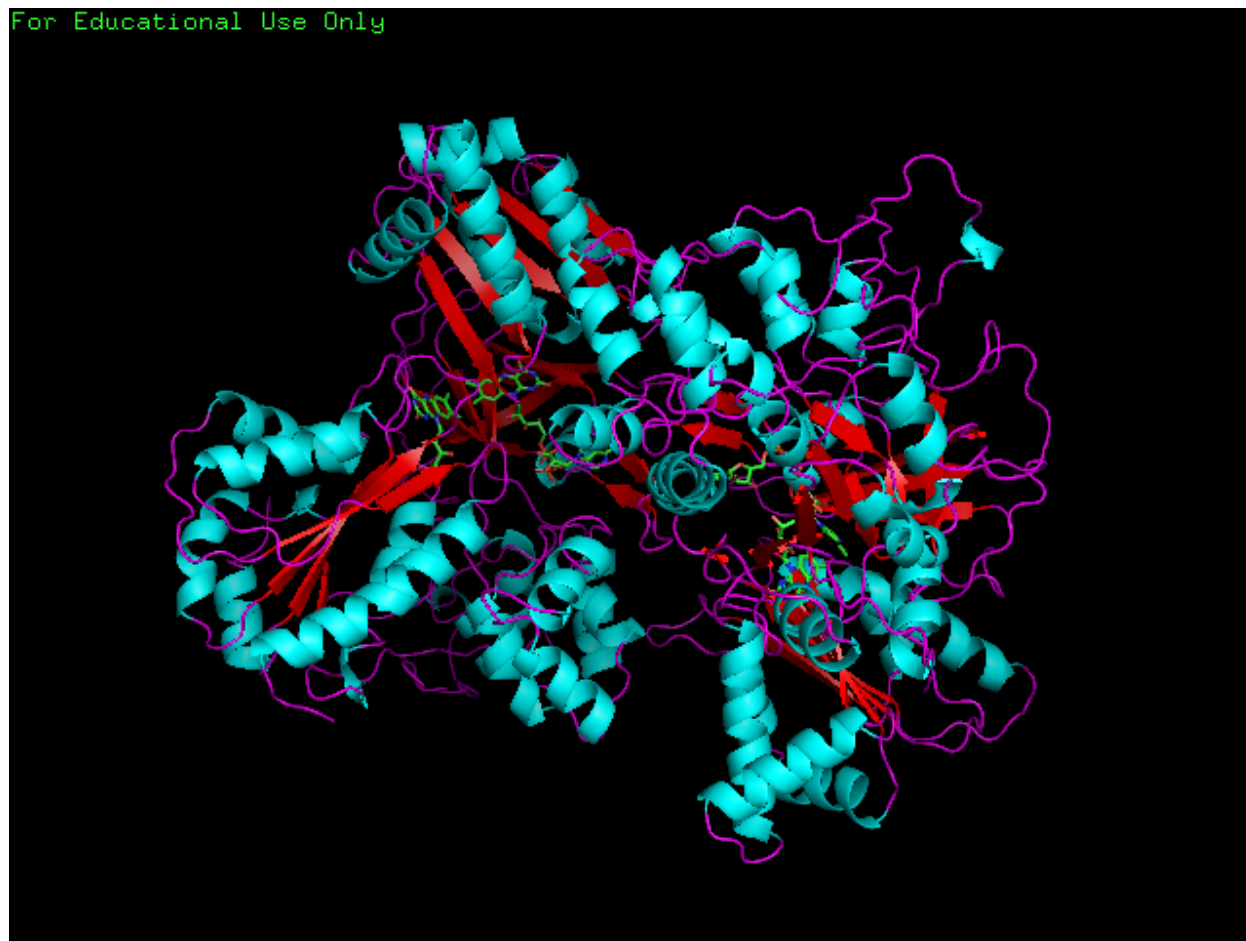
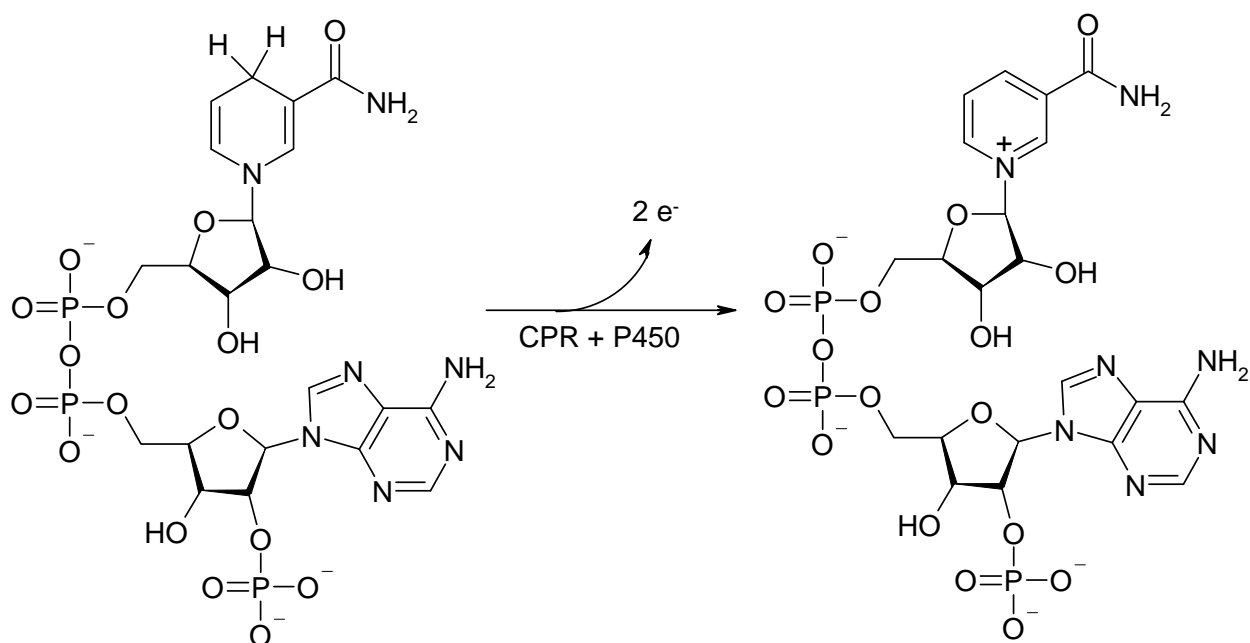


**Figure 1.2.** Crystal structure of CPR (1AMO.pdb) (ribbon diagram). Prosthetic FMN (left) and FMN (right) groups (stick diagram) are shown. Protein is presented as a dimer. Figure was rendered with Pymol ([www.pymol.com](http://www.pymol.com)).

#### 1.4. P450 Catalytic Cycle

Generally, P450 enzymes follow the catalytic reaction cycle to oxidize substrates, as shown in Scheme 1.2 below. The initiation of the cycle (**A**) occurs when a substrate (RH) enters enzyme and binds to the heme-iron contained within the active site of the P450 enzyme (**B**)<sup>14</sup>. This process changes the redox potential of the P450 and produces a situation where electrons can be favorably transferred from NADPH through the FAD and FMN moieties contained within CPR<sup>14,15</sup>. The oxidation of NADPH to NADP<sup>+</sup> is shown in Scheme 1.1.

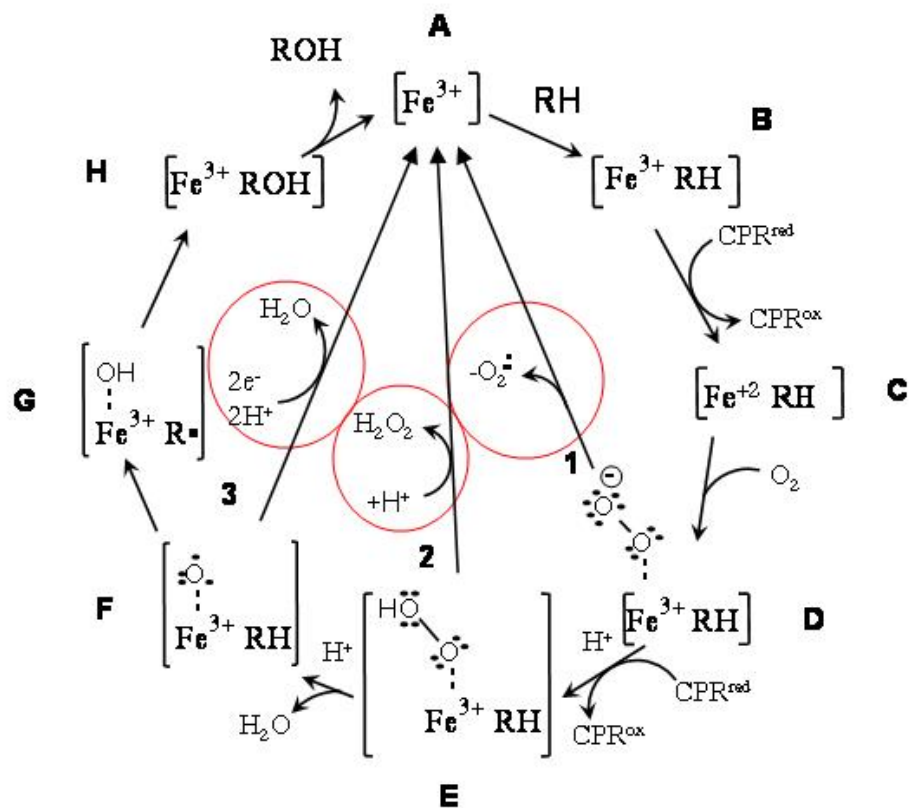


**Scheme 1.1.** Oxidation of NADPH to NADP<sup>+</sup>. Electrons from reaction are shuttled from NADPH through CPR to the heme-center of the P450 enzyme.

The first electron is transferred from the NADPH-CPR complex to reduce the heme-iron from Fe<sup>(III)</sup> to Fe<sup>(II)</sup> (**C**). The Fe<sup>(II)</sup> species is capable of binding molecular oxygen (O<sub>2</sub>), forming the dioxy-iron species<sup>16</sup>. Once bound, the reaction complex undergoes a second reduction of the heme-iron, suggesting a negatively charged superoxide complex<sup>17</sup> (**D**), which is referred to as the ferric-superoxide complex. This facilitates the transfer of a second electron, either from CPR or from cytochrome b5, forming the peroxo-ferric intermediate, which is rapidly protonated to form the ferric-hydroperoxo species<sup>18</sup> (**E**). Next, a second proton in the reaction solution migrates to the activated iron site, promoting the cleavage of the O-O bond in the hydroperoxo-iron, generating the iron-oxo species<sup>19</sup> (**F**). Next, the iron-oxo species abstracts a proton from the substrate (**G**) and reacts with the substrate present in the active site, forming a hydroxylated



substrate (ROH)<sup>20</sup> via (H). Finally the hydroxylated substrate (ROH) can leave the active site, at which point the P450 enzyme can conduct another oxidative cycle (A).



**Scheme 1.2.** Catalytic cycle of a Cytochrome P450 enzyme

### 1.5. Shunt Pathways of P450 Enzymes

In addition to the productive catalytic cycle described above, P450 enzymes may also undergo abortive pathways highlighted in Scheme 1.2 (1,2 or 3), which restore the enzyme to its resting state (A)<sup>21</sup>. This protects the activity of the enzyme by preventing degradation of the

heme moiety, if the substrate should happen to leave the active site during the catalytic cycle. Autooxidation of the ferric-superoxide complex can lead to uncoupling and release of the superoxide species as part of the superoxide shunt pathway (1). The cycle can also revert to its resting state by releasing hydrogen peroxide from the ferric-hydroperoxo species, and is referred to as the peroxide shunt pathway (2). Finally, the oxidase shunt pathway (3) forms after the activated iron-oxo species forms an excess water molecule after subsequent reduction with two additional electrons, and rapid protonation with two protons.

### **1.6. P450 Substrates and Subsequent Reactions**

Through the mapping of the human genome, it was determined that there were approximately 57 genes that coded for P450 enzymes. This class of enzymes oxidizes a wide variety of known substrates including sterols<sup>22</sup>, fatty acids<sup>3</sup>, eicosanoids<sup>22,23</sup>, vitamins<sup>24,25</sup> and xenobiotics<sup>26</sup>. Some of the more well characterized reactions catalyzed by P450 enzymes include hydroxylation of saturated carbon-hydrogen bonds<sup>27,28</sup>, N- and O- dealkylations<sup>29-31</sup>, hydroxylations of aromatic systems<sup>28</sup>, epoxidation of olefins<sup>32</sup>, aldehyde oxidations<sup>33</sup>, dehydrogenation, and heteroatom oxygenation reactions<sup>34,35</sup>. The major substrate classification for most human P450 enzymes can be seen in Table 1.1, below.

**Table 1.1.** Major substrate classification of known Cytochrome P450 isoforms.

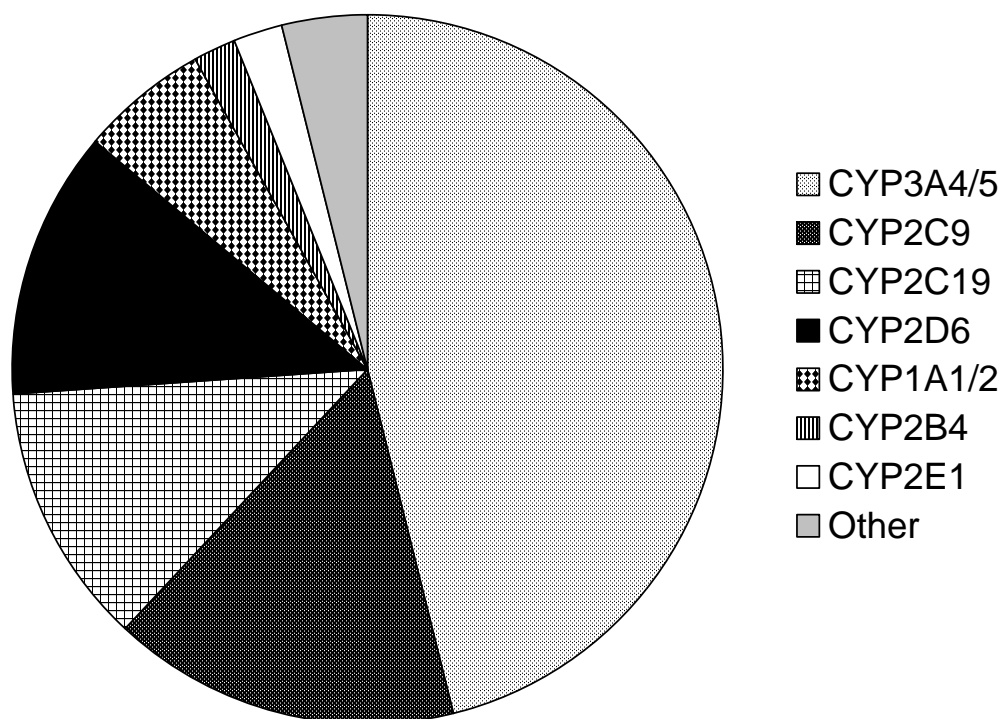
Sterols	Xenobiotics	Fatty Acids	Ecosanoids	Vitamins	Unknown
1B1	1A1	2J2	4F2	2R1	2A7
7A1	1A2	4A11	4F3	24A1	2S1
7B1	3A5	4B1	4F8	26A1	2U1
8B1	2A13	4F12	5A1	26B1	2W1
11A1	2B6		8A1	26C1	3A43
11B1	2C8			27B1	4A22
11B2	2C9				4F11
17A1	2C18				4V2
19A1	2C19				4X1
21A2	2D6				4Z1
27A1	2E1				20A1
39A1	2F1				27C1
46A1	3A4				
51A1	3A5				
	3A7				

Table was adapted from <sup>36-38</sup>.

### 1.7. The Role of Cytochrome P450 in the Clearance of Xenobiotics

The fate of drugs in the body follows three primary means of excretion from the body, biliary and renal excretion and biotransformation through metabolic processes, which functions to facilitate renal excretion by increasing the water solubility of a compound. The biological purpose of metabolism is to further facilitate excretion through either of the two formerly mentioned excretion routes. Approximately 75% of the most commonly prescribed pharmaceutical agents are thought to undergo some sort of metabolic biotransformation to facilitate their excretion<sup>39</sup>. Of the compounds that are biotransformed in the body, approximately 75% of those compounds are oxidized by P450 enzymes, accounting for the metabolism of more than two-thirds of commonly prescribed drugs<sup>40</sup>. As such, the relationship of xenobiotics and P450 metabolism are of major importance to the pharmaceutical industry. Approximately fifteen

P450 enzymes have been suggested to play a role in the metabolism of xenobiotics<sup>37</sup>, and six (1A2, 2C9, 2C19, 2D6, 3A4 and 3A5) of these enzymes are responsible for approximately 95% of xenobiotics metabolized<sup>39</sup>. The breakdown of the individual contribution of each P450 enzyme isoform is shown in Figure 1.3.



**Figure 1.3.** Contribution of each individual isoform to P450 mediated clearance. Figure 2 was adapted from <sup>39</sup>.

### 1.8. Formation of Reactive Metabolites

The insertion of oxygen by P450 enzymes into the chemical structure of many xenobiotics can often create reactive or otherwise toxic metabolites<sup>41</sup>, and represent a major hurdle for drug development. The reactivity of metabolites produced by P450 enzymes can be

attributed to electrophilic compounds which covalently bind to either protein<sup>42</sup> or DNA<sup>43</sup>. As a result, electrophilic P450 metabolites have been well characterized to generate hepatotoxicity<sup>44</sup>, carcinogenesis<sup>45</sup> and increased immune hypersensitivity<sup>46</sup>. Often, cytosolic glutathione is utilized to react with electrophilic metabolites and serves to protect the cell from damage. A classic example of this occurs with the oxidative metabolism of acetaminophen by CYP2E1<sup>47</sup>. This reaction generates N-acetyl-*p*-benzoquinone imine (NAPQI), a highly reactive metabolite which reacts readily with glutathione. If too much metabolite is produced, as is the case in overdose, or the cytosol is deficient in glutathione, the protective effect of glutathione is overwhelmed, NAPQI can then begin to react with proteins<sup>48</sup> and DNA<sup>49</sup>, leading to hepatotoxicity.

Reactive metabolites may also act as agents that act as mechanism-based inactivators towards P450 enzymes. Mechanism-based inactivation occurs when a reactive metabolite covalently binds to the active site of a P450 enzyme, rendering it inactive. Generally, the process of covalently bonding of the reactive metabolite to a P450 enzyme carries little inherent toxicity<sup>50</sup>, unless the inactivated P450 is involved in a physiologically relevant pathway. However, if a mechanism-based inactivator is concurrently administered with a drug that is oxidized by the same P450, as is the case with CYP3A and some HIV protease inhibitors<sup>51</sup>, drug-drug interaction becomes a concern in regards to toxicity.

### **1.9. Current *In-vitro* Model Systems of Cytochrome P450 Activity.**

In order to ensure prediction of the safety of a particular drug, two different *in-vitro* model systems of P450 enzymes are commonly used in early drug development scenarios. One of the more commonly used models of P450 metabolism consists of homogenized liver tissues,

where the smooth endoplasmic reticulum containing active P450 redox complex is purified by ultracentrifugation to form human liver microsomes. Human liver microsomes are valuable tools to better predict how a drug may be metabolized within the body. These microsomes generally contain all of the enzymes present in the liver and as such, they provide a reasonable *in-vitro* model to predict drug metabolism in early in drug development. However, because the entire complement of hepatic P450s is expressed, human liver microsomes offer little insight into which enzymes are primarily involved in metabolism of a drug, which is essential to mitigate inhibition of P450 enzymes.

Alternatively, recombinant expressed P450 enzymes developed in the early 1990's by Barnes and colleagues<sup>5</sup> are often used to elucidate the role of single P450 isoforms in regards to the metabolism of a particular drug. In order to properly mimic the natural environment of the P450 enzyme and facilitate their inherent catalytic activity, they are typically mixed with charged phospholipids<sup>52</sup>, which will generate a simulated microsomal structure and are thought to promote the interaction of P450 enzymes with redox partners such as CPR, thereby encouraging catalytic activity<sup>53</sup>. Once formed, these reconstituted "artificial microsomal" incubations are particularly useful in studies of P450-substrate interactions. Additionally, by having a system that can be tailored with variable amounts and types of enzymes present, these systems are useful in studying protein-protein interactions between P450 and CPR enzymes<sup>54</sup>, as well as P450-P450 interactions between different isoforms<sup>55</sup>.

## 1.10. Drug-drug Interactions

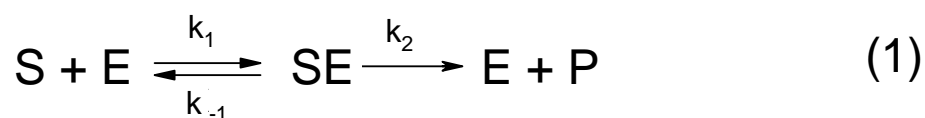
Solved crystal structures of P450 enzymes have shown that the active site of these enzymes is often quite large<sup>6</sup>, and P450 enzymes have been characterized to interact with and metabolize a wide variety of compounds<sup>56</sup>. As a result these enzymes are a major site for drug-drug interactions within the body. Knowledge of drug-drug interaction is continuously sought by the pharmaceutical industry and presents a major bottleneck for the further development of compounds. Interactions can be primarily generalized into two different categories including activation or inhibition of a P450 enzyme, and both have implications in clinical outcomes.

Most commonly, drug-drug interactions arise when the metabolism of a drug is inhibited by the simultaneous administration of a second drug, through, for example, competitive inhibition. This occurs when an inhibitor compound enters the active site, either reversibly or irreversibly, and prevents the access of a substrate molecule. By preventing access of substrate molecules, a situation is created where the metabolism of a drug is slowed significantly, altering metabolism kinetics. Clinically, this can lead to drug toxicity by leading to high levels of drug within the body.

Conversely, the large active site of P450 enzymes can often support two to three substrates, simultaneously in the active site in the enzyme. This scenario can present a situation where a substrate spends more time in a productive binding orientation in the effective enzyme of interest, creating a situation where the catalytic activity of the enzyme is dramatically increased<sup>57</sup>. Clinically, this can often equate to sub-therapeutic concentrations of drugs present within the body, and is a situation that should be avoided to increase the efficacy of a drug.

### 1.11. Kinetic Evaluation of P450 Enzymes

To measure enzyme kinetics as well as identify potential drug-drug interactions in reconstituted incubations using recombinant P450 enzymes, mathematical models have been developed to provide further insight into these processes. The simplest model for kinetic evaluation of a P450 enzyme-substrate interaction is typically based on a Michaelis-Menten model. This model, in a simple form is shown in Equation 1.



In this model, S is the substrate, E the enzyme, and P the product (metabolite) of the reaction between the substrate (S) and the enzyme (E). The reaction rates can be characterized as  $k_1$ , or the rate at which the substrate bound enzyme complex forms. The rate constant  $k_{-1}$  is a measurement of the rate at which the substrate bound enzyme complex dissociates into substrate and enzyme. Finally,  $k_2$ , is the reaction constant for the formation of the product, and is frequently the rate limiting step.

Through derivation of several equations regarding enzymatic rate as well as substrate and enzyme concentration, the Michaelis-Menten equation can be derived, shown in Equation 2. This equation allows one to determine the reaction velocity ( $V_0$ ) at any point at any substrate concentration ( $[S]$ ), given that you can obtain so information regarding the kinetics and binding of substrates.

$$V_0 = \frac{V_{\max} [S]}{K_m + [S]} \quad (2)$$



Typically, Michaelis-Menten like kinetics is a saturable process, meaning that as substrate concentration increases, the reaction will reach a maximum velocity ( $V_{\max}$ ). The  $V_{\max}$  term, shown in Equation 3, is derived from the rate limiting step, which is usually  $k_2$  (commonly referred to as the turnover rate) multiplied by the total enzyme concentration.

$$V_{\max} = k_2 [E]_{\text{tot}} \quad (3)$$

Finally, the  $K_m$  of the system, commonly referred to the Michaelis constant, is determined by the Equation 4 and is derived from the model of enzyme kinetics (Equation 1).

$$K_m = \frac{k_{-1} + k_2}{k_1} \quad (4)$$

The  $K_m$  is often related to the affinity of the enzyme for the substrate; however particular cases exist where this is not always the case. Conveniently, when generating Michaelis-Menten plots, the  $K_m$  value is the substrate concentration that generates approximately  $\frac{1}{2} V_{\max}$  value. To generate Michaelis-Menten like plots, the velocity of the reaction is measured, which in the case of P450 enzymes is typically determined by the concentration product formed, divided by time, divided by the concentration of P450 present in the incubation. By plotting the velocity of the reaction against the concentration of substrate, a sigmoidal curve is often generated, indicating that enzyme kinetics is a saturable process. An example of this type of curve can be seen in Figure 1.4 below.

## Michaelis-Menten Kinetics

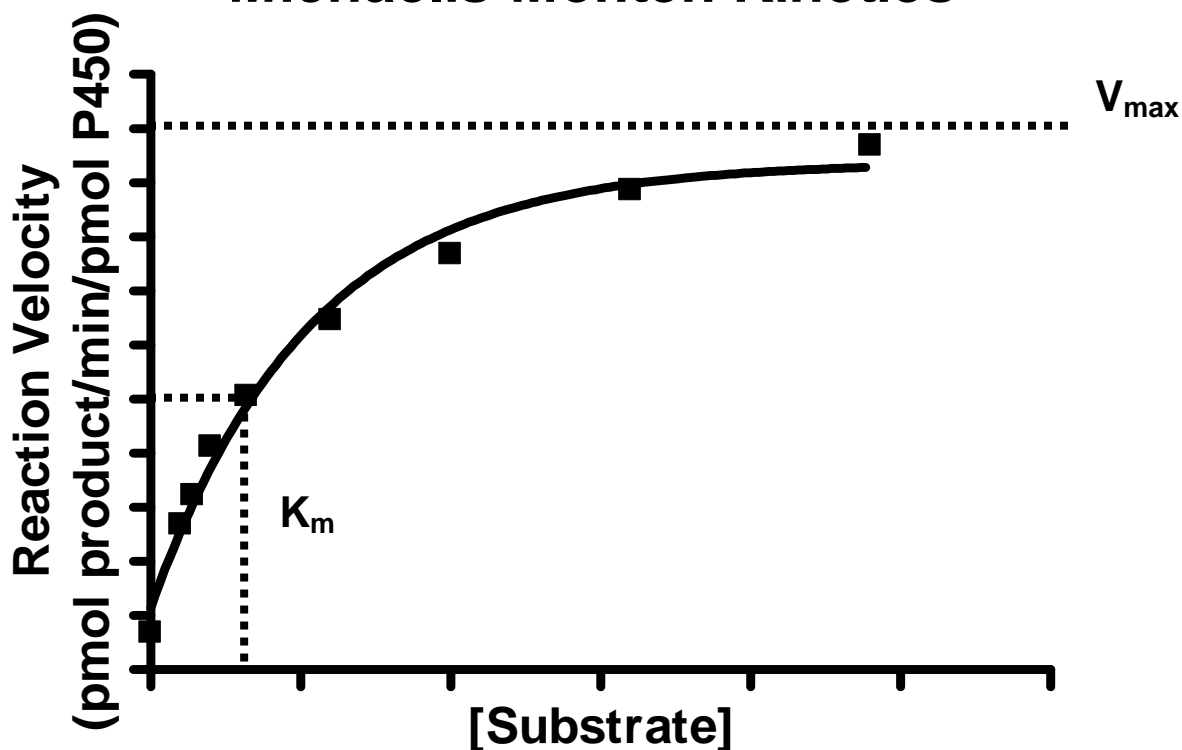


**Figure 1.4.** Generic plot representing Michaelis-Menten kinetics commonly observed in P450 biotransformation.

Essential to these Michaelis-Menten type studies using P450 enzymes is monitoring drug-drug interactions and their effect on  $K_m$  and  $V_{max}$ , and has also been observed in studies characterizing P450-P450 interaction. In cases of competitive inhibition, an inhibitor molecule will competitively bind to the active site, inhibiting substrate turnover, typically resulting in a decrease in  $V_{max}$  and an increase in  $K_m$ . The result of this can be observed in Figure 1.5, where a theoretical inhibitor decreases the catalytic turnover of a substrate.

## Michaelis-Menten Kinetics Inhibition

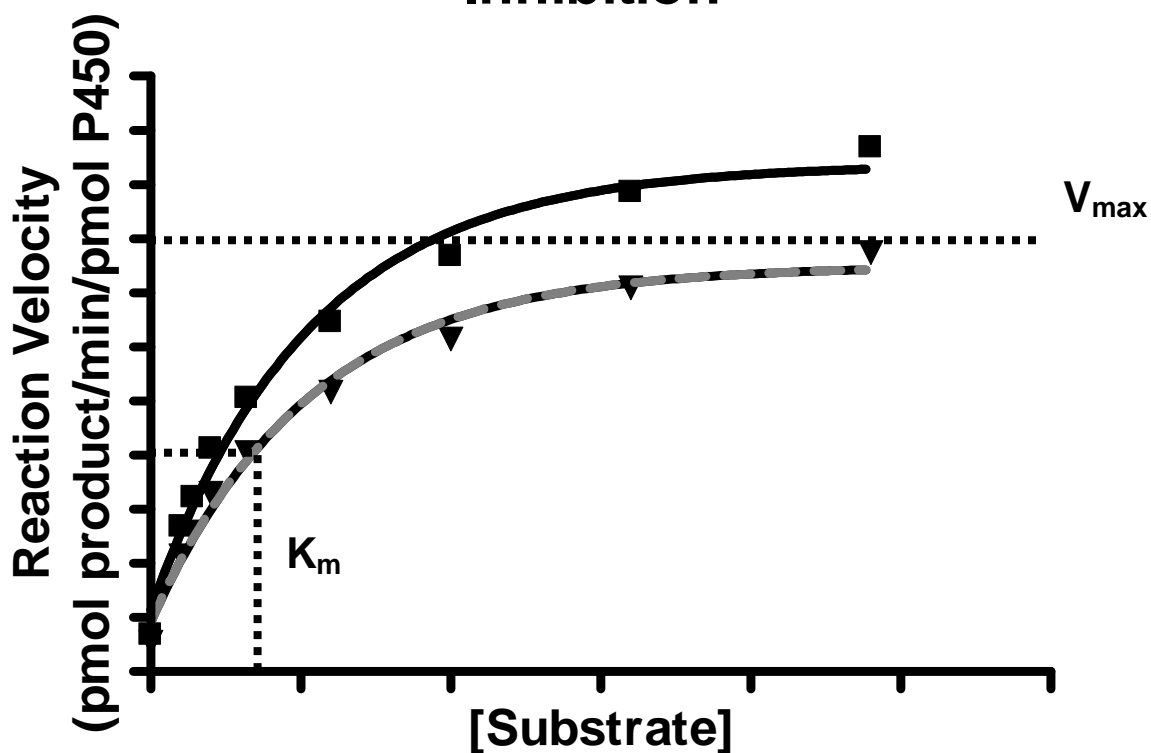


**Figure 1.5.** Generic plot representing inhibition in Michaelis-Menten kinetics (grey dashed line).

Michaelis-Menten like kinetics is commonly used as the simplest model to characterize enzyme kinetics, and often for studies involving drug-drug interactions in P450 enzymes, they are sufficient. However, kinetic modeling of enzymatic reactions is often extremely complex, and thus different models have been developed, accordingly, to deal with these issues.

### **1.12. Aggregation in *In-vitro* P450 Incubations**

Mammalian P450 enzymes exist as membrane-associated proteins, and as a result have several hydrophobic domains within their tertiary structure to interact with the endoplasmic reticulum<sup>10</sup>. Normally when a membrane is present, as is the case with intact hepatocytes, the P450 enzymes associate (bind) with the membrane and exist in a monomeric state. In contrast, when these enzymes are expressed and purified from *Escherichia coli* for use in biochemical experiments, the membrane components from these bacterial cells are washed away with a variety of detergents. The resulting P450 exists in solution with its hydrophobic, transmembrane domain exposed to water, and, as a result aggregation of P450 monomers through these hydrophobic domains forms large aggregates of P450 enzymes. Consequently, it becomes nearly impossible to distinguish deliberate protein-protein interactions thought to be involved in catalytic processes, from those interactions that occur as a result of exposed hydrophobic domains, which may contribute to random protein aggregation.

### **1.13. Flexibility in P450 Enzymes**

In addition to having a very large active site, several P450 enzymes exhibit extensive flexibility within their active site. Typically, substrates with large active sites, CYP2C9 and CYP3A4 being classic examples, demonstrate high levels of active site flexibility<sup>58</sup>. As a result, flexibility in the active site can modulate activity of a P450 towards a given substrate. Malleability of the active site may have effects on the catalytic activity of a P450 enzyme depending on both the substrate structure and absolute flexibility within the active site. Moreover, it is unclear to this point how aggregation of P450 enzymes may be affecting enzyme

flexibility, which may present a reasonable mechanism to explain altered catalytic activities as a result of P450 aggregation.

#### **1.14. Techniques to Reduce P450 Aggregation *In-vitro***

The role protein aggregation may play with purified P450 enzymes has been well characterized and often it has been shown that it can play a role in the catalytic activity of the P450 enzymes<sup>59</sup>. As a result, several different techniques have been explored to reduce or control the state of aggregation of recombinant P450 enzymes. Techniques include mutation of the enzyme structure such as mutation of key residues or truncation of the N-terminal domain, changes to the components of the enzyme incubation mixture including altering salt and detergent concentrations, use of a helical protein belt designed to make nanoscale lipid bilayer structures referred to in the literature as a Nanodiscs, and finally immobilization of the enzyme to a solid substrate.

##### *1.14.1. Enzyme Mutation*

With the development of recombinant DNA technology, production of P450 mutants has become an increasingly feasible technique to elucidate structural elements involved in P450 aggregation. Two main strategies are used to reduce aggregation of P450s: through enzyme mutation including 1) truncation of the N-terminus and 2) point mutations of amino acids thought to be involved in P450 protein-protein interactions. Truncation of the N-terminus has been probed in several different P450 isoforms including CYP2B4, CYP2E1<sup>60,61</sup> and CYP1A2<sup>62</sup>. These studies concluded that the N-terminus played a key role in the formation of P450

aggregates, through hydrophobic domains contained within the N-terminal domain of P450 enzymes. It was shown that removal of the N-terminal domain would tend to drive the P450 into pentameric or hexameric structures, preventing formation of large aggregates. None of the truncated P450 enzymes were found to form monomers in the absence of detergent<sup>60,61</sup>, and truncated CYP1A2 was found to form aggregates even in the presence of several detergents<sup>62</sup>. Moreover, many of the N-terminal truncated P450 enzymes show decreased activity over the wild type enzyme, making them unsuitable for probing changes in catalytic activity of a P450 enzyme as a function of aggregation state.

In addition to truncation of the N-terminal sequence of a P450 enzyme, point mutations of amino acid residues of CYP2C5 has also been shown to reduce the aggregation of P450 enzymes<sup>63</sup>. Interestingly, many of these mutations provided the enzyme the ability to exist in monomeric form in the absence of detergent. However, these mutations also produced a variety of catalytic activities depending on the location of a mutation. As a result, this approach makes it difficult to determine whether the resulting decrease (or increase) in catalytic activity is a result of a change in aggregation state or in the tertiary structure of the enzyme.

#### *1.14.2. Detergent*

As was previously discussed, detergents such sodium cholate were often used with truncated P450 enzymes to generate monomeric structures<sup>64</sup>. Furthermore, the use of Emulgen 913<sup>65</sup> or n-octylglucoside<sup>66</sup> on full length P450 enzymes has also been explored. One study in particular took an in depth look at the catalytic activity of CYP1A2 in incubations containing Emulgen 913<sup>65</sup>. It was discovered that at high concentrations of Emulgen 913 (8 g/L), P450

enzymes would form monomeric structures and from a kinetic standpoint, these monomeric forms of P450 enzymes were less active than their pentameric counterparts. Interestingly, it was also discovered that monomeric CYP1A2 has increased catalytic activity over aggregates of CYP1A2 in incubations containing no Emulgen 913. However, due to the high concentration of detergent involved in these studies, it is difficult to determine whether the decrease in catalytic activity is a true result of the monomeric state of the enzyme, or if these high concentrations of detergent hinder interaction between P450 and reductase, thereby reducing apparent activity.

#### *1.14.3. Nanodisc<sup>®</sup>*

The interaction of enzymes and receptors with lipid bilayer structures is essential to retaining activity and function of a membrane bound protein. Recently, techniques have been developed to study membrane bound proteins such as G-protein coupled receptors<sup>67</sup> and P450 enzymes<sup>68</sup> in discs of phospholipids bilayers of uniform shape and size. By forming a bilayer structure of specific dimensions, researchers can better produce a homogenous membrane environment, eliminating variables associated to membrane formation. Furthermore, in the case of P450 enzymes, these Nanodisc<sup>®</sup> structures have been used to reduce the aggregation of a P450 enzyme by providing a discoidal piece of membrane that is only capable of binding a single P450 enzyme. The presence of monomeric P450 enzymes has confirmed by atomic force microscopy (AFM) imaging<sup>69</sup>.

#### *1.14.4. Immobilization of P450 Enzymes*

A final approach to controlling the aggregation state of a P450 enzyme is to covalently immobilize these enzymes to a surface. Several groups have immobilized P450 enzymes to a variety of substrates including gold<sup>70,71</sup>, sol-gel films<sup>72</sup>, glassy carbon<sup>73</sup> and pyrolytic graphite.<sup>74</sup> A large majority of the research concerning immobilized P450 enzymes has taken advantage of the redox capabilities of this enzyme and coupled it to electroactive materials to elucidate the mechanism of electron transport<sup>75</sup> and substrate binding<sup>71</sup>. A key study conducted in our lab found that the presence of two CYP2C9 substrates, flurbiprofen and dapsone, capable of simultaneous binding to the heme-center of the P450 enzyme enabled the protein to remain metabolically active and utilize the natural cofactors (NADPH) and coenzymes (CPR)<sup>70</sup>. Upon inspection of the enzyme immobilized gold surface with AFM, it was demonstrated that this surface had a propensity to keep P450 enzymes in a monomeric state. As a result, this platform may be advantageous for both monitoring metabolic activity of monomeric CYP2C9 as well as probing for protein-protein interactions with other P450 enzymes. By utilizing this method, the use of mutations can be avoided since this may change the tertiary structure of the enzyme as well as eliminate the use of detergents within an incubation which may prevent interactions between P450 enzymes as well as interactions with reductase. Furthermore, by developing a construct based on gold thin films, we have provided additional capabilities, such as using the construct to examine interactions in real time, using techniques such as surface plasmon resonance (SPR).



### **1.15. Protein-Protein Interactions Between P450 Isoforms**

Given the presence of several different P450 enzymes in the endoplasmic reticulum of hepatocytes, protein-protein interactions between different P450 enzymes may be playing a role in the metabolism of xenobiotic compounds. Further supporting the idea of protein-protein interactions between different P450 enzymes is the low concentration of cytochrome P450 reductase present within hepatocyte cells. It has been estimated that concentrations of P450 to CPR in hepatocyte cells is approximately 20:1<sup>76</sup>, suggesting that CPR is a limiting factor in P450 reactions which requires a 1:1 complex of P450 to CPR for optimal function<sup>77</sup>. Several groups have characterized potential protein-protein interactions between P450 enzymes resulting in modulation of catalytic activity<sup>78-82</sup>. However, these experiments utilize reconstituted systems to conduct their incubation studies, which may be difficult to use in elucidating which protein-protein interactions are a result of a specific protein-protein interaction from those interactions of a non-specific, aggregative nature.

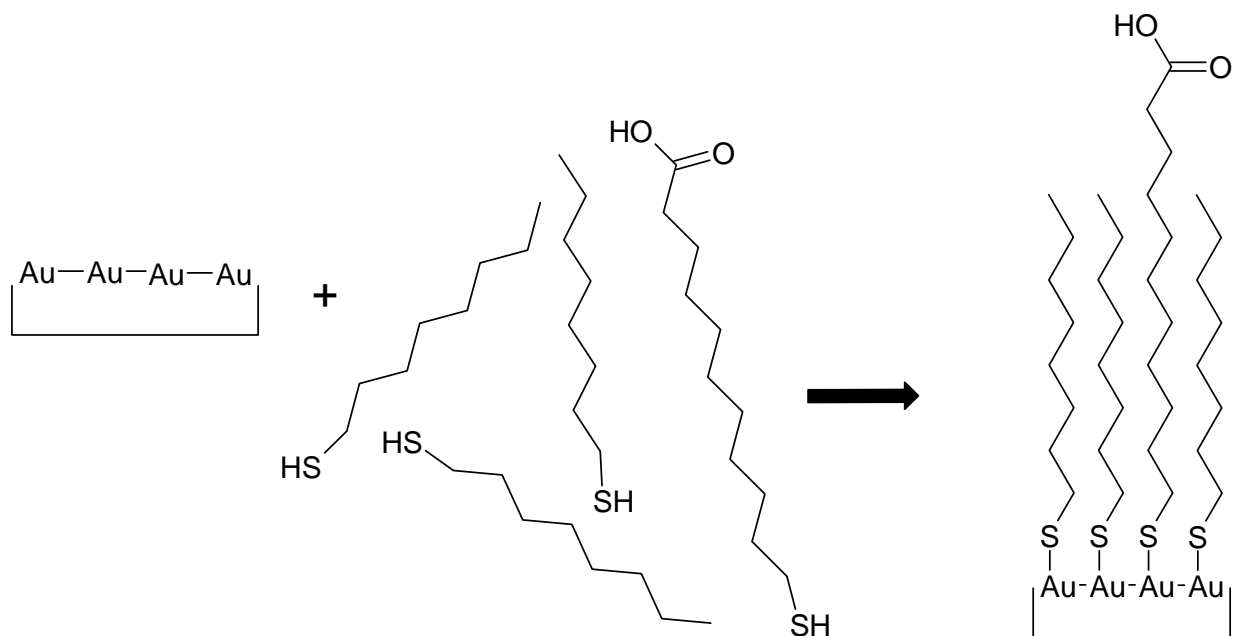
### **1.16. Self-assembled Monolayers**

Recent scientific discoveries in the field of materials science, particularly the formation of biomimetic surfaces, have found several applications in the field of biomedical sciences including use in cell culture substrates<sup>83</sup>, biosensors<sup>84</sup> and bioelectronics<sup>71</sup>. This research has been largely supported by the formation of well ordered films of monomolecular thickness, which owe their origins to work in biology, on a variety of different surfaces, commonly referred to as a self-assembled monolayer (SAM). SAMs can be formed by a variety of different ways,

but for the context presented here, we will describe the formation of two different types, thiol-gold SAMs as well as silane-silicon dioxide SAMs, both prepared from solution.

### 1.16.1. Thiol-gold Based SAMs

Certain metallic surfaces, when exposed to organothiol<sup>85</sup> or organoselenol<sup>86</sup> compounds are known to form ordered SAM structures. These organothiol (organoselenol) films on gold<sup>85</sup> have been well characterized in the literature, however, thiol-SAMs have also been characterized to form on copper<sup>87</sup>, silver<sup>88</sup> and palladium<sup>89</sup>, which only serve to increase their applications in bioelectronics and biomimetic surface fabrication. These SAMs are typically formed by immersing a thin film of metal, typically gold, in an ethanolic solution of thiol (selenol) resulting in the spontaneous formation the desired self-assembled monolayer. A schematic for this process is shown in Scheme 1.3.



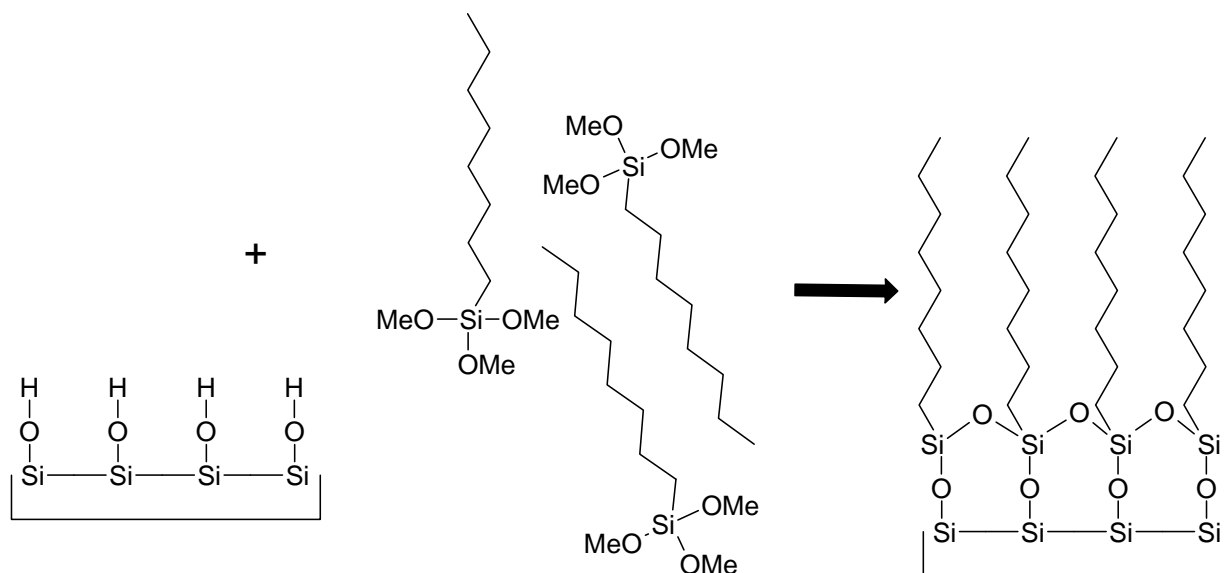
**Scheme 1.3.** Formation of a thiol-based SAM on a gold film.

The formation of self-assembled monolayers of organothiols on gold is a random and spontaneous process. As a result SAMs of mixed thiol composition often form unevenly distributed nano-sized domains of thiol-based structures within a particular thin film<sup>90</sup>. This can lead to large areas of the SAM structure to form heterogeneously mixed monolayers, often complicating the architecture of the biomimetic surface. As a result it would be ideal to generate nanostructure devices and biomimetic surfaces which can control uncertainty in formation of SAMs, and provide researchers with tools capable of precise control of interactions between engineered materials and biological entities.

#### *1.16.2. Silane-silicon Dioxide based SAMs*

SAMs can also be prepared on oxide-containing surfaces such as silicon dioxide<sup>91</sup>, when treated solutions containing silanes<sup>92</sup>. In addition to the formation of SAM structures on silicon dioxide, silane based SAMs have also been formed on various other oxide surfaces such as aluminum oxide<sup>93</sup>, germanium oxide<sup>94</sup> and indium tin oxide<sup>95</sup>. Typically, silanes in silane-based SAMs form a covalent bond between the silicon atom and a surface oxygen and bond as shown in Scheme 1.4. Interestingly, silane-based SAMs are typically more robust than gold thiol SAMs, however they are much more difficult to produce, largely because of their dependence on there being the correct amount of water being present for proper polymerization across the sample interface. Silane-based SAMs formed in deficient concentrations of water often form sparsely packed monolayer structures. In contrast, SAMs formed in high concentrations of water tend to form self-polymerized SAMs, which affect the structure of the SAM and cause the film

to lose its true monolayer form. Research has indicated that the proper concentration of water in a solution used for formation of silane-based SAMs is approximately 0.15mg/mL<sup>96</sup>.



**Scheme 1.4.** Formation of a silane-based SAM on a silicon dioxide wafer. .

### 1.17. Characterization of Gold-immobilized Constructs

Characterization of immobilized proteins to a variety of surfaces, to demonstrate bonding, can be accomplished by a wide array of techniques. For the purposes of this project, four different characterization techniques, three which were applied, will be discussed here. These are contact angle goniometry, x-ray photoelectron spectroscopy (XPS), surface plasmon resonance (SPR) and self-assembled monolayer desorption ionization mass spectrometry (SAMDI-MS).

### 1.17.1. Contact Angle Goniometry

One of the simplest means to characterize a SAM is through contact angle goniometry, a technique to measure surface wettability (tensiometry)<sup>97</sup>. Furthermore, with the development and formation of a variety of SAMs on a wide range of surfaces<sup>98,99</sup>, contact angle goniometry has become an indispensable technique to characterize surface energetics. To obtain static contact angle measurements, a drop of deionized water is placed on to a surface of interest, allowing for it to rest for a period of time to insure a thermodynamic equilibrium has been formed between the three separate phases: solid, liquid and gas. In its most simple form, static contact angles are determined by taking a measurement of the angle ( $\theta_Y$ ), formed by a liquid-gas interface when in contact with a solid surface. A diagram of this phenomenon and how  $\theta_Y$  is obtained is shown below in Figure 1.6. More complex measurements can be made using contact angle goniometry, such as advancing and receding contact angles which give greater insight to the free energy associated to the system<sup>97</sup>.

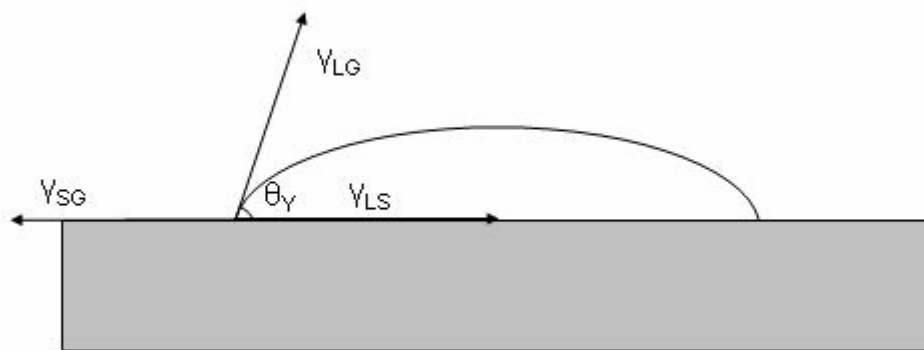


**Figure 1.6.** Diagram outlining the obtainment of ( $\theta_Y$ ) by using contact angle goniometry.

Measurement of static contact angles for immobilized constructs is a quick and robust way to characterize changes in surface chemistry. Measurement of static contact angles can be used in characterization of the formation of SAMs on gold<sup>100</sup> as well as silicon dioxide<sup>101</sup>. Moreover, contact angle goniometry can also be used to monitor changes in surface chemistry which are a result of a chemical reaction occurring at an interface<sup>100</sup>, particularly reactions involving the formation of N-hydroxysulfosuccinimide (NHS) esters. Finally, this technique can also be used to demonstrate changes in  $\theta_Y$  as proteins are adsorbed or bonded to a surface<sup>102</sup>.

#### *1.17.2. X-ray Photoelectron Spectroscopy*

Elemental analysis of a SAM or protein-immobilized-SAM surfaces can be accomplished by irradiating a sample with an x-ray beam and measuring the subsequent energy of electrons released from the sample<sup>103</sup>. This technique is referred to as x-ray photoelectron spectroscopy (XPS) or electron spectroscopy for chemical analysis (ESCA). The general principle of this technique is demonstrated in Figure 1.7. XPS allows for the measurement of the electron energies of ejected electrons from both core and valence levels, providing an advantage over ultraviolet photoelectron spectroscopy (UPS), which can only characterize electrons from valence levels<sup>104</sup>. The capability to characterize core electrons has led to the utilization of this technique to determine discrete energies of core electrons corresponding to individual elements, thus providing simple elemental analysis of surfaces or surface bound materials within approximately 10 nm of the sample interface. Furthermore this technique can be used to measure energy of ejected electrons as a function of localized environment, providing insight

into types of bonds. Here, there is particular interest for carbon and nitrogen<sup>104</sup>, at the surface as these elements are part of the SAM, protein or both.

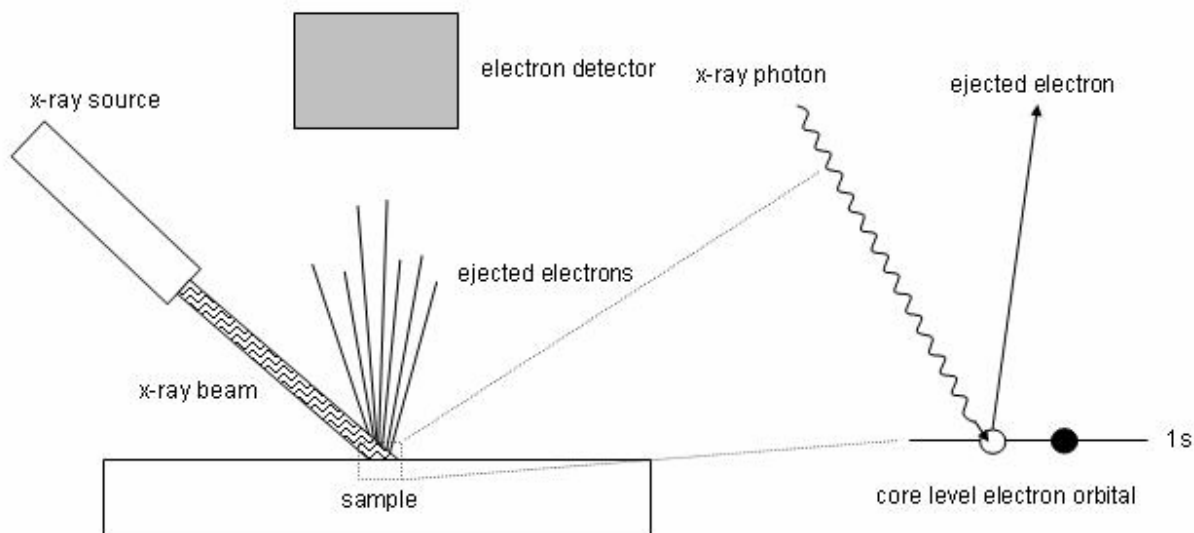


**Figure 1.7.** Diagram of X-ray Photoelectron Spectroscopy

### 1.17.3. Surface Plasmon Resonance

Initially, surface plasmon resonance sensors were used in the detection of gases<sup>105</sup>. The discovery and use of surface plasmon resonance (SPR) to characterize organic monolayers on thin films of silver occurred around the mid 1970's<sup>106</sup>. Coupling in formation with respect to SAM comprised of, for example alkanethiols based-films of monomolecular thickness on gold<sup>85</sup> increased the diversity of chemistry which could be applied to SPR substrates. Since that time, an explosion of research<sup>107</sup> in the field of SPR based sensors has occurred. This class of sensors has found further use for the detection of gases<sup>108,109</sup>, chemicals, including ions<sup>110</sup> and small molecules<sup>111</sup>, as well as detection of biomolecules such as proteins<sup>112</sup>, DNA<sup>113</sup> or RNA<sup>114</sup>.

To conduct SPR experiments, an SPR goniometer must be fabricated, for which the basic diagram of this set up is shown in Figure 1.8. In its most simple terms, SPR forms an extremely sensitive mass sensor. To accomplish this, a thin piece of glass is interfaced with a prism (bottom side) and a flow cell (top side). P-polarized light is transmitted through the prism where it interacts with the glass, which carries a higher refractive index than the dielectric media present in the flow cell (water). The difference in refractive index at the interface of the glass and water, induces total internal reflectance (TIR), resulting in all of the light being reflected from the interface.

SPR substrates are coated with a conducting material, typically gold or silver, of a very specific thickness (50 nm)<sup>115</sup>. As the p-polarized light strikes the gold coated glass slide, it induces the formation of a surface plasmon wave which propagates across the film. In addition to the formation of a plasmon wave, the reflectance spectra of a gold-coated glass slide has a characteristic trough or intensity minimum of the light reflected from the interface, for which the absolute minimum is referred to as the SPR angle ( $\theta_{\text{SPR}}$ ). The plasmon wave oscillates into the dielectric medium (water) and is extremely sensitive to changes in refractive index at the interface of the gold film and water. In the case of biosensors, proteins will covalently bond or adsorb to the surface and will modify the localized refractive index causing an effect in the propagation of the plasmon wave. As the plasmon wave is modulated by changes in localized refractive index, it generates a shift in  $\theta_{\text{SPR}}$ , which is measured as a change in response by the SPR spectrometer.



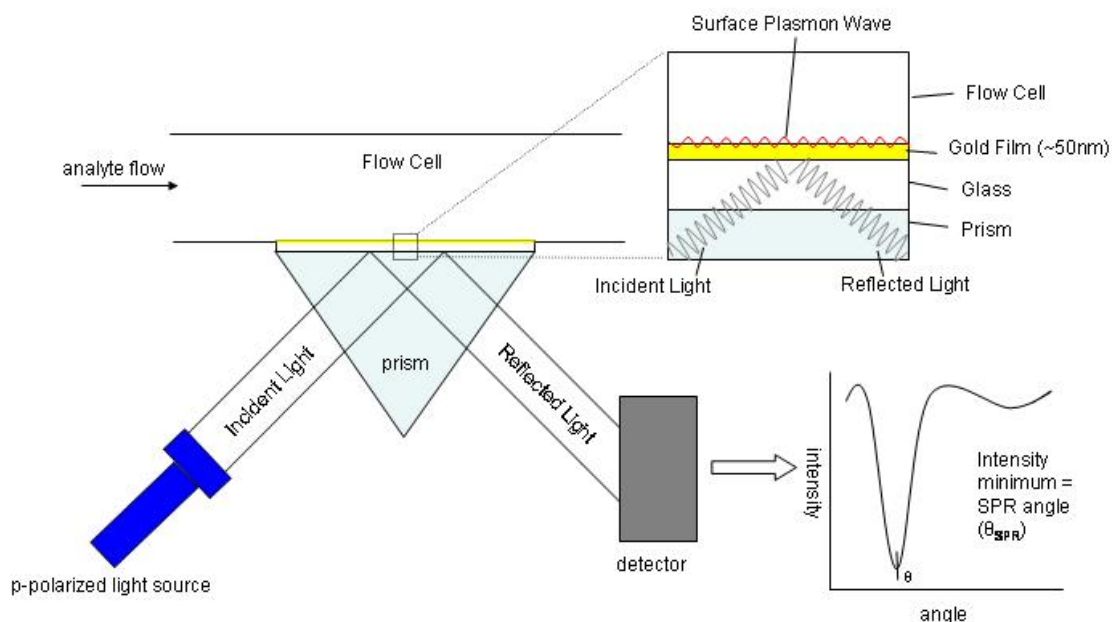


**Figure 1.8.** Diagram of Surface Plasmon Resonance Spectroscopy

SPR based biosensors have found application in several different areas of pharmaceutical sciences. In P450 research, SPR spectroscopy has been used to characterize binding of azoles to CYP3A4. Other applications of SPR involving small molecule binding to pharmacologically active targets including p38<sup>116</sup>, a protein involved in pro-inflammatory cascades. SPR surfaces can be modified to support membrane bound receptors, which are common pharmacological targets. The use of a biomimetic surface will support membrane associated receptors, such as g-protein coupled receptors<sup>117</sup>, which are common pharmacological targets. This may represent a simple approach to characterize small molecules binding to receptors. Finally, SPR has found

application in large molecule drugs as well, having been used in observing interactions of therapeutic antibodies with biological targets<sup>118</sup>.

#### *1.17.4. Atomic Force Microscopy*

Atomic force microscopy (AFM) is a type of scanning probe microscopy technique developed in the mid 1980's<sup>119</sup> to characterize surface topography of a variety of materials in a minimally invasive manner. Prior to this, imaging techniques, particularly of soft materials (protein, DNA) was conducted with transmission electron microscopy or scanning electron microscopy. In both of these cases, samples must be kept in a vacuum chamber during imaging, as an electron beam is directed at the target, and may be denatured under high vacuum conditions. Additionally, optical microscopy techniques, under ideal conditions (oil immersion lens) have a resolution of approximately 200 nm, far below the resolution needed to image a single P450 enzyme with a 6nm diameter. In contrast, AFM provides a resolution of around <1 nm, making it suitable to characterize proteins immobilized to a surface.

AFM can provide topographical images at the atomic-level using a specialized probe called an AFM tip. Normally, the tip is driven at resonance (z-direction) causing it to oscillate at a specific frequency. As the tip oscillates, it is moved along the surface (x-y direction) where the oscillations in the cantilever will be affected by changes in the topology of the surface. The oscillations of the tip are monitored with a laser, which is reflected onto a position detector, a photodiode array. As the tip comes into contact with the sample, the deflection of the laser off of the tip generates a topographical image. A schematic drawing of this is shown in Figure 1.9.

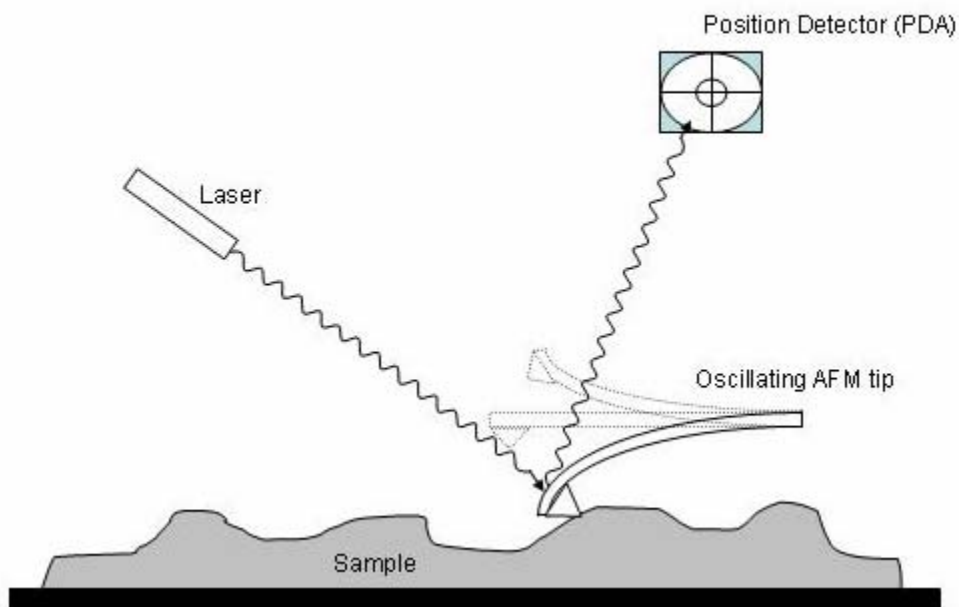


**Figure 1.9.** Diagram of the key parts of an atomic force microscopy (AFM) experiment

Since its invention in the mid 1980's, an explosion of atomic force microscopy research centered on the life sciences has occurred. AFM has been suggested as a complementary technique to x-ray diffraction in elucidation of protein structure<sup>120</sup>. Furthermore, because AFM can be used under physiological conditions, this technique has been useful in characterization of cell surface proteins using “wet” AFM<sup>121</sup> conducted in cell media. Additionally, protein-protein interaction experiments have been devised where an AFM tip is functionalized with a protein and is used to image a cellular surface. The tip-bound proteins will interact with cell membrane receptors, locating and quantifying them<sup>121,122</sup>. This technique is not only useful for developing molecular recognition images, but may also provide some insight into the biophysics of protein-protein interactions. With respect to P450 enzymes, AFM has been used to characterize the

formation of complexes of P450 enzymes with other enzymes<sup>123,124</sup>, as well as monitor interaction of P450 with membrane structures<sup>125</sup>.

#### *1.17.5. Self-Assembled Monolayer Desorption Ionization-Mass Spectrometry*

Analysis of proteins immobilized to self-assembled monolayers with mass spectrometry has led to the development of a technique<sup>126</sup> referred to as self-assembled monolayer desorption ionization-mass spectrometry (SAMDI-MS). This technique has several applications including monitoring chemical reactions that occur at interfaces<sup>127</sup> as well as probing protein-SAMs and protein-protein interactions<sup>128</sup>. Additionally the methods described here have also been coupled to SPR based sensing technologies to complement real-time monitoring of protein-protein interactions with the ability to identify adsorbed molecules<sup>129</sup>.

As SAMDI-MS was developed, it was still unclear how mass spectra from SAM structures were generated. Eventually, it was concluded that the mechanism surrounding the desorption of SAMs from a gold surface during SAMDI-MS was due to solubilization of the SAM molecules into the MALDI-MS matrix and solvent after application to the SAM<sup>130</sup>. Literature reports suggest that the Au-S bond made during the formation of SAMs, is regularly broken in solution. Free thiols from solution can readily exchange with thiols on the surface and vice versa<sup>131</sup>. As a result, in SAMDI-MS experiments, when thiol containing SAMs are treated with the SAMDI-MS matrix (2',4',6'-trihydroxyacetophenone in methanol), they become dislodged from the SAM and are dissolved into the matrix solution. Upon methanol evaporation, the resulting matrix crystals contain SAM components, co-crystallized within that matrix. The

matrix is then exposed to laser light, desorbing matrix components, and mass spectra are acquired. A schematic drawing for this process is shown in Figure 1.10.

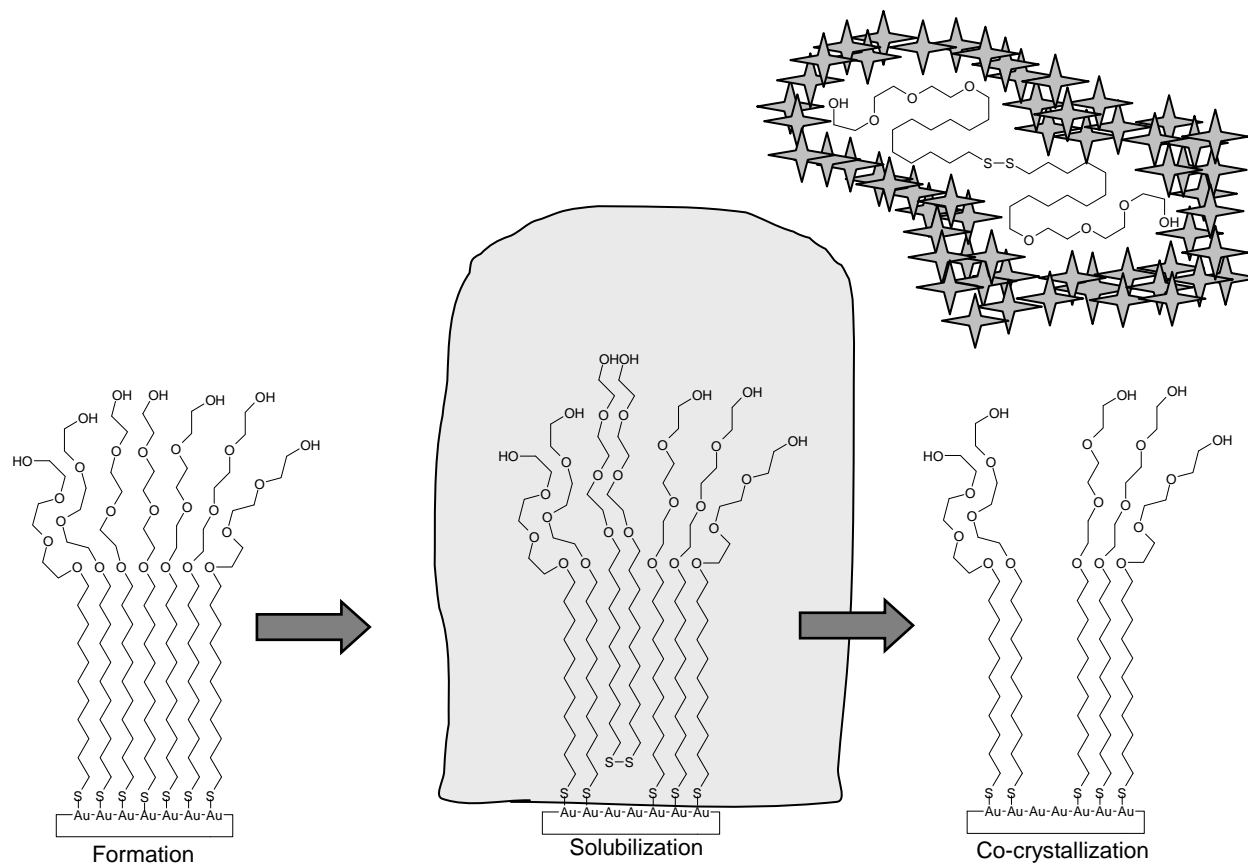


**Figure 1.10.** Diagram of SAM dissolution and crystallization in SAMDI matrix.

### 1.18. Project Aims

Prediction of *in-vivo* drug metabolism using reconstituted incubations of P450 enzymes *in-vitro* is a useful technique to establish metabolic parameters of a drug early in development. Generally these reconstituted incubations consist of P450, reductase, phospholipids and NADPH to generate a simulated microsomes. However, reconstituted incubations often promote the aggregation of P450 enzymes, which can often exhibit allosteric effects on the enzyme altering

its catalytic activity. Accordingly, the need for improved *in-vitro* models which can control the state of aggregation of a P450 enzyme must be developed.

P450 enzymes *in-vivo* are typically expressed along with the entire complement of P450 isoforms. The presence of sub-saturating concentrations of reductase present on the endoplasmic reticulum suggest that protein-protein interactions may be occurring within hepatocytes to affect the metabolism of a particular drug. To elucidate protein-protein interactions between P450 enzymes, mixed enzyme incubations containing two or more P450 enzymes are designed, and the resulting catalytic activity of the enzyme is measured. These mixed enzyme systems are also prone to aggregation as mentioned above, making it difficult to elucidate whether changes in catalytic activity are a result of a specific protein-protein interaction or a result of random aggregation. As a result, it would be extremely useful to develop models to which we can study interaction of monomeric P450 enzymes with one another.

The long term goals of this project are to develop *in-vitro* models designed to unequivocally control the aggregation state of a P450 enzyme. The use of these methods will assist in addressing the catalytic activity of monomeric P450 enzymes using an immobilized enzyme construct. These models will also provide a means to measure on-off rate kinetics to elucidate protein-protein interactions between P450 enzymes. In turn, these models may provide a better prediction of drug metabolism *in-vivo*, saving lost time and resources on compounds which have unacceptable metabolic characteristics. Moreover, these models, which contain active, immobilized P450 enzymes, can also be used for metabolite generation in bioreactor applications, providing a means to biosynthetically generate metabolites for toxicity studies.

### *Project Aims*

- 1.) Employ a nanostructure device designed to selectively bind enzymes to a surface to reduce the level of aggregation in reconstituted P450 incubations.
- 2.) Develop an immobilized P450 construct for applications probing protein-protein interactions as well as metabolite generation.

This dissertation will discuss the development of a nanostructure device designed to reduce the aggregation of P450 enzymes. The fabrication of this device and the methods used to characterize the device will be thoroughly discussed. Specifically we will use SPR to characterize real-time CYP2C9 adsorption to a variety of model self-assembled monolayers. We will use XPS to describe the adsorption of CYP2C9 to model self-assembled monolayers as well as use this technique to monitor changes in surface chemistry during the fabrication of the device. Finally, we will demonstrate that the P450 remains active on a surface containing ~100 nm “nano-beakers” demonstrating that proteins bound to the surface demonstrate activity in the presence of natural cofactors and coenzymes.

In addition to the nanostructure device, I will also describe the application of a method using SAMs of 3:1 octanethiol:mercaptoundecanoic acid to an SPR experiment. This experiment will directly measure on-off kinetic rates for immobilized CYP2C9 and solution CYP2D6, thus providing insight into protein-protein interactions between P450 enzymes. I will discuss how the immobilized CYP2C9 construct was used in an incubation containing increasing concentrations of CYP2D6, and this incubation exhibits no effect on the activity of immobilized CYP2C9. This information is in contrast to data presented in solution, further highlighting

differences between solution and immobilized P450 incubations. These differences may provide insight into the effect of protein aggregation and protein-protein interaction between P450 enzymes. Finally, I will use immobilized CYP2C9 to generate two approaches; a plug-flow and a batch bioreactor, capable of generating metabolites for use in toxicity studies. Ultimately, these approaches will assist in generating new *in-vitro* models which may provide better predictions of *in-vivo* drug metabolism and toxicity.



## **Chapter 2**

# **Applications of Immobilized CYP2C9 for Use in Bioreactor Constructs to Biosynthetically Generate Drug Metabolites**

## 2.1. Introduction

Cytochrome P450 (P450) enzymes have been shown to play a major role in the metabolism of pharmaceutical compounds<sup>132</sup>. In order to bring a new drug to market, or to determine the continued safety of currently marketed pharmaceuticals, drugs are screened with human enzymes for metabolism. When metabolites are formed, it is necessary to assess the toxicity of each particular metabolite<sup>133</sup>. In many cases, pharmaceutical compounds have been found to be metabolized by P450 enzymes and generate toxic reactive intermediates and/or metabolites<sup>134</sup>. Deleterious effects of these species include systemic and hepatotoxicity<sup>135,136</sup>, mechanism based inactivation of P450 enzymes<sup>137</sup>, or increased immune hypersensitivity.<sup>46</sup> Therefore, it is extremely important for pharmaceutical companies to identify compounds that are metabolized to toxic or reactive species early in the drug development process to mitigate losses of research dollars on compounds that are unsafe, and thus could not be brought to market. To accomplish this, researchers need to synthesize large quantities of metabolites to conduct toxicity testing.

Traditionally, metabolites and other compounds of interest to researchers were structurally elucidated using mass spectrometry (MS) and nuclear magnetic resonance (NMR) spectroscopy. Once compounds were characterized, synthetic schemes were generated and the compound then synthesized using traditional organic chemistry techniques. However, this process is often extremely time-consuming, resulting in increased labor costs and delaying the development process. Often the synthetic process required to produce the compounds of interest often requires harsh conditions and dangerous reagents, further emphasizing the need for safe and efficient production of compounds of interest.

Reactions of P450 enzymes are well known for producing compounds of very specific stereochemistry<sup>138</sup>. This increases the difficulty of synthesizing metabolites, as reactions typically generate racemates. While racemic mixtures can be separated, this can be difficult, reduces yields, and, in turn, increases the time and expense of preparing desired metabolites.

Furthermore, P450 enzymes have been characterized as extremely powerful oxidizing agents and have been shown to carry out a variety of reaction types, including N- and O-dealkylations, hydroxylations of aromatic systems as well as saturated carbon-hydrogen bonds, and heteroatom oxygenation reactions<sup>139</sup>. As a result, P450 enzymes have been shown to play a key role in the synthesis of several different compounds<sup>140,141</sup>, many of which would be very difficult to prepare with traditional synthetic organic chemistry.

Traditionally, bioreactors are devices which are designed to carry out some sort of bioprocess<sup>142</sup>. These bioprocesses can be conducted by either by living organisms, such as cultured cells<sup>143,144</sup> and bacteria<sup>145</sup>, or can consist components with biochemical activity such as enzymes<sup>146</sup>. In the pharmaceutical industry, bioreactors are commonly utilized to generate products of interest, such as small molecules<sup>147</sup> and proteins<sup>148</sup>.

The physical design of bioreactors traditionally fall into two general types of bioreactors commonly used in industrial applications. These include, batch and continuous flow bioreactors. Batch bioreactors have no flow of nutrients in and out of the bioreactor. They are generally inexpensive to make. However a major drawback of this approach is the build up of waste products, which may decrease the overall efficiency of the bioreactor.

In contrast, continuous flow bioreactors have a flow in and out of the reactor and have a variety of configurations possible, including bioreactors that are made of a simple tube or

channel to which reagents are supplied and are commonly referred to as plug-flow bioreactors. Generally these types of devices are highlighted by a tube-shaped structure which contains a catalyst on the walls of the tube and an inlet flow of reactant. The constant flow of media and/or chemicals into and out of the plug-flow bioreactors is advantageous in that these types of bioreactors have a continuous exchange of fluid flowing throughout the bioreactor. However, their design is generally more expensive to build when compared to batch bioreactors. The mixing of the reactant, particularly in the axial direction, in plug-flow bioreactors is usually significantly lower than in continuously stirred bioreactors. Finally, temperature in plug flow bioreactors is difficult to control, resulting in the formation of undesired temperature gradients.

Recent technological advantages including the production of recombinant P450 enzymes<sup>149</sup> has lead to the efficient production of enzyme at extremely high concentrations, in turn reinforcing their potential use as synthetic tools in bioreactor applications. Current strategies for bioreactor-based metabolite generation include the use of bacterial<sup>150</sup>, insect<sup>151,152</sup> and hepatocyte<sup>153</sup> cell-based systems. Other strategies include the coupling of human liver microsome (HLM) based systems to HPLC instrumentation<sup>154,155</sup> in a plug-flow set up. In the case of the latter system, these constructs provide a tool for structural determination of metabolites from pharmaceutical compounds, and are not intended for the generation of large quantities of metabolite necessary for toxicity testing or other research and development activities. Moreover, bioreactors containing whole cells require constant maintenance of the cell media, including removal of waste products and proper regulation of temperature, often requiring extensive and costly bioreactor setups.

Here we present two independent bioreactor designs one a plug-flow bioreactor, in which we chemically bond Cytochrome P450 2C9 (CYP2C9) to a PMMA surface and, the second a batch bioreactor where we utilize electrochemistry to oxidize substrates at an electrode bearing an immobilized P450 (CYP2C9). In both instances, amine directed coupling of recombinant CYP2C9 to a self-assembled monolayer (SAM) on gold or PMMA, is achieved conducting the bonding in the presence of two substrates, flurbiprofen and dapsone, which are hypothesized to stabilize the active site during the attachment (bonding) of the CYP2C9<sup>70</sup>. Furthermore, we have optimized several other factors including different attachment schemes, CYP2C9 attachment concentration and CYP2C9 attachment time on proof of concept bioreactor “chips” to increase metabolite output. Finally, we have fabricated PMMA based bioreactors using a plug-flow like channel and demonstrated its ability to generate metabolites of interest from a probe substrate, diclofenac.

## **2.2. Materials and Methods**

### **2.2.1. General**

Unless otherwise noted, phosphate buffer (KPi) was made by mixing 40mM solutions of both dibasic and monobasic potassium phosphate such that the resulting solution of mixed components had a measured pH of 7.4. Mixtures of N-(3-dimethylaminopropyl)-N'-ethylcarbodiimide hydrochloride (EDC) and N-hydroxysulfosuccinimide (NHS) used for enzyme immobilization consist of 3 mM EDC and 5 mM NHS in KPi. Solutions were combined in a 1:1 ratio (v/v) and substrates were immersed. The solution of flurbiprofen and dapsone, used during

CYP2C9 immobilization, was 40  $\mu$ M of each compound dissolved in KPi in a 1:1 ratio. Cryobuffer solution consists of KPi and glycerol (80:20, v/v)

### **2.2.2. Materials**

Diclofenac sodium, flurbiprofen, NHS, EDC, beta-nicotinamide adenine dinucleotide phosphate, reduced form (NADPH), beta-mercaptoethanol, 8-octanethiol (OT), 11-mercaptoundecanoic acid (MUA), warfarin, nickel chloride and N-phenylanthranilic acid were purchased from Sigma-Aldrich (Milwaukee, WI). 4'-hydroxydiclofenac was purchased from Toronto Research Chemicals (Toronto, Canada). Cytochrome P450 reductase (CPR) was purchased from BD Biosciences. Purified CYP2C9 and dapson were provided by Dr. Tim Tracy (Minneapolis, MN). Polyacrylamide gels and gel loading and running buffer were purchased from Biorad (Hercules, CA). Unless otherwise noted, chemicals were purchased from Sigma-Aldrich.

### **2.2.3. PMMA Chip Fabrication**

For initial, proof of concept experiments, small (4 mm x 6 mm) PMMA chips were cut from a PMMA sheet (Goodfellow, Oakdale, PA) using an Epilog Legend EXT carbon dioxide laser (Golden, CO). All of the PMMA chips were irradiated with UV light (Newport Corporation, Irvine, CA) (280 nm) for 15 minutes, per each side, prior to use.

### **2.2.4. PMMA Plug-flow Bioreactor Fabrication**

The PMMA based bioreactor was fabricated by micromilled using a Sherline Model 2010 milling station (Vista, CA) from PMMA plastic blanks (McMaster Carr, Elmhurst, IL). The

milling of the channel was conducted at Protea Biosciences (Morgantown, WV). Access holes and threads were all drilled with a standard drill press, and were designed to fit standard HPLC fittings (Upchurch Scientific, Oak Harbor, WA). The milling schematic for plug-flow PMMA bioreactor is shown in the figure 1. Both the top cover and milled channel were irradiated with UV light (Newport Corporation, Irvine CA) (280 nm) for 15 minutes on each side prior to fusing the two pieces together to finish the assembly of the PMMA bioreactor.

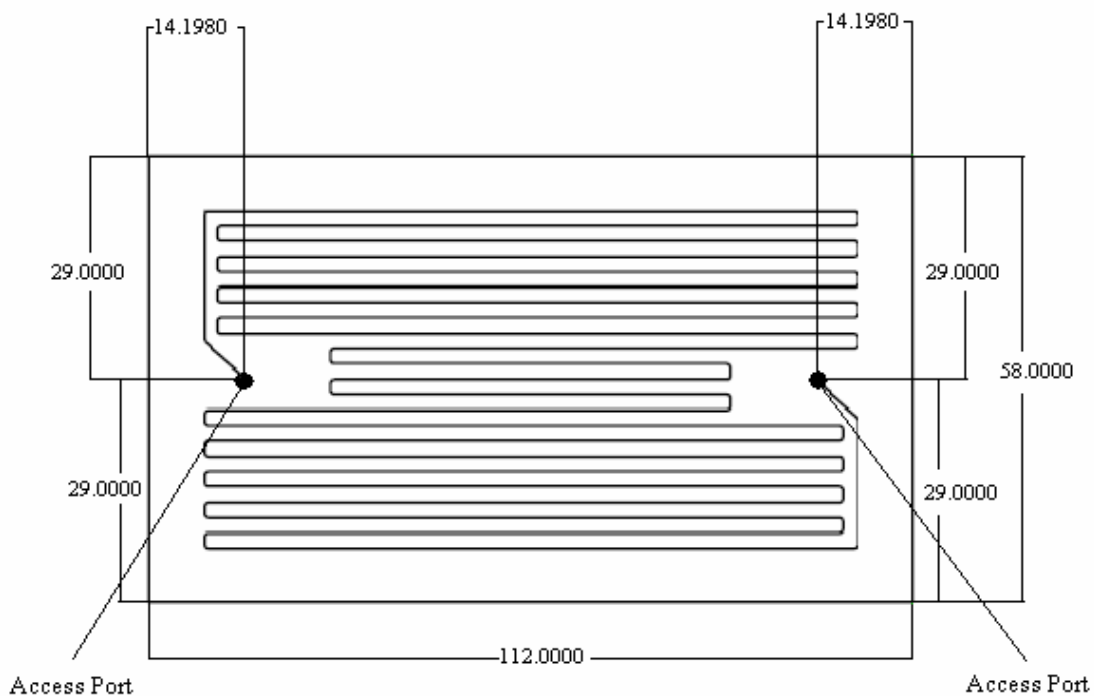


**Figure 2.1.** Milling schematic for the plug and flow bioreactor channel. Listed dimensions are given in millimeters (mm).

### **2.2.5. PMMA-CYP2C9 Chip Preparation**

PMMA chips (section x.2.3) were sonicated in KPi for a total of 5 min and placed in a solution containing EDC/NHS in KPi (10 mL) for a total of 2h. After activation of the surface carboxylic acids with NHS based esters, chips were rinsed KPi to remove excess EDC and NHS and were then treated with CYP2C9 (100 nM) in KPi containing a flurbiprofen and dapson, overnight, to allow for covalent bonding of CYP2C9 to NHS-activated esters. Finally, PMMA-CYP2C9 chips were rinsed in KPi before being stored in cryobuffer at -80°C prior to use.

### **2.2.6. PMMA-AcBzTacn-CYP2C9 Chip Fabrication**

PMMA chips (section x.2.3) were sonicated in KPi for a total of 5 minutes. After sonication, chips were removed from the KPi solution and transferred to vials containing EDC/NHS in KPi (10 mL) and were allowed to react for 2 h. Chips were rinsed with KPi and then were treated with (2 mL) AcBzTacn (20 mM) (A generous gift from Lisandra Martin, Monash University, Australia) previously dissolved in a potassium hydroxide solution (pH 10) for 30 hours. After the surface was functionalized with AcBzTacn, the surface was treated with (10 mL) nickel chloride (100 mM) for 1 h. Finally, the PMMA chips were treated with a solution (2 mL) of CYP2C9 (100 nM) in KPi containing flurbiprofen and dapson, overnight, to allow for Ni<sup>+2</sup> coordinated immobilization of CYP2C9 to the PMMA surface. After the PMMA-AcBzTacn-CYP2C9 construct was formed, chips were rinsed in KPi before being stored in cryobuffer at -80°C until use. All processes were performed under argon and at room temperature.



### **2.2.7. Gold-OT/MUA-CYP2C9 Chip Fabrication.**

Silicon wafers containing 50 nm gold on 5 nm chromium were diced into approximately 4 mm x 6mm chips and were sonicated in acetone for 5 minutes, rinsed with deionized water, and then soaked in Piranha solution (98% H<sub>2</sub>SO<sub>4</sub>: 30% H<sub>2</sub>O<sub>2</sub>, 3:1, v/v) at room temperature for 30 minutes. Chips were then rinsed with deionized water, ethanol, and then soaked in an ethanolic solution of 8-octanethiol (75 mM) and 11-mercaptoundecanoic acid (25 mM) for 18 hours to allow the SAM to form on the gold surface. Excess thiols were removed by subsequent rinsing the chips with pure ethanol, 95% ethanol, water and finally KPi. To bond the CYP2C9 to the SAM, the SAM-coated slides were immersed in a solution of EDC/NHS in KPi (10 mL) for a total of 2h. After activation of the surface carboxylic acids with NHS based esters, chips were rinsed KPi to remove excess EDC and NHS and were then treated with CYP2C9 (100 nM) in KPi containing a flurbiprofen and dapsone, overnight, to allow for covalent bonding of CYP2C9 to NHS-activated esters. Finally, Au-SAM-CYP2C9 chips were rinsed in KPi before being stored in cryobuffer at -80°C prior to use.

### **2.2.8. PMMA-CYP2C9 and Au-OT/MUA-CYP2C9 Chip Metabolic Incubation**

Both Au-SAM-CYP2C9 and PMMA-CYP2C9 chips were immersed in solutions containing Cytochrome P450 Reductase (200 nM, final concentration) and diclofenac (250 μM, final concentration) in KPi buffer in glass vials. To initiate the reaction, NADPH (250 μM, final concentration) in KPi was added, bringing the total reaction volume to 200 μL. The incubation

mixtures were incubated in a water bath overnight (16 h) at 37°C. Positive control experiments (200 µl, final volume) were conducted with solution CYP2C9 (2.5 nM, final concentration) containing 10 µL of dilaurophosphatidyl choline (1 mg/mL).

### **2.2.9. Fabrication of PMMA-2C9 Bioreactor EDC-NHS Construct (Dynamic Application)**

After fabrication of the PMMA bioreactor and its exposure to ultraviolet radiation, the plug and flow channel was cleaned by flowing KPi (10 ml, 40 mM) through the PMMA block at a rate of 500 µL/h using a Harvard Apparatus Pump II syringe pump (Holliston, MA). Once complete, the channel was filled (2 mL) with EDC/NHS in KPi. After the activation of the PMMA with the EDC/NHS mixture, the channel was rinsed with KPi (2 mL) for 2 hours at 1mL/h. Next, CYP2C9 (10 mL, 100 nM) dissolved in flurbiprofen and dapsone (1:1,v/v) in KPi was delivered through the channel continuously for a total of 20 h at 500 uL/h. After CYP2C9 immobilization, the channel was rinsed for a total 4 h with (2 mL) KPi at 500 uL/hr.

### **2.2.10. Fabrication of PMMA-2C9 Bioreactor EDC-NHS Construct (Static Application)**

Alternatively, a plug-flow bioreactor channel was fabricated using the same methods as above. However, during application of CYP2C9, the plug-flow channel was filled with a CYP2C9 solution (2 mL, 500 nM) dissolved in flurbiprofen and dapsone (1:1,v/v) in KPi. The CYP2C9 solution was applied to the channel in the absence of flow of CYP2C9 solution. After CYP2C9 immobilization, the channel was rinsed for a total 4 h with (2 mL) KPi at 500 uL/hr.

### **2.2.11. Fabrication of PMMA-2C9 Bioreactor AcBzTacn Construct**

For fabrication of a PMMA based bioreactor containing AcBzTacn, the plug-flow channel was cleaned by flowing KPi (10 mL, 40 mM) through the PMMA block at a rate of 500 uL/h using a Harvard Apparatus Pump II syringe pump (Holliston, MA). The bioreactor was then filled with EDC/NHS in KPi (2 mL) and allowed to react for 2 h. After activation of the PMMA with the EDC/NHS mixture, the channel was rinsed with KPi at (2 mL, 1 mL/h). Next, AcBzTacn (2 mL, 20 mM) in aqueous potassium hydroxide solution (pH 10) was applied by filling the channel and allowing the mixture to react with the surface for 30 h. The bioreactor was then treated with KPi at (2 mL, 1ml/hr). After the channel was rinsed free of excess AcBzTacn, the bioreactor was treated with CYP2C9 (10 mL, 100 nM, 20 h, 500  $\mu$ L/hr) in the presence of flurbiprofen and dapson (1:1, v/v). Finally, the channel was flushed with KPi (500 uL/h, 4 h) to remove residual enzyme solution.

### **2.2.12. Metabolite Generation of PMMA-CYP2C9 Bioreactor**

The basic set-up for the generation of 4'OH diclofenac is shown in Figure 2. The syringe and pump were coupled to HPLC style fittings and PEEK tubing. The block was placed into a jacketed beaker which is coupled to a circulating water bath to maintain the internal temperature of the jacketed beaker at 37°C. The physical set up is described in figure 2. Generation of metabolites is initiated by pumping of a solution containing diclofenac sodium (250  $\mu$ M, final concentration), NADPH (1mM, final concentration) and CPR (200 nM, final concentration) in KPi at 10mL, 500  $\mu$ L/h, 20 h). KPi solution containing metabolite leaves the bioreactor channel,

the PEEK tubing was positioned over a fraction collector. Fractions were continuously collected at a rate of one fraction per hour (500 uL) for a total of 20 h. The syringe was then refilled with KPi pumped through the bioreactor (2 mL, 500uL/h, 4h) to remove residual metabolite from the channel. The wash fractions were collected in the same procedure above, resulting in a total of 24 fractions. Fractions were centrifuged under, vacuum, to dryness using a Savant SC110 Speedvac (Thermo-Fisher, Pittsburgh, PA). Once dry, samples were reconstituted in aqueous acetonitrile (5% v/v, 200 uL).

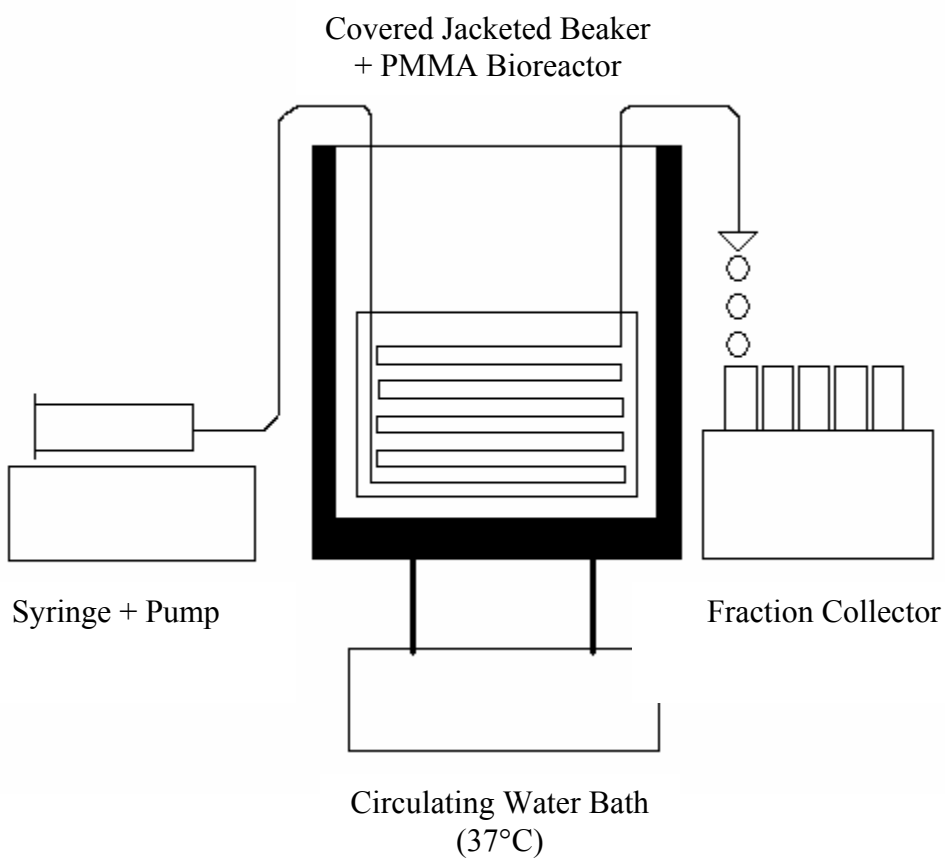


**Figure 2.2.** Setup corresponding to plug-flow PMMA-based bioreactor.

### **2.2.13. Chromatographic Detection of 4'-hydroxydiclofenac**

Metabolic reactions and bioreactor fractions were quenched by spiking with (50uL) acetic acid (50  $\mu$ L, HPLC grade) and an internal standard, N-phenylanthranilic acid in acetonitrile (50  $\mu$ L, 5  $\mu$ g/mL HPLC grade). Once completed, incubations were centrifuged (13,000 x g) for 10 min to precipitate protein. The supernatant (200  $\mu$ L) was removed and loaded into vials for chromatographic analysis. Separation of metabolite and parent compound was conducted using a Waters Alliance 2965 separations module (Milford, MA). Approximately 10uL of analyte was injected on to a Agilent Zorbax SB C-18 (150 mm X 4.6 mm, 5  $\mu$ m particle size) (Agilent Technologies, Santa Rosa, CA). Substrate and metabolite were eluted at 0.5ml/min using a mobile phase mixture of sodium acetate (75 mM, pH 5) and Acetonitrile (60:40, v/v). Eluted compounds were analyzed by a Waters 2487 Dual Absorbance Detector with absorbance detection at 280 nm. Data was processed by Waters Empower ver 2.0 software (Waters Corporation, Milford, MA). The peak corresponding to 4'-hydroxydiclofenac was determined by comparison to a 4'-hydroxydiclofenac standard.

### **2.2.14. Immobilization of CYP2C9 Enzyme on Gold electrode.**

Gold-coated glass slides (EMF Films, Ithaca, NY) were sonicated in acetone for 5 minutes, rinsed with deionized water, and then soaked in Piranha solution (98% H<sub>2</sub>SO<sub>4</sub>: 30% H<sub>2</sub>O<sub>2</sub>, 3:1, v/v) at 80° C for 15 minutes. The gold-coated glass slides were then rinsed with deionized water, ethanol, and then soaked in an ethanolic solution of 8-octanethiol (75 mM) and 11-mercaptoundecanoic acid (25 mM) overnight to allow the SAM to attach to the gold surface.

Excess thiols were removed by rinsing the SAM bearing gold-coated glass slides with absolute ethanol and PBS, each, three times. In order to bond the CYP2C9 to the SAM, the SAM-coated slides were covered with KPi containing EDC/NHS. The treated slides were then removed from the EDC/NHS solution and immersed in a KPi solution containing CYP2C9 (100 nM), flurbiprofen (40  $\mu$ M), and dapson (40  $\mu$ M) for 24 hr. All processes were performed under argon and at room temperature.

### **2.2.15. Electrocatalytic Metabolism of Warfarin**

Au-(MUA/OT)-CYP2C9 electrodes were immersed in an oxygen-saturated KPi solution containing NaCl (154 mM). A potential of -0.38 was applied using a potentiostat (Gamry Reference 600™, Warminster, PA), in the presence of a platinum wire (1 mm o.d.) counter electrode, an Ag/AgCl (3M KCl) reference electrode, and the CYP2C9-bonded gold electrode (CYP2C9-MUA/OT-Au) as the working electrode. The electrolysis was conducted for 2 hours. The electrode surface area was approximately 0.07 cm<sup>2</sup> and electrolysis solutions were magnetically stirred (150 RPM). The warfarin concentration in the electrolysis solution was 50  $\mu$ M. Upon completion of the electrolysis, the solution was concentrated to dryness, dissolved in acetonitrile (2 mL), filtered, and then concentrated to dryness. The residue was dissolved in KPi (200  $\mu$ L), spiked with 7-ethoxycoumarin (50  $\mu$ L, 1  $\mu$ g/ml) in acetonitrile, centrifuged (5 min @ 13,000x g) and loaded into HPLC vials for chromatographic analysis.

### **2.2.16. Reconstituted CYP2C9 Incubation with Warfarin**

Reconstituted CYP2C9 enzyme incubations with warfarin were conducted using enzyme prepared from insect cells infected with recombinant baculovirus containing a human CYP2C9\*1 cDNA and rabbit NADPH-P450 reductase. For these incubations, warfarin (50  $\mu$ M) was incubated with CYP2C9 (125 nM) in KPi, phospholipid (1.6 mM, final concentration), CPR (250 nM, final concentration) all in a total volume of 200  $\mu$ L. Samples were pre-incubated for 3 min at 37°C before the addition of NADPH (1mM, final concentration). Incubations were conducted for 20 min at 37°C, quenched by the addition of 7-ethoxycoumarin (50  $\mu$ L, 1  $\mu$ g/mL) in acetonitrile as the internal standard. The incubation mixture was then centrifuged (15 min @ 13000 x g) to pellet proteins. A total of 200  $\mu$ L of the supernatant was then loaded into liquid chromatography vials for analysis.

### **2.2.17. Chromatographic Analysis of Warfarin Metabolites**

Analysis of warfarin and its metabolites was performed with a Waters Alliance 2965 (Waters Corporation, Milford, MA) separations module using a Waters Symmetry column (150 mm  $\times$  4.6 mm, 3.6  $\mu$ m particle size, Waters Corporation, Milford, MA), eluting with aqueous phosphoric acid (0.5%) and acetonitrile (60:40, v/v, 1 mL/min), with fluorescence detection using a Waters 2475 dual channel fluorescence detector, ( $\lambda_{\text{ex}}$  = 320 nm,  $\lambda_{\text{em}}$  = 415 nm). nm) and an injection volume of 10  $\mu$ L. All chromatographic analysis was performed using Empower ver. 2.0 software (Waters Corporation, Milford, MA). The peak corresponding to 7-hydroxywarfarin was determined by comparison to a 7-hydroxywarfarin standard.

## **2.3. Results**

### **2.3.1. Introduction**

In order to maximize metabolite production of the completed plug-flow bioreactor, several different parameters were optimized on PMMA chips. Several PMMA chip studies were designed to look at optimal fabrication of PMMA-CYP2C9 chips. These include concentration of CYP2C9 exposed to NHS-activated PMMA, length of attachment time of CYP2C9 to NHS- activated PMMA and finally two different attachment schemes. Parameters which gave optimal metabolite output were then used in the fabrication of the plug-flow bioreactor.

### **2.3.2. Variation of CYP2C9 Immobilization Concentration**

In order to determine optimal concentration of CYP2C9, largely to prevent over crowding of CYP2C9 present on the PMMA surface, and enhance CPR access to the CPR binding site on the covalently immobilized CYP2C9, we conducted experiments varying the concentration of CYP2C9. PMMA chips were irradiated with UV light to cleave ester moieties within the PMMA polymer and form free carboxylic acids. Next, we incubated PMMA chips in EDC/NHS to form activated an NHS-ester, which will covalently bond any free amine in solution. Subsequently, we incubated the chips in 50, 100, 200 and 400 nM CYP2C9 respectively to bond the CYP2C9 to the chips. The activity of each chip was then determined by measuring the metabolism of diclofenac, a probe CYP2C9 substrate (process is outlined in Figure 2.3).



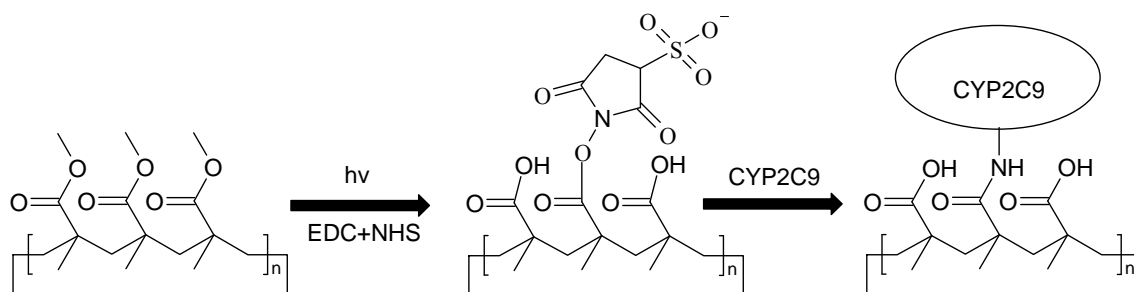


**Figure 2.3.** UV mediated cleavage of ester moieties present within the PMMA polymer. Subsequent EDC/NHS activation allows for the covalent linkage of CYP2C9 to the polymer surface.

Figure 2.4 shows the metabolism data for solution controls and PMMA chips. In this figure, the solid black bar represents the positive control experiment containing roughly 0.5 pmol CYP2C9 in solution. Negative control experiments omitted NADPH for each respective attachment concentration. Metabolite formation, 4'-hydroxydiclofenac, was not detected in the negative controls.

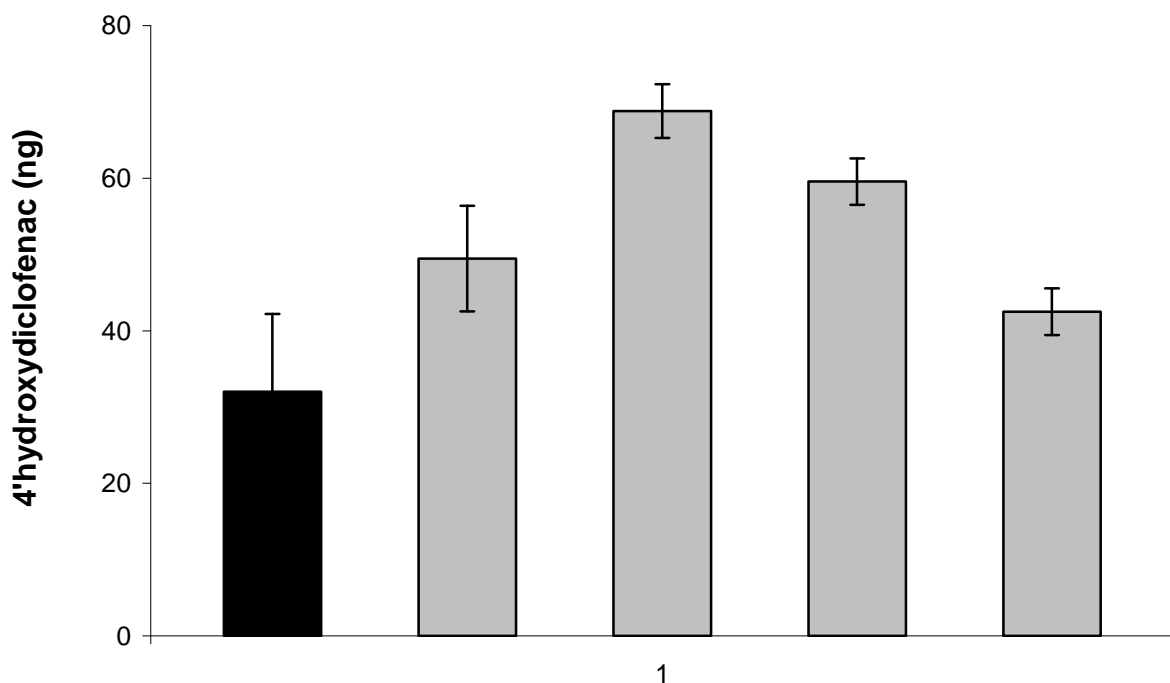


**Figure 2.4.** Metabolic formations from PMMA chips prepared with different concentrations (50, 100, 200, 400 nM) of CYP2C9 applied to EDC/NHS activated PMMA chips (grey). Solution incubation (black) contains 0.5 pmol CYP2C9 and dilaurophosphatidyl choline (black). All incubations contain CPR and NADPH.

### 2.3.3. CYP2C9 Attachment Time

In addition to determining the optimal enzyme concentration to treat the PMMA surface with and thus optimize metabolite output, we ran a series of experiments to optimize the PMMA chip exposure time to CYP2C9. The results are shown in Figure 5. This experiment used UV activated PMMA chips (4 mm x 6 mm) treated with EDC/NHS and then CYP2C9 (100 nM) solution for different time periods (2, 4, 6, 8 and 24 hours). Negative control experiments

omitted NADPH for each respective attachment time. Metabolite formation, 4'hydroxydiclofenac, was not detected in the negative controls.

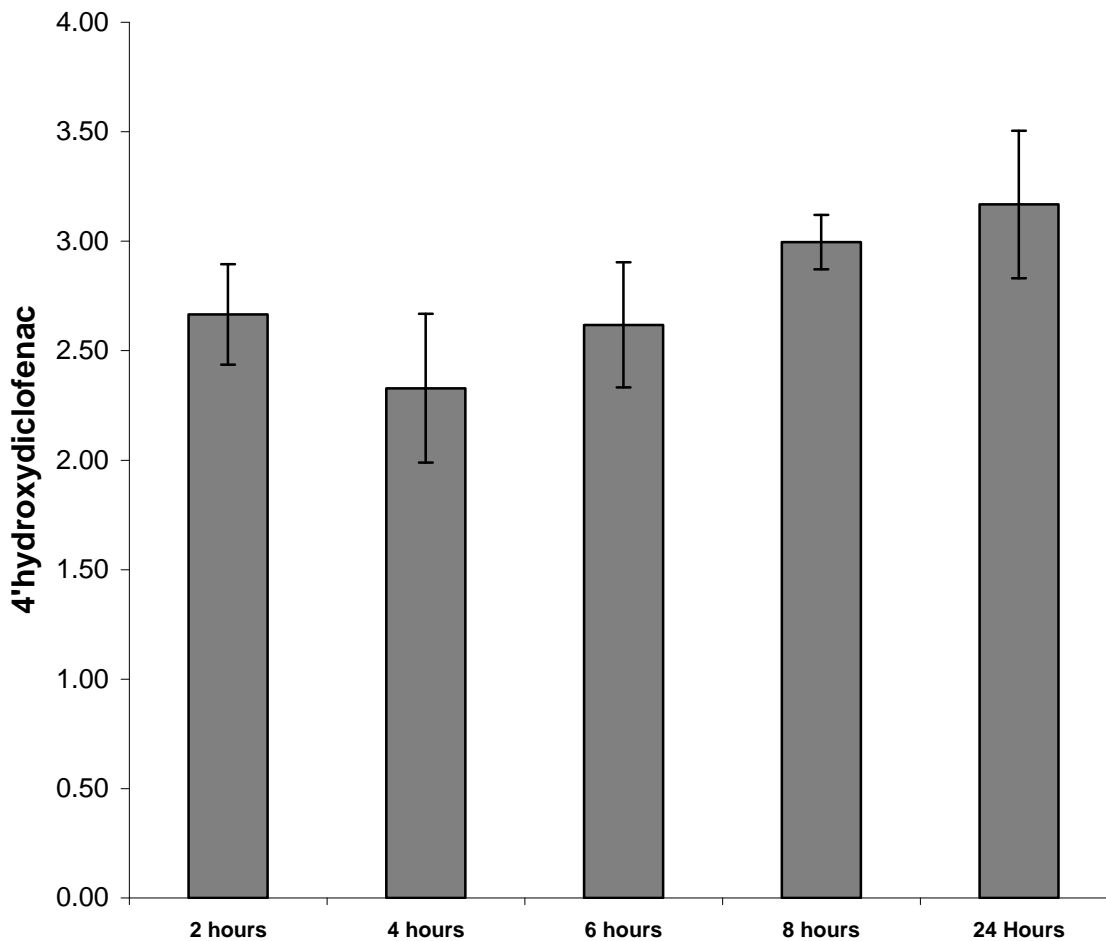


**Figure 2.5.** Incubation study optimizing CYP2C9 attachment time (2, 4, 6, 8, and 24 h) to an EDC/NHS activated PMMA chips.

### 2.3.4. CYP2C9 Attachment Type

A third parameter varied in addition to using different solution concentrations of CYP2C9 for protein attachment and different exposure times to optimize attachment, was to utilize two different attachment chemistries with the goal of optimizing metabolite production. One method

involves using EDC-NHS conjugation to form a covalent bond with a free amine at the N-terminus or on the surface of the protein. The second method used Acbztacn, a molecule capable of chelating divalent cations such as  $\text{Ni}^{+2}$ . Once this complex coordinates these divalent cations to the Acbztacn moiety, it can then bind the remaining coordination sites of the chelated species ( $\text{Ni}^{+2}$ ) to bind a his-tag, present on the C-terminus of the enzyme. This provides a way to specifically bind the protein at a specific site, in contrast to the EDC-NHS coupling, where the binding site is somewhat ambiguous. Figure 2.6 shows the amount of metabolite formation for solution incubations (solid black), the previously described CYP2C9 immobilized to a gold-thiol self-assembled monolayer (bricked) and from UV-exposed, PMMA chips (solid gray) that used AcBzTacn. The immobilized CYP2C9 experiments directly compare the metabolic activity of enzyme immobilized with EDC/NHS versus Acbztacn. Negative control experiments contain no NADPH for each respective attachment type and no metabolite was detected in any of these samples using our method of detection for 4'hydroxydiclofenac.

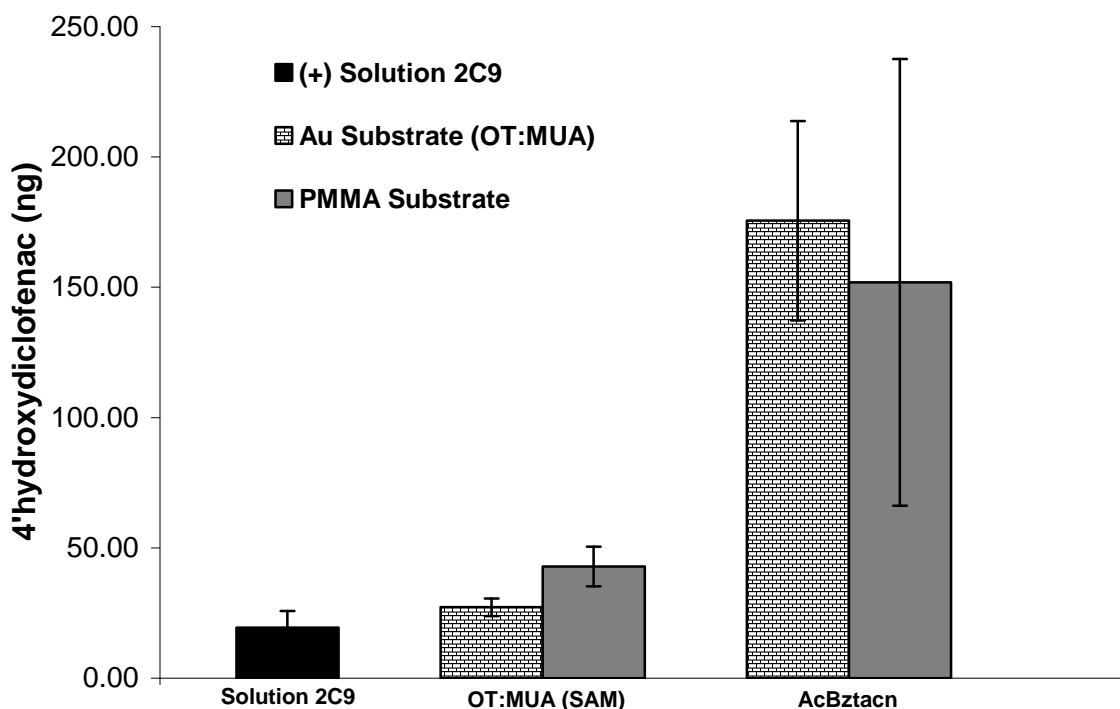


**Figure 2.6.** Comparison of metabolite production based on his-tag directed coordination (AcBzTacn) and covalent coupling (EDC/NHS) on gold-OT:MUA(3:1) self-assembled monolayer (bricked) or PMMA (grey). Incubations were conducted for 24 h.

### 2.3.4. Metabolite Production of Completed Bioreactor

After fabrication of the plug-flow bioreactor channel and subsequent coupling of CYP2C9, CPR and NADPH were flowed through the bioreactor (500 uL/hour). Samples were collected (500 uL) and metabolite production in each fraction determined by HPLC (Figure 7). Analysis of two different coupling chemistries, filled circles, representing Acbztacn coupling, and an EDC-NHS coupled bioreactor, represented by the filled squares were compared. Both of these bioreactors constructs were fabricated using a method where (10 mL) CYP2C9 (100 nM)

was flowed through the channel at a continuous rate (500 uL/hr) for a total of 20 hours. In contrast, we have also monitored the production of metabolites based on an EDC-NHS based bioreactor which is treated with the same amount of CYP2C9 (1 nmol), however the enzyme is applied by filling the channel with a single volume of (2 mL) CYP2C9 (500nM), and is represented by filled triangles. Total metabolite production for each bioreactor were 1.) Acbztacn coupled (114.1 ng), 2.) EDC-NHS coupled (295.7 ng) (dynamic application) and 3.) EDC-NHS in the absence of flow (static application) through the channel during CYP2C9 application (437.3 ng).

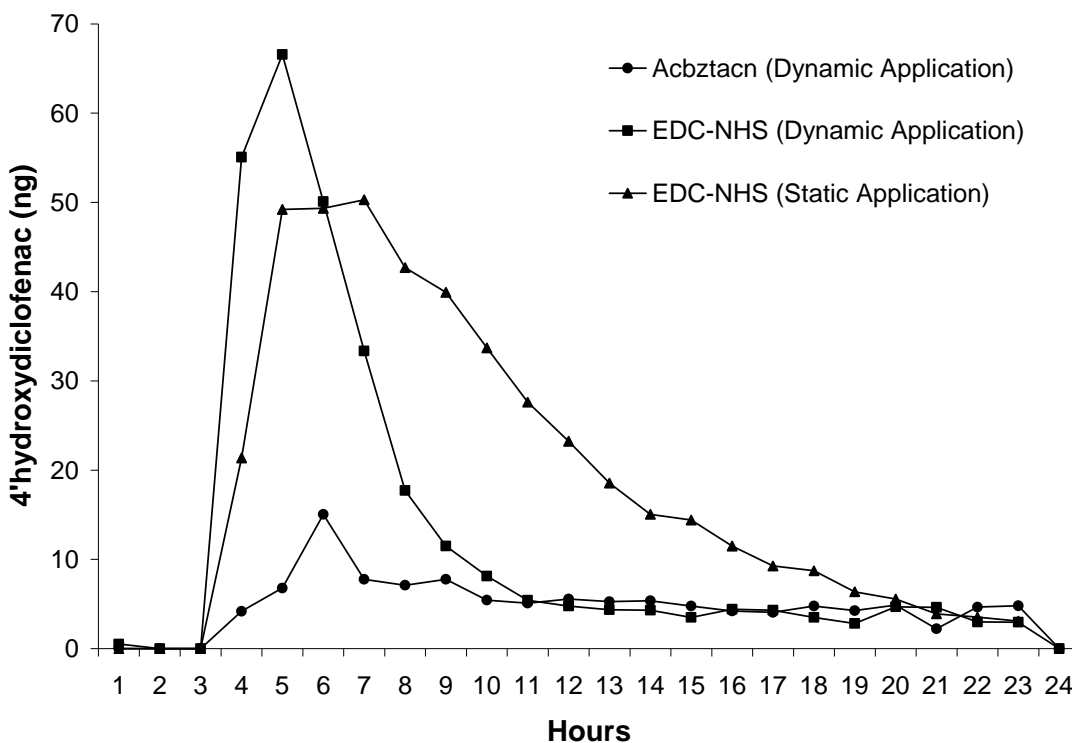


**Figure 2.7.** Time course analysis of metabolite production by a CYP2C9 immobilized plug and flow PMMA bioreactor. His-tag directed coordination with Acbztacn (circles) is compared to plug and flow channels fabricated using EDC/NHS covalent immobilization. Further comparison of EDC/NHS immobilization techniques is shown by continuous injection (10 mL, continuously injected at 500  $\mu$ L per hour for 20 h total) of CYP2C9 (100 nM) (squares) and static injection (2 mL, injected immediately, for 20 h) (triangles) of CYP2C9 (500 nM).

### 2.3.6. Alternative Bioreactor Generated Warfarin Metabolites

An alternative approach to producing useful quantities of metabolite is to use the immobilize enzyme as an electrode. Therefore, a model for a batch biochemical reactor was explored using an electrochemical cell with a gold electrode to which was attached CYP2C9 via an OT:MUA (3:1) self-assembled monolayer. The electrochemical bioreactor was filled with warfarin (50  $\mu$ M) in water, KPi and sodium chloride (154 mM) and held at a potential of -0.38 V

for a period of 2 h. Metabolite formation in the control potential electrolysis of warfarin was compared with a solution incubation by HPLC and the data is shown in Figure 8. Curve A in figure 8 is the chromatogram obtained from the solution incubation. As indicated in Figure 8, the major metabolite formed is 7-hydroxywarfarin (retention time 6.8 min). A second peak, with a retention time of 6.4 min was not identified by may be 6-hydroxywarfarin. The dashed curve above Curve A is the negative control (-NADPH) and lacks the peak corresponding to the 7-hydroxywarfarin. Curve B in Figure 8 is the chromatogram of the controlled potential electrolysis mixture. The formation of the expected metabolite (7-hydroxywarfarin) is apparent (retention time = 6.8 min), as is a second peak (retention time = 6.4 min) that was also observed in the solution incubation. A third peak (retention time = 4.2 min) is observed but was not seen in the solution incubation. The identity of this peak is unknown. Finally, the dashed curve above curve B is of the same system except that no electrochemical potential was applied to the system (negative control).



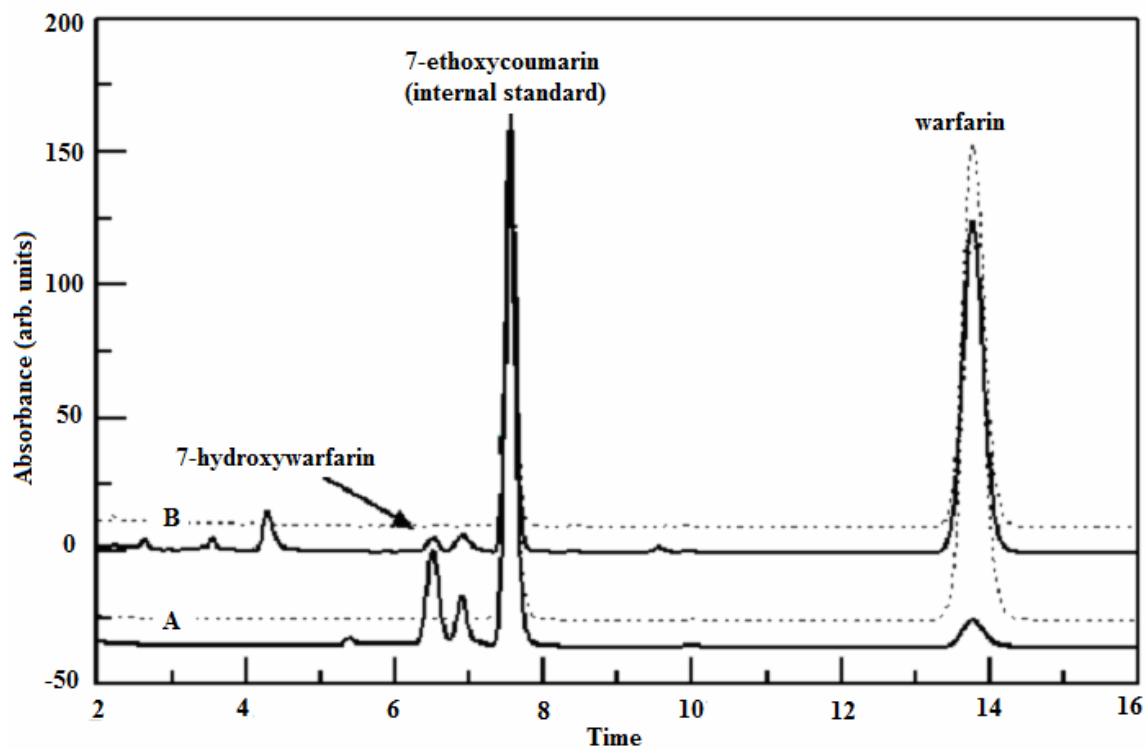


**Figure 2.8.** Chromatogram trace representing the production of warfarin metabolites. Chromatographic trace (A) represents solution incubation of CYP2C9 baculosomes in the presence of NADPH. Dashed chromatographic trace above (A) represents an NADPH-free CYP2C9 baculosome incubation. Chromatographic trace (B) represents warfarin metabolites generated from a CYP2C9 immobilized electrode. Dashed line above (B) represents electrochemical analyte when no potential is applied to the enzyme-electrode.

## 2.4. Discussion

### 2.4.1. PMMA Based Plug-Flow Bioreactor

Here we present a novel method to generate drug metabolites by utilizing chemically immobilized P450 enzymes in plug-flow bioreactor construct. The use of recombinant enzymes in bioreactor systems as described here, is an approach to generate specific metabolites, using a single P450 isoform of interest. The bioreactor constructs presented here are very easy to fabricate and only relies on simple, well established procedures including bioconjugation chemistry and microfluidic fabrication techniques. This is in contrast to previously described

methods to generate metabolites. The primary alternative for production of metabolites often requires synthetic approaches entailing several steps and can be a very expensive, time consuming and labor intensive process.

We have attempted to optimize the coverage of enzyme on the surface by modulating the concentration of CYP2C9 present during the immobilization. We found that an optimal immobilization concentration of CYP2C9 to be around 100 nM. We hypothesize that a lower concentration of CYP2C9 present for immobilization would likely generate a surface which to sparsely populated with enzyme, thus generating lower levels of metabolite produced when compared to the 100 nM attachment concentration. In contrast, attachment of CYP2C9 at higher concentrations probably leads to a surface which is tightly packed with enzyme, thereby reducing the access of CPR to the CYP2C9 located on the surface.

In addition to monitoring the concentration of P450 available for attachment, we also wanted to observe the amount of time the enzyme could be exposed to a PMMA chip without losing activity. We see an increase in metabolite produced over a period of 24 hours, without losing activity of the CYP2C9 over the 24 hour period. This indicates that the CYP2C9 is a fairly robust enzyme and does not lose activity over long periods of time at room temperature, making it an excellent candidate for use in the proposed bioreactor construct. The ability of CYP2C9 to remain active over a long period of time without losing activity will allow for fabrication of the bioreactor under low-flow conditions, which will expose the inside of the channel to decreased levels of shearing force, which should reduce CYP2C9 denaturation during the immobilization process.

In addition to having the enzyme immobilized in a covalent manner, a comparison was made to monitor the activity of chips using AcBzTacn based immobilization, which is based on  $\text{Ni}^{+2}$  mediated coordination of a C-terminal his-tag present on CYP2C9. From experiments conducted on PMMA and gold-thiol SAMs, we demonstrate that Acbztacn immobilized protein showed greater activity when compared to the EDC-NHS conjugated chips. This may be a result of the enzyme being oriented in a more favorable binding orientation to interact with CPR. By specifically attaching to the C-terminus, the enzyme likely exists in a single orientation, whereas with the EDC/NHS covalent immobilization, the enzyme may be immobilized at the N-terminus but could also be immobilized to any one of numerous surface lysine residues that exist on the surface. In turn this could affect the binding of CPR, as the CYP2C9 could potentially have this binding site blocked. Moreover, the random orientation of the CYP2C9 on the surface could also block the substrate access channel, which would have a detrimental affect on the activity of the enzyme. As a result, we chose to compare enzyme immobilization methods in plug-flow bioreactors to determine which of the methods is best for optimal metabolite production. However, in these experiments, much less metabolite is produced from the Acbztacn immobilized protein when compared to the EDC/NHS immobilized based bioreactor, suggesting that EDC/NHS immobilized CYP2C9 may be the optimal choice for the plug-flow bioreactor construct.

Furthermore, experiments comparing the application method of CYP2C9 to the bioreactor channel were compared to evaluate metabolic activity of each bioreactor construct. Two different plug-flow bioreactors were compared, one where enzyme was applied and immobilized CYP2C9 by delivering 2 mL of CYP2C9 solution to the channel immediately. The

second approach applied 10 mL of CYP2C9 solution from a syringe at a constant flow for a total of 20 hours. Both systems were treated with an equivalent amount of CYP2C9 (1 nmol) to allow for proper comparison. Results of this experiment suggest the static application of CYP2C9 produced more metabolite over the 24 hour experiment than the dynamic application of CYP2C9 flowed through the bioreactor channel during immobilization of CYP2C9. This may be attributed to enzyme crowding, where the static system generates a surface more evenly covered with CYP2C9. In contrast, when the enzyme is continuously applied, a situation may arise where the CYP2C9 at the beginning of the channel could be tightly packed due to the high concentration of enzyme present at the beginning of the channel, in turn hindering CPR binding. Moreover, near the end of the channel we have a situation where enzyme at the end of the channel is much more dispersed, creating a situation where little enzyme is present to metabolize substrates.

Previously, we have described that an excess of CPR is necessary to generate metabolites in immobilized chip systems<sup>70</sup>. This is, in large part, due to the localized nature of CYP2C9 (on the chip) in relation to the dispersed nature of the CPR through out the solution. More to the point, in a typical incubation conducted in solution, it is common to use a 2:1 ratio of CPR:P450, as these two components are evenly mixed throughout the solution. However in the case with the enzyme immobilized on the PMMA chip, these two components are heterogeneously mixed, resulting in the requirement for excess reductase to achieve sufficient concentration at the surface and therefore generate enough metabolite to be able to reliably quantitate P450 mediated metabolite production.

In contrast, the plug-flow bioreactor was found to generate metabolite without having the large excess concentration of CPR required with the chip incubations. That is to say that the concentration of CPR applied to the channel during the metabolism experiment is approximately 2 fold (2 nmol) greater than the amount of CYP2C9 that is applied through the channel during the immobilization experiment. It is hypothesized that this difference may be due to the difference in surface area/volume ratio between the two systems. The cross section of the plug-flow channel is 1 mm by 1 mm and the channel is 2.1 m long. This generates a channel with an internal volume of approximately 2100  $\mu\text{L}$  and a surface area of 8400  $\text{mm}^2$ . In comparison, the immobilized chip experiments, conducted in 200  $\mu\text{L}$  of solution and contain an activated surface area of approximately of 48  $\text{mm}^2$ . In comparing the ratio of surface area to volume, we see the plug-flow bioreactor channel has a much higher ratio (4  $\text{mm}^2/\mu\text{L}$ ) when compared to the immobilized chip system (0.24  $\text{mm}^2/\mu\text{L}$ ).

Further complicating the issue of CPR access is the reduced mixing present in the channel of a plug-flow bioreactor, particularly in the axial direction. As a result, the impaired mixing of the reactant may contribute to poor interaction of CPR on the P450-PMMA surface. Moreover, the decreased mixing may also hinder mixing of other components necessary for P450 mediated metabolism, such as NADPH,  $\text{O}_2$  and substrate. The lack of proper and homogeneous mixing in plug-flow reactors may help to explain the low levels of metabolite produced (as a function of CYP2C9 concentration).

Accordingly, it would be optimal to use a concentration of CPR such that there was a ratio of CPR:P450 based on our estimate of the amount of P450 immobilized to the channel. This significantly reduces the amount of CPR used in running the bioreactor, and has several

advantages including the reduced cost to run the bioreactor (10 fold less CPR in each incubation compared to chip based experiments). Second, this system more accurately reflects common *in-vitro* experiments that typically use a 2:1 ratio of CPR:P450.

Further optimization of the bioreactor construct is still necessary before such a device is ready for commercialized use. For example, the CPR:P450 ratio has not been optimized, nor has flow rate, as both of these parameters differ significantly between the proof of concept chips and plug-flow bioreactor construct. This is due in large part to the ratio of volume to surface area between the two systems. In the immobilized chip system, we have optimized reductase concentrations that are approximately 20:1 (CPR:P450). This largely based on previous calculations of enzyme concentration, determined electrochemically, by similar sized chips made with a (3:1) OT:MUA self-assembled monolayer on gold<sup>71</sup>, a construct that serves to simulate the chemistry present on the PMMA surface. Additionally, we see similar levels of metabolite between both the PMMA and gold-immobilized systems and thus we crudely estimate the level of enzyme immobilized to the PMMA and gold-self-assembled monolayer construct to be similar. At the present time a reliable method to quantitate enzyme levels present on a PMMA surface has not been found. Unfortunately this hinders the optimization process of the PMMA-P450 chip, and we will look to address this in future experiments.

Previously, several groups have attempted to make metabolite using plug-flow bioreactors using HLM preparations<sup>154,155</sup>. Advantages of the plug-flow bioreactor utilizing recombinant CYP2C9, when compared to systems including HLMs includes the fact that this bioreactor uses a single P450 isoform and could thus be used to form only the metabolite(s) of interest. This is particularly advantageous when trying to generate a specific metabolite or

compound for toxicological studies or for use as an analytical standard. In contrast, HLM based systems contain the entire compliment of P450 enzymes present in the liver and thus will potentially form many metabolites. In several instances, reactive and toxic metabolites are often not the dominant metabolite produced and are often generated in very low quantities. The system we describe here could be designed, by using any P450 enzyme of interest, to target the formation of specific compounds and would allow for researchers to generate these compounds in sufficient quantities to provide more definitive answers pertaining to the toxic mechanism of a particular metabolite. Finally, the use of HLM based bioreactors, since multiple metabolites may form, increases the difficulty of separating the compounds generated, often requiring complex chromatographic separations to in order to collect all the metabolites of interest. Thus, it is likely that these HLM based systems are better suited for early stage screening and structural elucidation of metabolites.

However systems do exist that will generate large quantities of metabolite, particularly insect-cell based systems designed by Rushmore, et. al<sup>151</sup>. These systems are efficient for metabolite production and can be tailored by transfection of a P450 baculosome into insect-cell lines to produce specific metabolites of interest. Though several disadvantages of this system are still apparent and should be addressed. First, to generate the cell line of interest, it is necessary to be skilled in the growth and maintenance of cell lines, as well as the adequate transfection of the cell line. Additionally, if it happens that you are trying to generate a metabolite which produces some cytotoxic effect, for example, through DNA-damage, then this presents a situation where production of metabolite(s) in a cell based bioreactor becomes counter-productive, because the metabolites may cause cytotoxic effects to cells in the bioreactor.

Moreover, compounds that are specifically designed to cause cytotoxic effects, such as chemotherapeutic agents, may be compatible with our system, as it remains a cell free system.

Additionally, bioreactors containing living cells used for the generation of compounds of interest have several issues associated to their use that makes them undesirable candidates for use in bioreactors, particularly when compared to immobilized enzyme constructs. For one temperature issues are well know to plague batch and fed-batch bioreactors, and often require complex temperature control systems. Additionally, cell-based systems will generate a tremendous amount of waste, which needs to be removed from the system in order to keep the bioreactor functional.

The use of a plug-flow bioreactor based on PMMA conjugated P450 enzymes could be easily converted into a system for its commercial use. Commercially available PMMA tubing can be found at extremely reasonable prices. Purchasing commercially available tubing eliminates the need to mill PMMA blocks and hence the associated costs (time, labor, equipment). we avoid having to purchase a costly milling station and eliminate the time required by the mill the PMMA block. Furthermore, it is possible to couple the PMMA tubing to HPLC-like fittings, which could potentially assist in high throughput metabolite generation and gives the device additional functionality to be used as a screening tool in early drug development situations. Additionally, several functionalized PMMA tubes could be bundled and utilized in hollow fiber bioreactor constructs<sup>156</sup>, thus serving to further increase the metabolite output of PMMA immobilized P450 bioreactor.



#### *2.4.2. Electrochemical Batch Bioreactor*

As an alternative to the production of metabolites with a plug-flow PMMA bioreactor, an electrochemical based system to generate metabolites was utilized. This system replaces the electron source CPR/NADPH with electrochemically supplied electrons via an enzyme-based electrode. Based on the levels of metabolite produced in relation to the amount of P450 used in each system, the electrocatalytic oxidation of CYP2C9 substrates is far more efficient in comparison to the plug-flow bioreactor described above. Additionally, only substrate and buffer salts are necessary to run the electrochemical mediated synthesis, creating a cost effective method to generate metabolite. In contrast, the plug-flow bioreactor channel uses substantial amounts of P450 as well as CPR and NADPH to carry out the catalytic oxidation of a given substrate. In the long run this is an extremely costly process, and future research and resources should likely be applied to optimize the P450-electrode based metabolite synthesis.

The downside of this approach is that the presence of CPR and NADPH contribute to the regiospecificity of metabolites that are produced. As a result, the electrochemical bioreactor may produce metabolites that would not be found when using CPR and NADPH. Evidence for this is shown in Figure 2.8, where a peak corresponding to a warfarin metabolite(s) elutes at 4.2 min. The chromatographic peak seen here may be a result of a metabolite eluting from the column which is not typically produced by P450 enzymes in the presence of CPR/NADPH. Conversely, it may be a result of two subsequent oxidations of a warfarin molecule by the P450-electrode.

To compare the metabolic profile of warfarin produced electrocatalytically, we performed an incubation of CYP2C9 baculosomes in KPi containing NADPH and racemic warfarin. The retention times of the species of interest in each chromatogram as they relate to the

retention time of the internal standard peak, demonstrate the formation of 7-hydroxywarfarin. This is the major metabolite of CYP2C9-mediated metabolism of warfarin and here it was formed with the application of an electrical potential to an enzyme-immobilized modified gold electrode. Moreover, the chromatographic traces suggest that the electrocatalytically driven metabolism of racemic warfarin also results in the formation of other metabolites commonly observed by CYP2C9 metabolism. The solution metabolism appears to yield much greater amounts of metabolite than the electrochemically driven system, based solely on peak area. However, when comparing the relative enzyme content of the two systems, the CYP2C9 baculosome incubation contained approximately 25 picomoles of CYP2C9 whereas the covalently bound CYP2C9 electrode contains approximately 0.06 picomoles, nearly 500 fold less CYP2C9<sup>71</sup>. These findings suggest the electrocatalytically generated method of metabolite production is a far more efficient method of metabolite production when compared to the plug-flow reactor. The preparation of metabolites using the plug-flow PMMA bioreactor, designed as-is, becomes somewhat cost prohibitive, particularly when you take into account the amount of purified enzyme required and the minimal amount of metabolite that is ultimately produced is taken into account.

### *2.4.3. Conclusion*

In summary, we have shown the ability of immobilized CYP2C9 to produce drug metabolites of interest. The methods described herein provide a significant advantage over traditional organic synthesis in that we can produce the metabolites in a rapid and high-throughput fashion, with a high level of regiochemical control. Additionally we can synthesize

metabolites without the use of harsh reagents, thus eliminating safety hazards presented by traditional synthesis. We propose this as a novel system to produce large quantities of metabolites for pharmaceutical companies to conduct toxicity testing. We believe that this technique could be used to potentially save pharmaceutical companies time and money by eliminating the need to produce compounds in traditional medicinal chemistry laboratories

## **Chapter 3**

# **Nanostructure Device Designed to Control Aggregation between CYP2C9 Enzymes**

### 3.1. Introduction

Cytochrome P450 (P450) enzymes are a family of oxoferroreductase enzymes containing a heme moiety and are well known to be involved in the metabolism of a wide variety of endogenous and xenobiotic materials. It is estimated that roughly 75% of all pharmaceutical compounds are metabolized by these enzymes and of these, approximately 90% are processed by five of the major human isoforms including CYP3A4, CYP2C9, CYP2C19, CYP2D6 and CYP1A2.<sup>39,157</sup>

P450 enzymes involved in metabolism are present as a membrane bound proteins, bound to the endoplasmic reticulum. Early P450-mediated metabolism studies demonstrated that P450-mediated metabolism required a membrane-bound complex containing a P450 enzyme and Cytochrome P450 reductase (CPR). This finding provided a template for which model reconstituted systems would be developed and metabolism studies would be conducted<sup>3</sup>. Utilization of solution studies involving P450 enzymes has been extremely useful in determining and demonstrating overall drug safety. The approach provides an inexpensive and efficient way to determine viable drug candidates from the standpoint of drug metabolism (e.g., P450 binding, inhibition, toxic metabolite production) before more costly and extensive studies are undertaken. However, several issues still exist with solution systems for P450 incubations and metabolic differences between these model systems and *in-vivo* conditions have been described<sup>158</sup>.

Among the issues which persist with respect to the current use of recombinant P450 enzymes is the tendency of these enzymes to form aggregates with one another that may result in alterations in catalytic activity. It is believed that after purification from bacterial cells, the hydrophobic nature of these proteins tends to promote aggregation at the N-terminal membrane

associated domain<sup>60</sup>. Experimentally, P450 aggregates can be dispersed by truncation of N-terminal hydrophobic domains<sup>60,61</sup>, mutation of key residues involved in aggregation of P450 enzymes<sup>63</sup> through the use of non-denaturing detergents<sup>61,159</sup>, by incorporation into nanodiscs<sup>68</sup>, or by immobilization of the P450 enzyme to a solid substrate<sup>3,70,160</sup>.

In instances where P450 enzymes are truncated to prevent the formation of aggregates<sup>60,61</sup>, the N-terminal domain is removed. In the case of truncated-CYP2E1, residues 3-29 were removed from the protein sequence. Once removed this enzyme displayed a decreased tendency to form large aggregates and were restricted, primarily, to pentameric structures. However, given the nature of the N-terminal domain to associate with membrane-like structures and form an active redox complex with Cytochrome P450 Reductase, this mutation may also alter the catalytic activity and may not provide results that accurately reflect the true activity of the monomeric P450 enzymes.

Additionally, mutations to key residues thought to be located in the F-helix or FG loop of P450 enzymes have also been addressed to reduce levels of aggregates<sup>63</sup>. In studies involving mutations of the F-helix and FG-loop, it was found that some mutants displayed significantly decreased activity while others displayed increased activity over wild-type P450 enzymes. These observations could be the result of a reduced state of aggregation though it is also possible that it is an artifact of a change in the structure of the enzyme that produced the alteration in enzymatic activity. Utilization of mutations, therefore, may only be useful for assessing the mechanism of aggregation, and may not be suitable for studies that assess catalytic activity.

An alternative approach to reduce or eliminate aggregation is to use detergents, such as Emulgen 913, within the incubation<sup>161</sup>. By using this detergent at controlled concentrations, it

was demonstrated that monomeric forms of P450 could be produced. Furthermore, it was shown that the formation of P450 aggregates can lead to large differences in the catalytic activity of CYP1A2. This study demonstrated that large P450 aggregates are much less catalytically active than either the pentameric monomeric forms. At the same time, it was also shown that pentameric aggregates of CYP1A2 were more catalytically efficient than monomers, when normalized for protein concentration. The caveat is that variation in the concentration the detergent may be a contributing factor to the poor activity seen in the monomeric forms, as this could hinder interactions with redox partner proteins, alter the membrane anchoring domains which are commonly used to generate a reconstituted incubation, or occupy/bind to the active site.

Recently, nanometer-scale discoidal membranes have been synthesized by mixing membrane proteins with a helical belt protein to form a Nanodisc<sup>68,69</sup>. This particular approach has been useful in the study of transmembrane proteins such as g-protein coupled receptors<sup>67</sup> and P450 enzymes<sup>69</sup>. By controlling the size of the membrane disc, and thereby reducing the capacity of the discoidal membrane to bind large P450 aggregates, researchers have developed a system to reduce heterogeneity in P450 enzymes by generating monomeric P450 enzymes for kinetic analysis<sup>68</sup>.

We have developed approaches to reduce aggregation of P450 enzymes by selective immobilization of P450 enzymes to a solid surface<sup>70</sup>. In general, this platform will create a tethering point for P450 enzymes to remain stationary on the surface and in a monomeric form. However, given the tendency of mixed-thiol self-assembled monolayer films to produce non-uniform (random distribution of thiols) mono-layers,<sup>90</sup> it may be the case that domains will be

present in these self-assembled films that will carry a hydrophobic character and promote the formation of aggregates. As discussed earlier, the likely mechanism of thiol aggregation is through the interaction of hydrophobic domains and these hydrophobic domains in SAMs promote localized aggregation and/or non-specific binding of proteins at a given point on the surface. As a result it is likely that an immobilized P450 (e.g., CYP2C9) is both bonded and non-specifically bound to nanosized domains of octanethiol which are, in turn, bonded to the surface.

There have been several recent advances in the creation of patterned nanostructures. The formation of these regular (patterned) nanostructures is effected through several different methods of fabrication including nano-imprint lithography<sup>162</sup>, near-field optical lithography<sup>163</sup>, dip-pen nanolithography<sup>164</sup>, scanning-probe microscope based nanoscale patterning<sup>165</sup>, self-assembly of monolayers<sup>166</sup>, and pattern formation based on phase separation of polymers<sup>167</sup>. However as is the case with many of these methods, they often create nanostructures of non-uniform size or periodicity or they are only optimized to form nanostructures over a very small area. As a result many of these techniques may be insufficient when it is desired to create a nano-patterned surface of sufficient area such they bear sufficient enzyme for the generation of sufficient product for detection and quantitation.

Here we describe a nanostructure device that, in principle, can be used to unequivocally control the aggregation state of CYP2C9. In order to accomplish, we utilize polystyrene nanosphere based lithography<sup>168</sup> to generate nanostructures of uniform size (here, 100 nm) and periodicity (500nm, presented here) over a large area such that approximately 100 billion ‘nanowells’ are present in an area of 1 X 1 cm. This is sufficiently large to ensure that enough enzyme is present on the surface (~ 100 fmol) to detect metabolite by conventional methods



(HPLC, LC/MS). By immobilizing enzymes to this nanostructure device, we can unequivocally control the state of aggregation of these P450 enzymes to provide insight into the relationship of aggregation on catalytic activity.

## **3.2. Materials and Methods**

### **3.2.1. General**

Unless otherwise noted, phosphate buffer (KPi) was made by mixing 40mM solutions of both dibasic and monobasic potassium phosphate such that the resulting solution of mixed components had a measured pH of 7.4. Running buffer for SPR experiments includes the addition of sodium chloride (150 mM, final concentration) to KPi buffer and shall be referred to as phosphate buffered saline (PBS). The solution of flurbiprofen and dapsone, used during CYP2C9 adsorption, was 40  $\mu$ M of each compound dissolved in KPi in a 1:1 ratio. The cryobuffer solution consists of KPi and glycerol (80:20, v/v)

### **3.2.2. Materials**

Diclofenac sodium, flurbiprofen, beta-nicotinamide adenine dinucleotide phosphate, reduced form (NADPH), 8-octanethiol (OT), (11-mercaptoundecyl)tri(ethylene glycol), and N-phenylanthranilic acid were purchased from Sigma-Aldrich (Milwaukee, WI). 4'-hydroxydiclofenac was purchased from Toronto Research Chemicals (Toronto, Canada). Cytochrome P450 reductase (CPR) was purchased from BD Biosciences (San Jose, CA). Purified CYP2C9 and dapsone were provided by Dr. Tim Tracy (Minneapolis, MN). N-octyltrimethoxysilane and 2-[methoxy(polyethyleneoxy)propyl]trimethoxysilane were purchased

from Gelest (Morrisville, PA). Microscope cover slides were purchased from VWR (Radnor, PA). SPR substrate holders were purchased as part of an SIA Au kit from GE Healthcare (Piscataway, NJ). Gold coated glass microscope slides were purchased from Evaporated Metal Films (Ithaca, NY).

### **3.2.3. SPR Film Fabrication.**

Microscope cover slides (40 mm x 24 mm, No. 2) (VWR, Radnor, PA) were cut into 12 mm x 10 mm rectangles and were loaded into a Temescal BJD-2000 (Edwards Vacuum, Phoenix, AZ) system with an Inficon XTC/2 deposition controller (Inficon, East Syracuse, NY) for metal evaporation. The chamber was pumped down to a pressure  $\leq 1.0 \times 10^{-5}$  Torr. The system was set to a voltage of 10.0 kV. Typical currents were approximately 40 mA for titanium and 80 mA for gold. All metals were purchased from the Kurt J. Lesker Company (Clariton, PA). Samples were rotated 1-2 RPM in the chamber to ensure uniform coverage. A crystal monitor with gold 6 MHz piezoelectric crystals (Kurt J. Lesker Co.) were used to monitor metal thickness during evaporation.

Emission current was first allowed to stabilize at 12-13 mA to melt metal sources. Upon stabilization, the current was slowly ramped up 5 mA until the metal began to melt. Once the metal was ready, the shutter was opened and evaporation onto the SPR substrates would begin. The deposition rate onto the samples was controlled by adjusting the emission current and was typically maintained at 0.3-0.5 Å/s. The Inficon XTC/2 deposition controller automatically closed the shutter when the desired final thickness had been reached. The emission current was slowly turned down until it reached 0 mA. Upon completion of each metal evaporation onto a

sample, the chamber was brought back to atmospheric pressure and samples were left inside to cool for 30-60 minutes before removal.

#### **3.2.4. X-ray Photoelectron Spectroscopy Analysis**

XPS analysis performed with a Physical Electronics VersaProbe 5000 XPS (Chanhassen, MN), which was equipped with an EA125 energy analyzer. Photoemission was stimulated by a monochromated Al K $\alpha$  X-ray (1486.6 eV). Nitrogen 1s (N1s) core level scans were scanned from 411-391 eV. Carbon 1s (C1s) core level scans were scanned from 299-279 eV. Electron counts were analyzed every 0.1 eV for high resolution core-level scans. Spectra (C1s, N1s) were acquired for the protein-adsorbed and nano-array samples using a pass energy of 58.7 eV. Peak binding energies were referenced to the Au 4f peak at 84.0 eV.

#### **3.2.5. Gold-thiol Self-assembled Monolayer Fabrication**

Thin films of gold coated microscope slides (XPS analysis) or gold coated microscope cover slides (SPR analysis) were rinsed in distilled water (x3) and ethanol (x3) before being submerged in solutions containing octanethiol (10mM, 5mL total volume) or (11-mercaptoundecyl) tri(ethylene glycol) (10 mM, 5 mL total volume) dissolved in 100% ethanol overnight (16 h). Once complete, gold-SAM films were rinsed with ethanol (x3) and distilled water (x3) and were dried under a gentle stream of nitrogen.

### **3.2.6. Silicon Dioxide-silane Self-assembled Monolayer Fabrication**

Thin films of silicon dioxide (10 nm) on gold coated microscope slides (XPS analysis) or gold coated microscope cover slides (SPR analysis) were rinsed in distilled water (x3) and ethanol (x3) and anhydrous toluene (x3) before being submerged in solutions containing N-octyltrimethoxysilane (6 mM, 5 mL total volume) or 2-[methoxy(polyethyleneoxy)propyl]trimethoxysilane (6 mM, 5 mL total volume) dissolved in anhydrous toluene containing triethylamine (1%, v/v) overnight (16 h). Once complete, silane-SAM films were rinsed with anhydrous toluene (x3), ethanol (x3), and distilled water (x3) and were dried under a gentle stream of nitrogen.

### **3.2.7. SPR Binding Analysis**

SPR substrates chips, with pre-formed self-assembled monolayers, were taped down with double sided tape to SPR substrate holders acquired from a Biacore SIA Au chip kit. Assembled SPR cartridges were loaded into a Biacore X100 SPR (GE Healthcare, Piscataway, NJ) for analysis. SPR experiments were conducted with a continuous flow of (PBS) at 10  $\mu$ L/min. Running buffer was flowed over the sensor surface for a total of 90 sec followed by CYP2C9 in PBS (100 nM, 10  $\mu$ L/min) for 480 sec, and then running buffer for an additional 480 sec.

### **3.2.8. Quantitation of CYP2C9 Surface Coverage**

Quantitation of approximate surface coverage was determined by measuring response values before (90 sec) and after (700 sec) injection of CYP2C9 to determine  $\Delta$ RU. Values were selected at time points before and after injection that would allow sufficient stabilization of the

SPR system. It has been approximated in the literature that a change of one response unit ( $\Delta RU$ ) is equivalent to  $1 \text{ pg/mm}^2$  protein coverage<sup>169</sup>.

### **3.2.9. Adsorbed Enzyme Constructs**

Gold coated microscope slides containing thiol or silane SAMs described above, were treated with CYP2C9 (100 nM) dissolved in KPi (1 mL, total volume) overnight (16 h). Once complete, protein treated SAM surfaces were rinsed in KPi (x3) and distilled water (x3) and were dried under a gentle stream of nitrogen.

### **3.2.10. Preparation of Adsorbed CYP2C9 Constructs for Metabolic Incubation**

Silicon wafers containing 50 nm gold on 5 nm chromium were diced into approximately 4 mm x 6mm chips and were sonicated in acetone for 5 min, rinsed with deionized water, and then soaked in Piranha solution (98% H<sub>2</sub>SO<sub>4</sub>: 30% H<sub>2</sub>O<sub>2</sub>, 3:1, v/v) at room temperature for 30 minutes. Chips were then rinsed with deionized water, ethanol, and then soaked in an (20 mL) ethanolic solution of OT (10 mM), EG3 (10 mM) or a 3:1 ratio of OT to mercaptoundecanoic acid (MUA) (10 mM total thiol concentration) for 18 hours to allow the SAM to form on the gold surface. Excess thiols were removed by subsequent rinsing the chips with pure ethanol, 95% ethanol, water and finally KPi. To bond the CYP2C9 to the OT/MUA SAM chip, the SAM-coated slides were immersed in a solution of EDC/NHS in KPi (10 mL) for a total of 2 h. Chips with SAMs which do not covalently bond CYP2C9 (OT + EG3) were treated with KPi for 2 h instead of the EDC/NHS mixture. To bind CYP2C9, chips were rinsed in KPi and were then treated with CYP2C9 (100 nM) in KPi containing a flurbiprofen and dapson, overnight, to

allow for binding of CYP2C9 to the SAM surface. Finally, Au-SAM-CYP2C9 chips were rinsed in KPi before being stored in cryobuffer at  $-80^{\circ}\text{C}$  prior to use. Incubation procedure used to assess metabolic activity is shown in section 3.2.13.

### **3.2.10. Nano-array Fabrication**

A large-area close-packed polystyrene sphere monolayer template was prepared. Briefly, a silicon substrate ( $> 15 \text{ mm} \times 15 \text{ mm}$ ) with a resistivity of  $> 2000 \Omega \text{ cm}^{-1}$  (p-type,  $111^{\circ} 1^{\circ}$ , undoped) was pretreated in piranha solution ( $\text{H}_2\text{O}_2:\text{H}_2\text{SO}_4$ , 3:7, v/v) for 1 h (Caution: piranha solution reacts violently with organic chemicals). The Si chip was then sonicated in a mixture solution ( $\text{NH}_3:\text{H}_2\text{O}_2:\text{H}_2\text{O}$ , 1:1:5, v/v) for 1 h to obtain a hydrophilic surface. Polystyrene spheres (PS) (500 nm diameter) were purchased from Thermo-Fisher Scientific (Waltham, MA). The 10% (w/v) aqueous solution of PS was diluted by mixing with an equivalent amount of ethanol prior to use. Approximately  $5 \mu\text{l}$  of this PS suspension solution was dispensed onto the pretreated silicon substrate. The sphere covered silicon chip was then slowly immersed into deionized water in a glass Petri dish to release the PS spheres from the Si surface to form a self-assembled close-packed PS monolayer on the water surface. A gold chip that was pretreated in the piranha solution ( $\text{H}_2\text{O}_2:\text{H}_2\text{SO}_4$ , 3:7, v/v) for 10 min was dipped into water and then slowly pulled out of the water surface. As a result, a close-packed PS monolayer was transferred onto the gold substrate from the water surface. To etch the PS monolayer present on the gold surface, a March PX-250 Plasma Asher (Nordson Corporation, Westlake, OH) was utilized, power 50 watt, at 110 mtorr for 5-30 min to reduce the size of the polystyrene spheres. After reducing the PS radius, a thin film of  $\text{SiO}_2$  was deposited by e-beam evaporation as described above. The 10

nm deposition was conducted at 5-10 Å/s. Finally, samples were soaked in an ethanol solution and sonicated for 30 min to remove the PS monolayer.

### **3.2.11. Nano-array Imaging**

Image characterization of the morphology of the nano-array was conducted with a Hitachi S-4700 Field Emission Scanning Electron Microscope (Hitachi High Technologies America, Inc., Pleasanton, CA). Atomic Force Microscope (AFM) images were generated using a Veeco SPM (Veeco, Plainview, NY).

### **3.2.12. Metabolic Incubation of the Nano-array**

Nanohole array chips were immersed in solutions containing Cytochrome P450 Reductase (200 nM, final concentration) and diclofenac (250 µM, final concentration) dissolved in KPi buffer contained in Eppendorf tubes. To initiate the reaction, NADPH (1 mM, final concentration) in KPi was added (final volume 1 mL). The mixtures were incubated in a water bath overnight (16 h) at 37°C. Positive control experiments (1 mL, final volume) were conducted with solution CYP2C9 (2.5 nM, final concentration) containing dilaurophosphatidyl choline (50 µL, 1 mg/mL). Incubations were quenched with glacial acetic acid (250 µL) containing N-phenylanthranilic acid (internal standard) in acetonitrile (250 µL, 5 µg/mL HPLC grade). Once incubations were completed, they were dried down (Savant SC110 Speedvac (Thermo-Fisher, Pittsburgh, PA)). Once dry, samples were reconstituted in (200 µL) sodium acetate buffer (75 mM, pH 5) and acetonitrile (60:40, v/v), and loaded into HPLC vials for analysis.

### **3.2.13. Chromatographic Detection of Diclofenac**

Metabolic reactions were quenched by spiking with acetic acid (50  $\mu$ L, HPLC grade) and N-phenylanthranilic acid (internal standard) in acetonitrile (50  $\mu$ L, 5  $\mu$ g/mL HPLC grade). Incubation mixtures were then centrifuged (13,000 x g) for 10 min to precipitate protein the supernatant (200  $\mu$ L) was removed and loaded into vials for chromatographic analysis. Separation of metabolite and parent compound was conducted using a Waters Alliance 2965 separations module (Milford, MA). Approximately 10  $\mu$ L of analyte was injected on to a Agilent Zorbax SB C-18 (150 mm X 4.6 mm, 5  $\mu$ m particle size (Agilent Technologies, Santa Rosa, CA.)). Substrate and metabolite were eluted at 0.5 ml/min using a mobile phase mixture of sodium acetate (75 mM, pH 5) and acetonitrile (60:40, v/v). Eluted compounds were analyzed on a Waters 2487 Dual Absorbance Detector at 280 nm. Data was processed using the Waters Empower ver. 2.0 software (Waters Corporation, Milford, MA). The peak corresponding to 4'-hydroxydiclofenac was determined by comparison to a 4'-hydroxydiclofenac standard. Approximate retention times for diclofenac, 4'-hydroxydiclofenac and N-phenylanthranilic acid were 23.4 mins, 10.2 mins, and 20.5 mins respectively.

## **3.3. Results**

### **3.3.1. Biocatalysis of Diclofenac by Adsorbed CYP2C9**

The goal here is to selectively immobilize CYP2C9 to a SAM that is, in turn, bonded to a gold surface and, at the same time, prevent “non-specific binding to silicon dioxide. If this is the can be achieved then the CYP2C9 will be solely located in the nano-array well. Our approach was to first demonstrate that binding was dependent on the functional groups of the SMA that are



exposed to the medium. It has been well demonstrated in the literature that hydrophobic proteins tend to strongly bind to alkyl groups but not to PEG terminated SAMs<sup>170,171</sup>. Furthermore, it has been reported that thiols will bond to gold and not silicon (as long as dilute solutions are used). Consequently, the bottom of the nano-array well will bear an alkanethiol SAM and the remainder of the chip, PEG-silane.

SAMs were prepared that were solely composed of octane thiol (OT) or 11-mercaptoundecyl-triethylene glycol (EG3), treated with a solution of CYP2C9 and the resulting chip used in to effect metabolism of diclofenac. The data are shown in Figure 1. The data from three control experiments are shown, CYP2C9 in solution with and without NADPH, and our standard Au-(OT/MUA)-CYP2C9 chip (CYP2C9 bonded to MUA with NHS/EDC<sup>70</sup>). Chips with OT SAMs produced metabolite (4'-hydroxydiclofenac) at about 75% of the level produced in solution or on the Au-(OT/MUA)-CYP2C9 chip while the SAM comprised of EG3 produced metabolite at about 10-15% of this level. Thus, the OT layer appears to adsorb CYP2C9 much more strongly than did the EG3 SAM. Alternatively, both SAMs may bind similar amounts of CYP2C9 but when bound to the EG3 SAM the enzyme activity is less than when bound to the OT SAM.

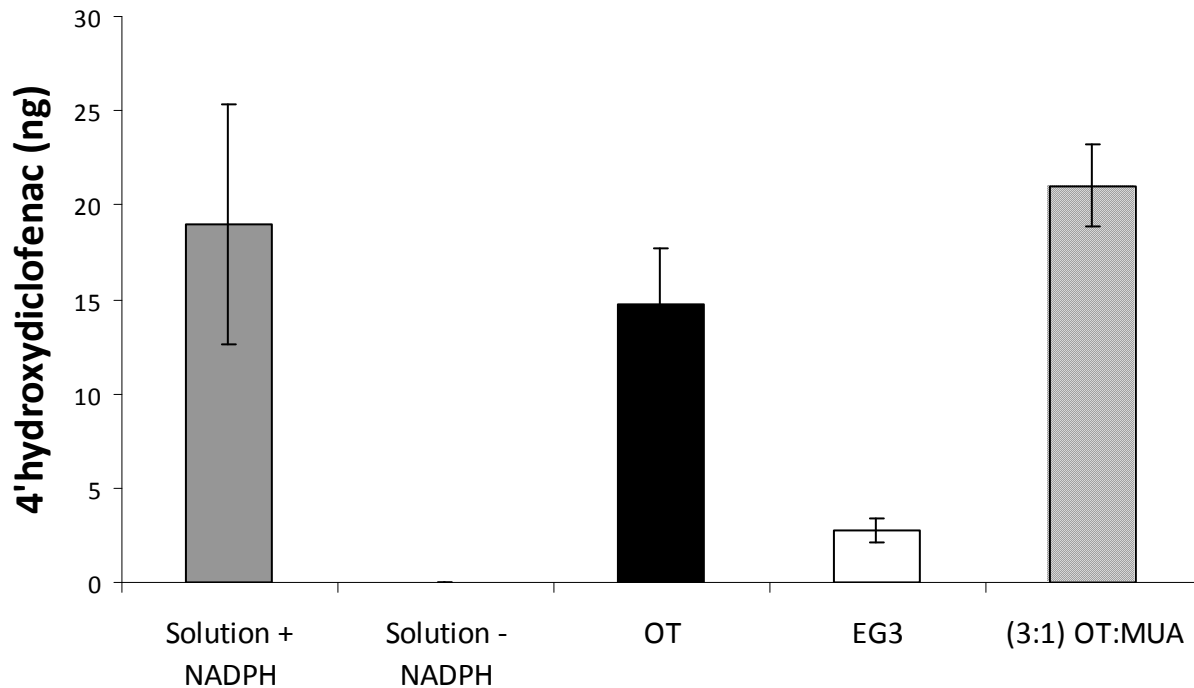


**Figure 3.1.** Effect of SAM composition on metabolic activity of CYP2C9. Solution mixtures contained CYP2C9, CPR, diclofenac and phospholipid. Chip immobilized mixture were comprised of gold chips with the indicated SAM, bound (OT and EG3) or bonded ((3:1) OT:MUA) CYP2C9, diclofenac, CPR and NADPH.

### 3.3.2. SPR Characterization of CYP2C9 Adsorption

In order to explain the trend in the metabolic data presented in Figure 1, an SPR experiment was designed to monitor adsorption of CYP2C9 to model surfaces. The adsorption of CYP2C9 to the OT and EG3 SAMs was monitored in real time by SPR spectroscopy. In Figure 2A is shown the sensorgrams obtained for the adsorption of CYP2C9 to OT (black) or EG3 (gray) SAMs. Figure 2B displays the sensorgrams for CYP2C9 adsorption to silane containing SAMs made of either n-octyltrimethoxysilane (black) or 2-[methoxy(polyethyleneoxy)propyl] trimethoxysilane (gray) For each experiment, sensor surfaces were equilibrated with running

buffer. Then CYP2C9, in running buffer, is injected on to the surface of the sensor (arrow 1), the interaction of CYP2C9 with SAM allowed to occur for approximately 480 seconds, and then returned to running buffer (arrow 2) alone. Each sensorgram trace is an average of three separate injections and each injection measurement was conducted on a freshly made SPR sensor film.

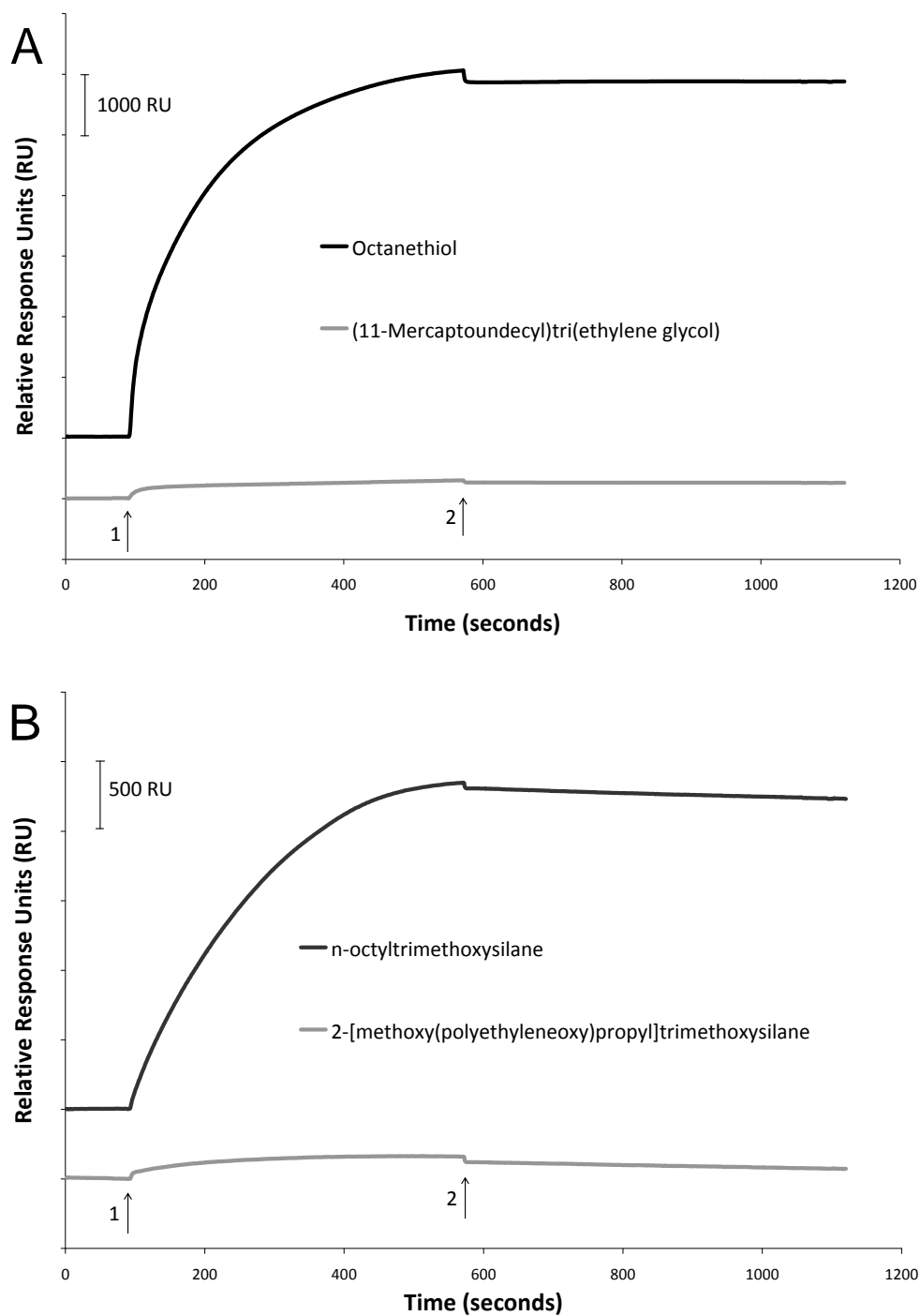


**Figure 3.2.** SPR sensorgram comparing interaction of CYP2C9 with self-assembled monolayers produced from A. Gold-thiol self-assembled monolayers (octanethiol) (black) and (11-Mercaptoundecyl)tri(ethylene glycol) (gray) and B. Silane-silicon dioxide self-assembled monolayers (n-octyltrimethoxysilane (black) and 2-[methoxy(polyethyleneoxy)propyl]trimethoxy silane (gray)). Each sensorgram trace represents an average of 3 separate experiments.

The change in response ( $\Delta$ RU) is determined by subtraction of the response value taken before protein injection ( $t = 90$  sec), from the response observed at the end of the run ( $t=700$  sec) after protein injection had ceased. Previous studies conducted with radioactive proteins<sup>172</sup> suggest that a change in response ( $\Delta$ RU) of 1 RU correspond to a coverage of protein equivalent to  $1 \text{ pg/mm}^2$ . Values of  $\Delta$ RU and the corresponding protein coverage obtained from the sensorgrams in Figures 2A and B are compiled in Table 1.

**Table 3.1.** Observed  $\Delta$ RU and Calculated Protein Coverage on Various SAMs<sup>a</sup>

Self-assembled Monolayer	$\Delta$ RU	Protein Coverage ( $\text{ng/mm}^2$ ) <sup>b</sup>
Octanethiol (OT)	$5853 \pm 150$	$5.853 \pm 0.15$
(11-Mercaptoundecyl)tri(ethylene glycol) (EG3)	$260 \pm 230$	$0.260 \pm 0.23$
N-Octyltrimethoxysilane	$2287 \pm 480$	$2.287 \pm 0.48$
2-[Methoxy(polyethyleneoxy)propyl] trimethoxysilane	$109 \pm 100$	$0.109 \pm 0.10$

Values calculating the difference between the baseline response during buffer washes over the sensor surface both before (90 s) and after (700 s) the injection of CYP2C9 injection.<sup>b</sup> A change in response ( $\Delta$ RU) of 1 RU corresponds to a protein coverage of approximately  $1 \text{ pg/mm}^2$ .

### 3.3.3. XPS Characterization of CYP2C9 Adsorption

We also determined protein adsorption to a variety of self-assembled monolayers using XPS. XPS provides information concerning the bond types, and, therefore, the identity of the atoms that are present on a surface. Since amide bonds are unique to bound protein (i.e., not otherwise present in the SAM or supporting substrate), N1s core spectra, which corresponds to

binding energies in the range of 412 to 392 eV, were measured to determine if protein was present on the SAMs. Minor contributions to the N1s spectra are expected, arising from the guanidium group of arginine, primary amine groups on lysine, proline, glutamine, and asparagine, secondary amine groups of tryptophan and histidine. Information regarding the peak binding energy of various N-containing bonds is shown in Table 2. Electron counts were taken approximately every 0.1 eV and each spectrum represents the summation of 15 successive scans. XPS spectra of CYP2C9 treated OT (black) or EG3 (gray) SAMs on gold are shown in Figure 3A. CYP2C9 adsorption to silane self-assembled monolayers made from either n-octyltrimethoxysilane (black) or 2-[methoxy(polyethyleneoxy)propyl] trimethoxysilane (gray) are shown in Figure 3B.

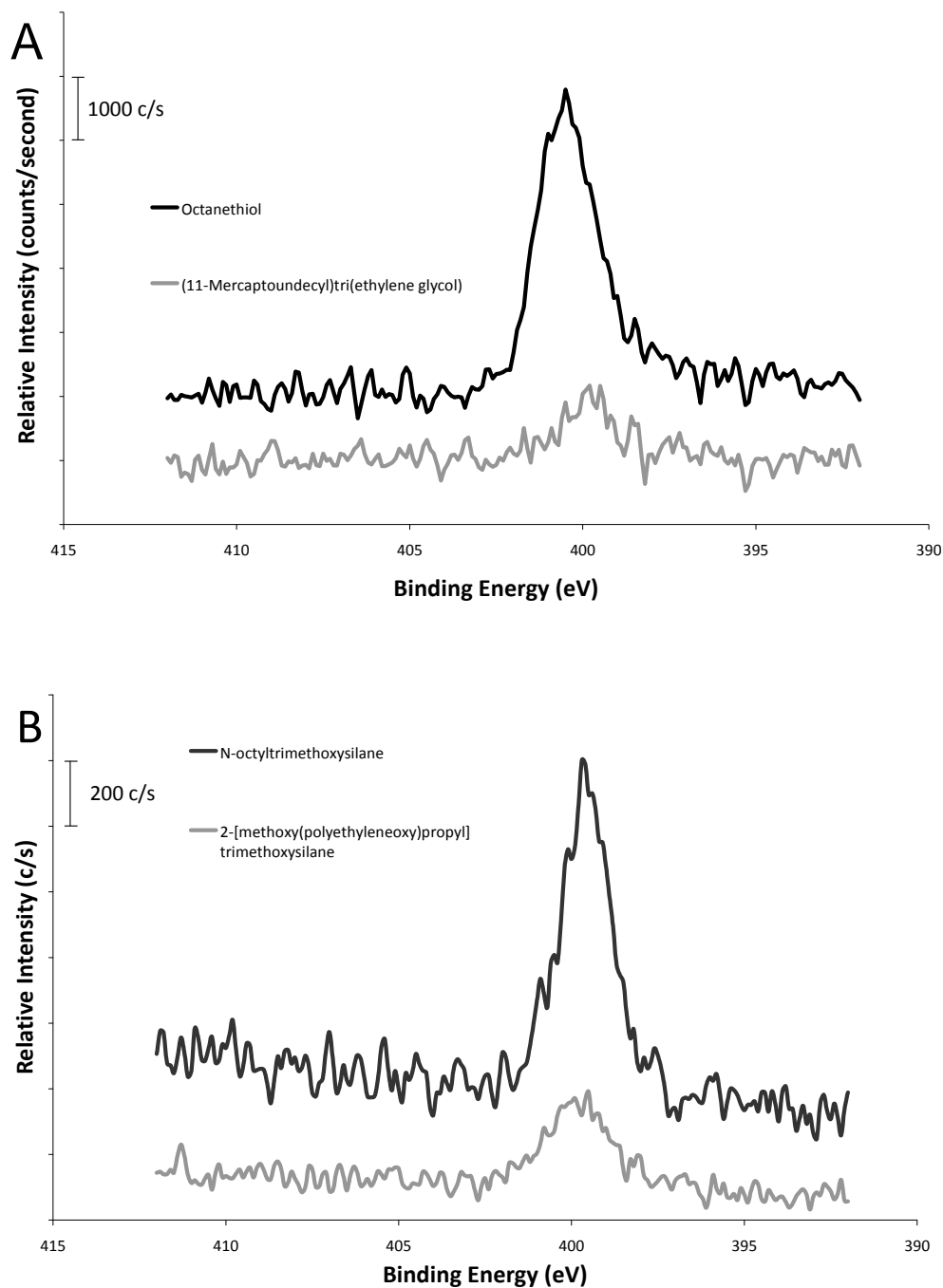


**Figure 3.3.** X-ray photoelectron spectra comparing N1s core level scans of CYP2C9 adsorbed to self-assembled monolayers comprised of A) octanethiol (black) and (11-Mercaptoundecyl)tri(ethylene glycol) (gray) on gold and B) N-octyltrimethoxysilane (black) and 2-methoxy(polyethyleneoxy)propyl] trimethoxysilane (gray) on silicon dioxide. Each spectrum is the sum of 15 scans.

**Table 3.2.** XPS Bond energies (N1s)

<b>Chemical Bond</b>	<b>Peak energy (eV)</b>
<b>N-C</b>	<b>399.5</b>
<b>N-H</b>	<b>399.8</b>
<b>N-C(O)</b>	<b>399.6</b>
<b>N=C</b>	<b>398.9</b>

Approximate energy of N1s electrons as a function of bonding environment. All values were obtained from an online XPS database<sup>173</sup>

#### **3.3.4. AFM Imaging of Nano-array**

AFM images of the nano-array surface before SAM functionalization are shown in Figure 4. The diameter, as determined by AFM, of each of the nanowells comprising the array is approximately 100 nm. The periodicity of nanowells is approximately 500 nm. Areas which appear lighter in color are regions which are coated in silicon dioxide. Darker regions represent the nano-hole and contain exposed gold at the bottom of the well structure.



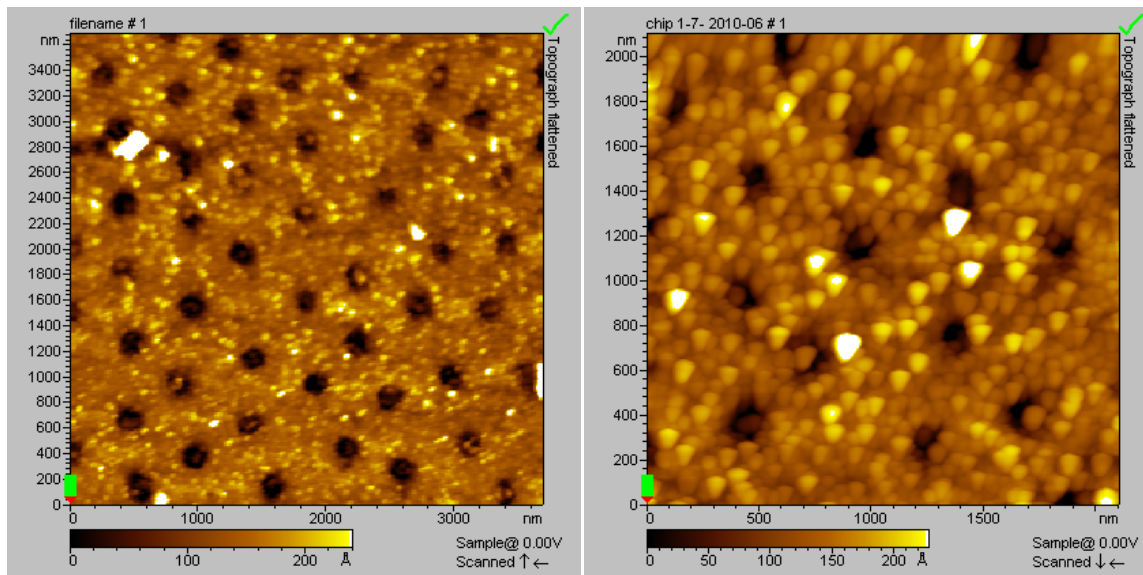


**Figure 3.4.** Atomic force images of the nanowell array structure.

### 3.3.5. SEM Imaging of Nano-array

The SEM image of the nanohole surface is shown in Figure 5. The use of low magnification (Figure 5A) of the sample area demonstrates the regularity of the pattern over a large area. At higher magnification of the sample (Figure 5B) provides confirmatory evidence of the dimensions of the nanowell (diameter 100 nm) and periodicity between (500 nm).

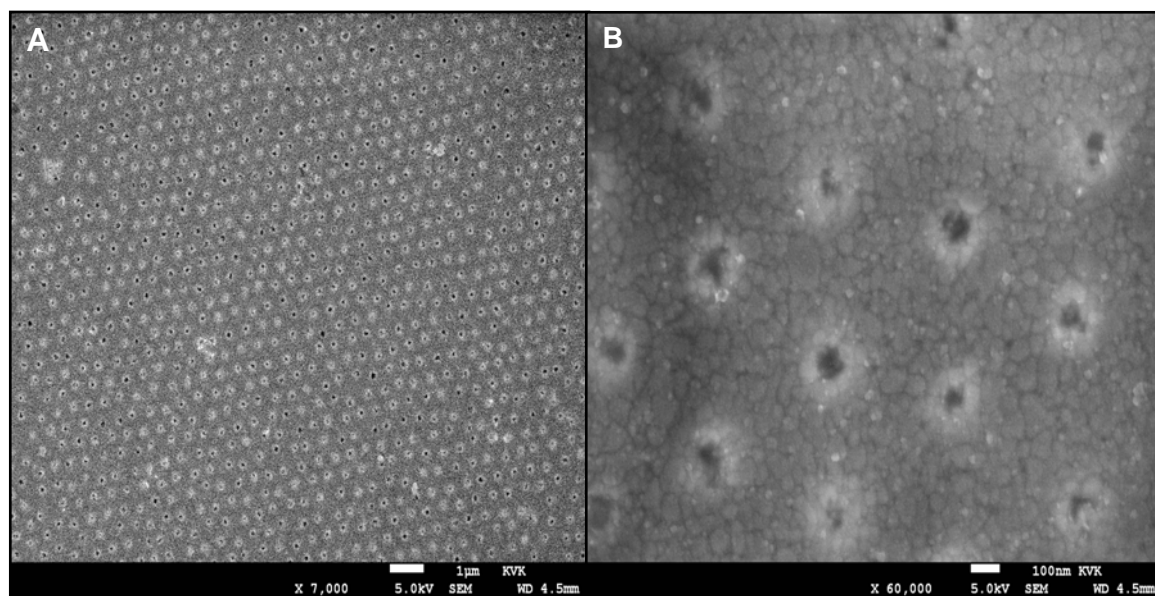


**Figure 3.5.** (A) Low magnification scanning electron micrograph (SEM) of the nanowell array. (B) High magnification SEM image of the nanowell array.

### 3.3.6. XPS Characterization of Nano-array Fabrication

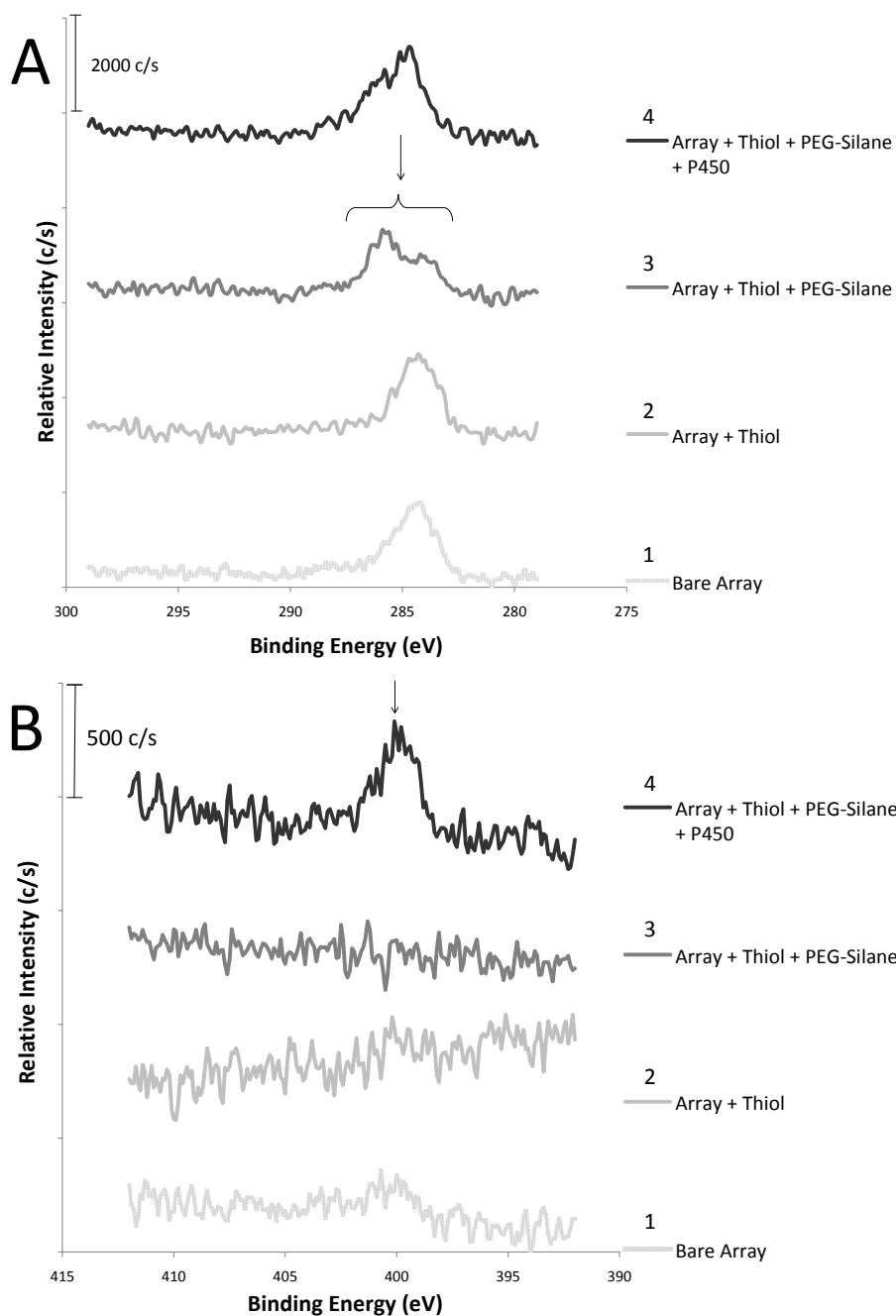
The nanowell array was examined by XPS at each step of the fabrication process. Spectra for the bare array (1), with the OT self-assembled monolayer (2), with the octanethiol and 2-[methoxy(polyethyleneoxy)propyl]trimethoxysilane self-assembled monolayers (3) and finally the completed nanowell array with both the octanethiol and 2-[methoxy(polyethyleneoxy)propyl]trimethoxysilane self-assembled monolayers and adsorbed CYP2C9 (4) are shown in Figure 6. Here, we measured both the C1s (Figure 6A) and N1s (Figure 6B) core-level spectra of the nanowell array. Spectrum 3 in Figure 6A, exhibits a characteristic double peak indicated by an arrow, suggesting the presence of a C-O bond, which implies that a SAM consisting of 2-[methoxy(polyethyleneoxy)propyl]trimethoxysilane has formed on the nano-array surface. For reference, information regarding the peak binding energies of various C-containing bonds, including C-O, is shown in Table 3.3. Spectrum 4 in

Figure 6B, suggests the presence of nitrogen on the surface, highlighted by the arrow, supporting the claim that CYP2C9 is adsorbed to the nano-array surface. See Table 3.2 for information on peak energies of N-containing bonds.

**Table 3.3. XPS Peak Bond Energies (C1s)**

<b>Chemical Bond</b>	<b>Peak energy (eV)</b>
<b>C-C</b>	<b>284.6</b>
<b>C-O</b>	<b>286.5</b>
<b>C-H</b>	<b>284.6</b>
<b>C=O</b>	<b>286.8</b>
<b>C(O)-N</b>	<b>288.2</b>
<b>C-N</b>	<b>285.7</b>
<b>C-S</b>	<b>286.8</b>

Approximate energy of C1s electrons as a function of bonding environment. All values were obtained from an online XPS database<sup>173</sup>



**Figure 3.6.** XPS spectra of the A) C1s core level spectra and B) N1s core level spectra obtained during fabrication of the nanowell chip bearing OT and 2-[methoxy(polyethyleneoxy)propyl]trimethoxysilane and CYP2C9. Successive spectra (from bottom) in each panel are of the step-by-step fabrication of the nanowell array and are 1) the bare

array, 2) (1) + OT SAM, 3) (2) + 2-[methoxy(polyethyleneoxy)propyl]-trimethoxysilane, 4) (3) + CYP2C9.

### 3.3.7. Metabolic Activity of the Completed Nano-array.

After the adsorption of CYP2C9 to the nano-array, we evaluated the metabolic activity of the CYP2C9 bearing array probing for the biotransformation of diclofenac into its primary CYP2C9-mediated metabolite, 4'hydroxydiclofenac. Nano-array incubations contained NADPH (1 mM, final concentration) as an electron donor, CYP2C9, CPR, and diclofenac. The solution control was similarly constituted but also contained phospholipid. Negative control experiments omitted NADPH. Results are shown in Table 2.

**Table 2.4. CYP2C9-Nanowell Metabolite Production from Diclofenac.<sup>a</sup>**

<b>Experiment Conditions</b>	<b>4'hydroxydiclofenac (ng/mL)</b>
Solution CYP2C9 (+NADPH)	12.56 ± 0.56
Solution CYP2C9 (-NADPH)	ND
Nanowell CYP2C9 (+NADPH)	7.41 ± 0.32
Nanowell CYP2C9 (-NADPH)	ND

Incubation conditions: Solution incubations contained CYP2C9 (0.5 pmol), CPR (10 pmol), phospholipid (1 mg/ml) and diclofenac (250 μM). Positive controls also contained NADPH (1 mM). Nanowell incubations contained CYP2C9 adsorbed Nano-array, CPR (10 pmol), diclofenac (250 μM). Metabolite formation determined by HPLC.

### 3.4. Discussion

Cytochrome P450 enzymes are well known to form aggregates in solution. It is thought that aggregation can have a profound effect on the catalytic activity of the enzyme. In order to unequivocally control the state of aggregation of a P450 enzyme, several different approaches have been taken including truncation of N-terminal domains believed to be involved in aggregation, mutation of key residues thought to be involved in aggregation, the use of detergents, binding to Nanodiscs<sup>®</sup>, and immobilization of the protein to a solid surface. Of the above listed approaches to inhibit the aggregation of these proteins, only binding to Nanodiscs<sup>®</sup> or immobilization to a solid substrate provides a reasonable means to maintain the protein in a non-aggregated state without modifying the incubation conditions (e.g., addition of detergent) or modification of the protein (e.g., N-terminal truncation, FG loop or F helix residue mutation, etc). Further, only immobilization to a solid substrate will permit the selective creation of more complex structures (e.g., homo- or hetero-dimers, trimers, etc.). As a result we have proposed a nanostructure device and have been developing it that is designed to unequivocally control the state of aggregation of P450 enzymes by providing a surface to which P450 enzymes bind, or bond, in an area with well defined surface topology.

A key feature of nanowell arrays is the bottom of the nanowell is gold while the surrounding material is silicon dioxide, permitting the selective formation of OT SAMs on the floor of the nanowell surrounded by a thin layer (10 nm) silicon dioxide bearing a 2-[methoxy(polyethyleneoxy)propyl]trimethoxysilane SAM. By doing this the nanowell surfaces have been selectively functionalized. The hydrophobic nature of OT presents a SAM for P450

binding while the polyethylene glycol bearing silane is resistant to protein adsorption and will thus promote the adsorption of a P450 of interest in the nanowell.

Cross-reactivity of silane to gold as well as thiol to silicon dioxide is a potential issue, making the step wise fabrication of the device occur in a specific order (thiol first, silane second). Literature sources have suggested that formation of silane based SAMs on gold do in fact occur<sup>174</sup>. As a result, the OT containing SAM was first formed on gold by treating with OT first. This will block the silane from forming a self-assembled monolayer on gold. Thiols have shown the ability to form self-assembled monolayers on oxide surfaces<sup>175</sup>, however, it has been demonstrated that thiol-based self-assembled monolayers form on oxide surfaces only when thiol solutions are neat, or by chemical vapor deposition. This evidence suggests that our thiol should not interact (i.e., form a SAM) with the silicon dioxide surface.

The fabrication of a nanostructure device on a large scale (1 cm x 1 cm) is a potentially difficult task to accomplish. With this in mind, we designed the nanostructure array to be reusable, utilizing the strong association of the CYP2C9 to the surface, but also a strong detergent will dissociate the CYP2C9 from the surface and permit the CYP2C9 to be washed away from the surface. In turn, this should make the nanostructure device reusable. This will be especially useful, as the complexity of device fabrication increases as the dimensions of the nano-well decrease.

In order to verify the activity of the CYP2C9 that was adsorbed to a surface, a study was conducted where CYP2C9 was adsorbed to a surface using both OT and EG3 thiol-based SAMs. These chips were created and transferred to a reaction incubation after allowing for CYP2C9 to adsorb, in the presence of flurbiprofen and dapson, to the surface of interest. The adsorbed

constructs were compared to a well described immobilized P450 enzyme construct and demonstrate statistically similar levels of metabolite formation. Furthermore, the data shown in Figure 1 indicates that greater activity is seen in gold chips bearing OT SAMs as opposed to EG3 based SAMs. This result can be explained by two potential hypotheses, either 1) PEG-thiol based SAMs have significantly less CYP2C9 bound to the surface than their OT counterparts, providing less enzyme for metabolic transformation or 2) PEG-based SAM's interact with CYP2C9 in, for an example, a denaturing manner to reduce the metabolic activity of the adsorbed CYP2C9. Under the premise that the first hypothesis is correct, it is reasonable that very little CYP2C9 adsorption to PEG monolayers may occur, and that most of the CYP2C9 adsorbs to the exposed silicon dioxide wafer on the back of the chip<sup>176</sup>, explaining the minimal activity seen with EG3 thiol-based SAM's.

SPR was used to resolve the question of whether or not CYP2C9 was being adsorbed to SAMs of OT and EG3 on gold as well as 2-[methoxy(polyethyleneoxy)propyl]trimethoxysilane and N-octyltrimethoxy silane on silicon dioxide. SPR spectra for these experiments are shown in Figure 2A for SAMs formed on gold, and Figure 2B for SAMs formed on silicon dioxide. Here, SPR spectra demonstrate, in real time, that CYP2C9 is non-specifically adsorbing to OT based self-assembled monolayers on gold as well as N-octyltrimethoxysilane based self-assembled monolayers formed on silicon dioxide-covered gold SPR films. Interestingly, in triplicate experiments comparing the relative response between the two hydrophobic SAM's, thiol based SAMs demonstrate a two-fold greater response when compared to silane based SAMs. Differences in response seen between gold-thiol and silicon dioxide-silane SAMs may be attributed to the fact that gold-thiol SAMs typically form well ordered films on the gold surface.



In contrast, silane based self-assembled monolayers often exhibit decreased order in formation, either through insufficient packing<sup>91</sup> or through self polymerization<sup>177</sup> of silane components. It is hypothesized that differences in observed SPR response regarding the adsorption of CYP2C9 to SAMs of OT or N-octyltrimethoxy silane may be attributed to differences in the formation of SAMs on two chemically different materials, gold and silicon dioxide.

SPR experiments were also designed to observe an *in situ* interaction of CYP2C9 on hydrophobic thiol- and silane-based SAMs, SPR films were also functionalized with PEG based SAMs (EG3 and 2-[methoxy(polyethyleneoxy)propyl]trimethoxysilane) and subsequently their interaction with CYP2C9 are shown in Figure 2A and Figure 2B and the sensorgrams indicate that the binding of CYP2C9 to PEG-based SAMs is significantly less, roughly 20-fold, than the analogous binding to the hydrocarbon (OT and N-octyltrimethoxy silane) based SAMs. The small response observed for CYP2C9 exposure to PEG-based SAMs is likely due to imperfections in the SAM structure, or bare areas which may allow adsorption of CYP2C9.

In addition to looking at an *in situ* interaction of CYP2C9 to a SAM, we can also measure protein coverage by monitoring SPR response. Studies conducted with radioactive-labeled proteins established that a change in response equal to 1 RU is approximately equal to a 1 pg/mm<sup>2</sup> coverage of protein<sup>172</sup>. From this, we can measure the amount of CYP2C9 adsorbed to either gold-thiol or silane-silicon dioxide SAMs by monitoring the difference in response before and after protein injection, as determined from the SPR data (see Table 3.2). We observed coverage levels for hydrophobic SAMs composed of OT ( $5.853 \pm 0.15$  ng/mm<sup>2</sup>) or N-octyltrimethoxy silane ( $2.287 \pm 0.48$  ng/mm<sup>2</sup>). In contrast PEG SAMs made from EG3 ( $0.260 \pm 0.23$  ng/mm<sup>2</sup>) or 2-[methoxy(polyethyleneoxy)propyl]trimethoxysilane ( $0.109 \pm 0.10$  ng/mm<sup>2</sup>)

solutions exhibit significantly lower coverage, supporting the idea the CYP2C9 will bind to the well, avoiding the areas of silicon dioxide in between each gold well.

SPR experiments are useful to demonstrate protein adsorption to surfaces, however, SPR experiments are run over a short time (540 sec) of protein exposure. As a result, the experiment designed here may provide a poor model for chip-preparation, which typically expose the surface to CYP2C9 overnight (16 h). To counter this, several model surfaces were incubated and functionalized with the same SAMs in the SPR experiment (see Figure 2). These samples were analyzed with XPS, and the respective spectra are shown in Figure 3 (A and B). The XPS spectra suggest that binding of CYP2C9 to surfaces with OT and N-octyltrimethoxysilane exhibit high levels of protein adsorption based on peak intensity as compared to either EG3 or 2-[methoxy(polyethyleneoxy)propyl]trimethoxysilane SAMs. The results suggest that SPR data is reflective of CYP2C9 binding under long-term immersion. Furthermore, data indicates that CYP2C9 will likely have a preference for the hydrophobic SAM present in the bottom of the nanostructure array and will selectively bind in the nanowell..

XPS measurements at each step of the fabrication of the array proved to be extremely useful to monitor the changing characteristics of the array surface. The data shown in Figure 6A shows changes in peak shape corresponding to alterations in C1s core electron energies as a function of bonding environment. Figure 6A spectrum (1) is an XPS spectrum of the bare array. The peak present in this spectrum is likely due to atmospheric hydrocarbons non-specifically adsorbed to the surface. Next in Figure 6A spectrum (2), we see the addition of OT SAM to the array surface. Interestingly, Figure 6A spectrum (3) displays a characteristic “double peak” after the application of PEG silane self-assembled monolayers<sup>178</sup>. Values of binding energy

associated to C1s bonds can be observed in Table 3.3. The peak values for C-C and C-H, both 284.6 eV differ from the peak energy from C-O bonds (286.5) and give rise to the double peak characteristic seen in Figure 6A spectrum (3). This data indicates that the silane self-assembled monolayer containing 2-[methoxy(polyethyleneoxy)propyl]trimethoxysilane has formed on the device. Furthermore, the XPS data, after the addition of protein in spectrum 4, suggests CYP2C9 is adsorbed to the surface. This result is by the data shown in confirmed in Figure 4. XPS spectra of N1s core level electrons is shown in Figure 6B and spectrum (4) indicates that after the treatment of the device with CYP2C9 enzyme is bound to the surface.

After fabrication of the array surface and immersion in CYP2C9, the nano-array was immersed in an incubation containing CPR and NADPH to probe for metabolic activity. Data regarding the metabolic activity of the completed array was compiled and shown in Table 3.4. Samples containing the completed nanoarray with NADPH indicate that CYP2C9 remains active when bound to the array surface. In contrast, when NADPH is absent from the incubation mixture, no metabolite (4'-hydroxydiclofenac) was detected. This data suggests that CYP2C9 immobilized on the array surface in the presence of natural co-factors and co-enzymes remains metabolically active. Moreover, when compared to data obtained from solution incubations containing dilaurophosphatidyl choline, array incubations generate metabolites with identical retention times, indicating that the metabolite formed is likely 4'-hydroxydiclofenac.

The amount of CYP2C9 bound to the nano-array can be roughly predicted by making a few assumptions regarding the array. If the diameter of CYP2C9 is approximately 7 nm in diameter, then the number of congruent circles (CYP2C9) which can fit inside a larger 100 nm circle (nano-array well) has been probed with computer programs<sup>179</sup>. These programs predict the

ideal packing of a perfectly circular CYP2C9 in a 100 nm nano-array well results in 231 enzymes present in a single well. Perfect packing of the congruent CYP2C9 is likely not occurring. If this were the case, little room would be available in the nano-array well to allow for CPR binding. As a result, we can approximate the number of enzymes in a single well to correspond to the median value of enzymes (115 enzymes) that may be found in a well. Assuming that the distribution of enzymes in wells across the surface is uniform, the median number of enzymes present in a well corresponds to an average value of enzymes present in a well. With that assumption, we can predict the amount of 100 nm nano-array wells, with 500 nm periodicity, in a 1 cm by 1 cm square to be  $4 \times 10^8$  wells. Assuming 200 enzymes are in each well, the total amount of enzyme present on the surface is  $4.6 \times 10^{10}$  enzymes, around 75 femtomoles. Typical pharmaceutical incubations utilize anywhere from 1 to 10 picomoles of enzyme, approximately 10- to 100-fold more enzyme than is present on the device. As a result, metabolic incubations utilizing the nanostructure array will likely need to employ high-turnover substrates or ultra-sensitive detection methods to evaluate metabolic activity.

In summary, here we have shown the interaction of CYP2C9 with a variety of SAMs. The information presented here suggests that CYP2C9 should be localizing to areas of hydrophobic SAM at the bottom of the nano-well structure. In turn, we aim to fabricate this device with further reduced the dimensions of the nano-array elements, so that it is only capable, unequivocally, of binding a single P450 enzyme per well with space for CPR. In turn, we would like to make use of this device to make predictions regarding *in-vivo* metabolism of drugs, using this improved *in-vitro* model. Ultimately this device may be very useful in early drug

development and may help to answer mechanistic discrepancies between actual *in-vivo* drug metabolism and traditional *in-vitro* solution experiments

## **Chapter 4**

# **Gold-Immobilized CYP2C9 as a Platform to Characterize Protein- Protein Interactions Occuring in P450 Enzymes**

#### 4.1. Introduction

Cytochrome P450 (P450) enzymes are a family of oxoferroreductase enzymes containing a heme moiety and are well known to be involved in the metabolism of a wide variety of endogenous and xenobiotic materials. It is estimated that roughly 75% of all pharmaceutical compounds are metabolized by these enzymes and of these, approximately 90% are processed by five of the major human isoforms including CYP3A4, CYP2C9, CYP2C19, CYP2D6 and CYP1A2.<sup>39,180</sup>

P450 enzymes are expressed in all tissues, but have particularly high expression in hepatic tissues, where most of the oxidative drug metabolism is thought to be carried out. To form a functional complex, cytochrome P450 enzymes combine with cytochrome P450 reductase (CPR) to transfer electrons from NADPH to the heme-center of the P450 enzyme<sup>77,181</sup>, where drugs are then oxidized. Cytochrome P450 reductase interacts with the cytochrome P450 in a 1:1 stoichiometry to generate metabolite, however it has been described in the literature that ratios of P450 to CPR in hepatocytes are around 10:1 to 20:1<sup>182</sup>. As a result, interaction between P450 enzymes may be occurring to facilitate sub-optimal concentrations of CPR in hepatocytes.

Protein-protein interactions between different P450 enzymes in hepatocytes has been demonstrated to occur *in-vivo*<sup>183</sup>. In order to provide some insight into interactions which may be occurring between specific P450 isoforms, several groups have used recombinant expressed enzyme incubations to probe for catalytic alterations exacerbated by the presence of a second P450 isoform. Specific instances of protein-protein interactions between P450 enzymes include interactions between CYP2C9 and CYP2C19 in the oxidation of methoxychlor<sup>79</sup>, CYP2C9 and CYP2D6 in the oxidation of both flurbiprofen and dextromethorphan<sup>81</sup>, CYP2C9 and CYP3A4

in the metabolism of testosterone and naproxen<sup>184</sup>, and CYP2B4 and CYP1A2 in oxidation of 7-pentoxoresorufin<sup>185</sup>.

Reconstituted incubations containing recombinantly prepared P450 enzymes are advantageous in that concentrations of individual enzymes present in an incubation can be easily controlled. Furthermore, with the advent of recombinant DNA technology, interactions between virtually any combinations of P450s can be studied. However, reconstituted P450 enzymes are prone to aggregation, which has been shown to affect the catalytic activity of P450 enzyme<sup>65</sup>. Furthermore, it is conceivable that protein-protein interactions observed using reconstituted solution incubations may be an artifact of the system. In short, alterations in catalytic activity occur as a result of the mixed enzyme aggregates that form in model systems which may exhibit different catalytic activities than would be observed by monomeric proteins interacting alone.

Ideally, it would be useful to selectively control the aggregation state of a P450 enzyme and monitor their interaction with other P450 enzymes. Several attempts have been made to reduce aggregation of P450 enzymes, including mutation of key residues involved in P450 aggregation<sup>63</sup>, truncation of N-terminal domains<sup>60,61</sup>, the use of detergents designed to keep P450 enzymes in monomeric form<sup>65</sup>, formation of discoidal lipid nanostructures referred to as Nanodiscs®<sup>68</sup> which limit the area of membrane to dimensions which can only bind a single enzyme, and finally immobilization of the protein to a solid surface<sup>70</sup>. With the exception of Nanodiscs® and immobilization to solid surfaces, the techniques used to control aggregation either change the incubation conditions or mutate the enzyme, and the resulting data may be a poor reflection of *in-vivo* conditions and activity.



Current techniques for characterizing protein-protein interactions include monitoring changes in catalytic activity<sup>79,81,184,185</sup>, Förster resonance energy transfer (FRET)<sup>186</sup>, isothermal titration calorimetry<sup>187</sup>, circular dichroism<sup>188</sup> and surface plasmon resonance (SPR)<sup>189</sup>. FRET and other related techniques carry the disadvantage of requiring protein modifications (e.g., attachment of a fluorescent tag), which may affect protein-protein interactions. Other techniques such as circular dichroism and isothermal titration calorimetry often require large volumes of highly concentrated samples to properly establish biophysical constants of protein-protein interaction. On the other hand, SPR based experiments that monitor protein-protein interactions have the advantage of requiring small amounts of sample. Additionally, P450 enzymes have similar refractive indices associated with them, thus samples are already “tagged” in their native form. Moreover, the change in response in SPR experiments is linearly proportional to the amount of protein (change in refractive index) at the surface, providing what equates to an extremely sensitive mass sensor.

Typically, SPR experiments are conducted on a carboxymethyl-dextran gel which is grafted on to a thin film of gold, necessary for the SPR experiment<sup>190</sup>. The carboxymethyl-dextran gel contains free carboxylic acid groups which will allow for the surface to be bonded with proteins and/or enzymes once activated with N-hydroxysulfosuccinimide (NHS) and N-(3-Dimethylaminopropyl)-N'-ethyl-carbodiimide hydrochloride (EDC). Unfortunately, the physical nature of the carbohydrate on the surface, which makes it difficult to image with AFM, which is used as a secondary measure of the protein aggregation state. However, gold with self-assembled monolayers (SAMs) can be used in SPR, permitting the direct transfer of the methods

we have described in the literature<sup>70</sup>, where the formation of monomeric P450 enzymes has been shown.

Here we describe the interaction of solution CYP2D6 with an OT/MUA immobilized CYP2C9. Using SPR, both on ( $k_a$ ) and off rates ( $k_d$ ) for solution CYP2D6 to immobilized, monomeric CYP2C9 are determined and thereby  $K_D$  ( $k_d/k_a$ ). Additionally we demonstrate that the presence of CYP2D6 has little effect on the metabolism of flurbiprofen by immobilized CYP2C9. This is in contrast with solution data that has been published, which suggests that the addition of CYP2D6 to incubations of flurbiprofen and CYP2C9 causes an inhibitory effect. We hypothesize that the differences observed are a result of the decreased state of aggregation of the Au-OT/MUA immobilized CYP2C9 versus solution incubations. In turn, the work presented here could be useful in describing protein-protein interactions between cytochrome P450 enzymes and may help make better predictions of *in-vivo* drug metabolism based on improved *in-vitro* models.

## **4.2. Materials and Methods**

### **4.2.1 General**

Unless otherwise noted, chemicals were purchased from Sigma-Aldrich. Inorganic phosphate buffer (KPi) was made by mixing 40mM solutions of both dibasic and monobasic potassium phosphate until the solution of mixed components had a measured pH of 7.4. Mixtures of EDC and NHS used for enzyme immobilization consist of 3 mM EDC and 5 mM NHS in KPi for chip-based incubations. SPR experiments utilize 0.4 M EDC and 0.1 M NHS in KPi. In both instances, solutions were combined in a 1:1 ratio (v/v) and applied to surfaces of interest. Running buffer for SPR experiments contains 4-(2-hydroxyethyl)-1-piperazineethanesulfonic

acid (HEPES) (10 mM), sodium chloride (154 mM), sodium ethylenediaminetetraacetic acid (EDTA) (3 mM), and TWEEN 20 (0.05%) and is referred to as HBS+EP. The solution of flurbiprofen and dapsone, used during CYP2C9 immobilization, was 40  $\mu$ M of each compound dissolved in KPi in a 1:1 ratio. Cryobuffer solution consists of 80:20 KPi to glycerol (v/v).

#### **4.2.2. Materials**

Flurbiprofen, NHS, EDC, Nicotinamide adenine dinucleotide phosphate reduced form (NADPH),  $\beta$ -mercaptoethanol, 8-octanethiol (OT), and 11-mercaptopundecanoic acid (MUA) were purchased from Sigma Aldrich (Milwaukee, WI). Cytochrome P450 reductase was purchased from BD Biosciences (Franklin Lakes, NJ). Purified CYP2C9, CYP2D6, 4'-hydroxyflurbiprofen, 2-fluoro-4-biphenyl acetic acid and dapsone were provided by Dr. Tim Tracy (Lexington, KY).

#### **4.2.3. SPR Substrate Fabrication**

Microscope cover slides (40 mm x 24 mm, No. 2) (VWR, Radnor PA) were cut into 12 mm x 10 mm rectangles (SPR experiment) or 3" silicon wafers (metabolic experiment) (University Wafer, South Boston, MA) and were loaded into a Temescal BJD-2000 (Edwards Vacuum, Phoenix, AZ) system with an Inficon XTC/2 deposition controller (Inficon, East Syracuse, NY) for metal evaporation. The chamber was pumped down to a pressure  $\leq 1.0 \times 10^{-5}$  Torr. The system was set to a voltage of 10.0 kV. Typical currents were approximately 40 mA for titanium and 80 mA for gold. All metals were purchased from the Kurt J. Lesker Company (Clariton, PA). Samples were rotated at 1-2 rpm in the chamber to ensure uniform coverage. A

crystal monitor with gold 6 MHz piezoelectric crystals (Kurt J. Lesker Co.) were used to monitor metal thickness during evaporation.

The emission current was first allowed to stabilize at 12-13 mA to melt metal sources. Upon stabilization, the current was slowly ramped up an additional 5 mA until the metal began to melt. Once the metal was molten, the shutter was opened and evaporation onto the SPR substrates began. The deposition rate onto the samples was controlled by adjusting the emission current and was typically maintained at 0.3-0.5 Å/s. The Inficon XTC/2 deposition controller automatically closed the shutter when the desired final thickness had been reached. The emission current was slowly turned down until it reached 0 mA. Upon completion of each metal evaporation onto a sample, the chamber was brought back to atmospheric pressure and samples were left inside to cool for 30-60 minutes before removal.

#### **4.2.4. Gold-thiol self-assembled monolayer fabrication (SPR)**

Thin films of gold coated microscope cover slides (SPR analysis) were rinsed with distilled water (x3) and ethanol (x3) before being submerged in a solution (12 mL total) of octanethiol (10mM, 9mL total volume) and 11-mercaptoundecanoic acid (10 mM, 3 mL total volume) (3:1) dissolved in 100% ethanol overnight (16 h). The gold-SAM films were then rinsed with ethanol (x3) and distilled water (x3) and then dried under a gentle stream of nitrogen.

#### **4.2.5. SPR Immobilization**

SPR sensor substrates, with pre-formed self-assembled monolayers, were taped down to SPR substrate holders acquired from a Biacore SIA Au chip kit using double-sided tape.

Assembled SPR cartridges were loaded into a Biacore X100 SPR (GE Healthcare, Piscataway, NJ) for analysis. SPR experiments were conducted with a continuous flow of (HBS+EP) at 10  $\mu$ L/min. Running buffer was flowed over the sensor surface for a total of  $\sim$ 200 sec to generate a baseline value. Next the sensor surface was treated with a 1:1 mixture of EDC (0.4 M) and NHS (0.1 M) for a total of 480 sec. The sensor surface was rinsed with HBS+EP for 270 sec. Next the surface was treated with CYP2C9 (100 nM), dissolved in HBS+EP, for 420 sec and then rinsed with HBS+EP for 270 sec. Unreacted NHS esters were destroyed by treating with a solution of ethanolamine (1 M), dissolved in water, for 540 sec and were rinsed with HBS+EP (270 sec). Finally, the surface was rinsed with cetyltrimethylammonium bromide (CTAB) (3.9 mM), dissolved in water, for 540 sec and then with HBS+EP (270sec). The negative control (reference) alternated the order of injection so that ethanolamine was first injected, followed by CYP2C9. HBS+EP washes serve to rinse the surface, and, also are designed for intermittent response measurements.

#### **4.2.6. Binding of Immobilized CYP2C9 with CYP2D6**

After the formation of the immobilized CYP2C9 sample and reference flow cells, SPR sensor surfaces were treated with varying concentrations of CYP2D6 (0 nM, 5 nM, 10 nM, 50 nM, 100 nM, 500 nM). To reduce large fluctuations in the bulk refractive index of CYP2D6 containing solutions and to allow for proper blank-subtraction of kinetic sensorgrams, protein-free cryobuffer was added to generate solutions of CYP2D6 which are identical to one another with the exception of CYP2D6 concentrations. Contact times for CYP2D6 solutions were approximately 180 sec followed by a dissociation period of 900 sec, during which time the

sample cell washed with HBS+EP. Changes in response values are represented as a difference, where the response in the reference flow cell is subtracted from the sample flow cell to correct for non-specific interaction of CYP2C9 with the surface of interest. Fitting of kinetic data was accomplished by Biacore X100 evaluation software.

#### **4.2.7. Gold-OT/MUA-CYP2C9 Chip Fabrication.**

Silicon wafers containing a 50 nm gold layer on a 5 nm chromium layer were diced into approximately 4 mm x 6mm chips, sonicated in acetone for 5 minutes, rinsed with deionized water, and then soaked in Piranha solution (98% H<sub>2</sub>SO<sub>4</sub>: 30% H<sub>2</sub>O<sub>2</sub>, 3:1, v/v) at room temperature for 30 minutes (CAUTION: *Piranha solution reacts violently with organic chemicals*). Chips were then rinsed with deionized water, ethanol, and then soaked in an ethanolic solution containing a 3:1 ratio of OT (10 mM) and MUA (10 mM) overnight to allow for the SAM to form a bond and attach to the gold surface. Non-specifically adsorbed thiols were removed by rinsing the chips with 100% ethanol, 95% ethanol, water and finally KPi. To bond the CYP2C9 to the SAM, the SAM-coated slides were immersed with KPi (10 mL) containing EDC/NHS (2 mM and 5 mM, respectively). The treated chips were then removed from the EDC/NHS solution and immersed in a KPi (4 mL) solution containing CYP2C9 (100 nM), flurbiprofen (40 μM), and dapsone (40 μM) for 24 hr. All processes were performed under argon and at room temperature. CYP2C9 chips were then immersed and removed from a KPi solution before being stored in cryobuffer at -80°C until use.

#### **4.2.8. Metabolic incubation of CYP2C9 chips with flurbiprofen**

Gold-OT/MUA chips bearing CYP2C9 were immersed in vials containing Cytochrome P450 Reductase (200 nM, final concentration), cytochrome b<sub>5</sub> (100 nM) and flurbiprofen (250 μM, final concentration) in KPi buffer. To initiate the reaction, samples were spiked with NADPH (250 μM, final concentration) in KPi, bringing the total reaction volume to 200 μL. The vials were then incubated for ~16h at 37°C (water bath) at 37°C. Positive control experiments (200 μL, final volume) replace Gold-CYP2C9 chips with solution CYP2C9 (2.5 nM, final concentration) containing 10 μL of dilaurophosphatidyl choline (1 mg/mL). Final concentrations of CYP2D6 added to incubations of CYP2C9 are (0.75 nM (0.3:1)), (1.25 nM (0.5:1)), (2.5 nM (1:1)) and (5 nM (2:1)). The amount of CYP2D6 added assumed the amount of bonded CYP2C9 was ~0.5 pmol.

#### **4.2.9. Chromatographic Detection of 4'hydroxyflurbiprofen**

Flurbiprofen containing incubations were quenched with acetonitrile containing 200 ng/mL 2-fluoro-4-biphenylacetic acid (internal standard) (50 μL) and a 50% phosphoric acid solution (50 μL). Samples were centrifuged for 10 min and supernatant (200 μL) was loaded into liquid chromatography vials. Chromatography was conducted using a Waters Alliance 2965 separations module, an Alltech Econosphere C-18 column (150mm X 4.6mm, 5 μm particle size)(Grace-Davison, Deerfield, IL) with a 10 μL injection volume. Substrate and metabolite were eluted at 1 ml/min (60:40) mobile phase mixture of potassium phosphate (20 mM, pH 3) and acetonitrile. Eluted compounds were detected with a Waters 2475 fluorescence detector ( $\lambda_{\text{ex}}$  = 260nm,  $\lambda_{\text{em}}$  = 260nm). Data was processed by using the Waters Empower software (ver 2.0).

The peak corresponding to 4'-hydroxyflurbiprofen was determined by comparison to a 4'-hydroxyflurbiprofen standard. Approximate retention times for flurbiprofen, 4'-hydroxyflurbiprofen and 2-fluoro-4-biphenyl acetic acid were 15.2 mins, 10.1 mins, and 6.3 mins respectively.

### **4.3. Results**

#### **4.3.1. SPR based real-time immobilization of CYP2C9 to OT:MUA**

Real time immobilization of CYP2C9 to a self-assembled monolayer containing a 3:1 ratio of OT to MUA was conducted on a thin film of gold (50 nm) and was monitored by SPR spectroscopy in Figure 4.1. Initially the sensor surface was treated with running buffer to generate a baseline response value. Next the surface was treated with a 1:1 EDC:NHS mixture to react with free carboxylic acid groups presented by the SAM. The surface was subsequently rinsed with running buffer in preparation for the next step. In the active flow cell (black line), the surface was treated with CYP2C9 followed by ethanolamine to block unreacted NHS esters, and demonstrate an increase in response relative to the baseline generated in the initial washing. In contrast, the blank flow cell was treated with ethanolamine after EDC-NHS activation followed by CYP2C9 treatment. By treating with ethanolamine first, activated NHS esters will react with the amine group of the ethanolamine, preventing further functionalization with protein. Both surfaces were finally treated with CTAB, which has been demonstrated to remove non-specifically bound proteins<sup>191</sup>. After CTAB rinsing, the surface was rinsed a final time in running buffer. Surfaces treated with CYP2C9 followed by ethanolamine demonstrate a positive response ( $\approx 375$  RU) compared to a blank immobilized flow cell which should be unable to



covalently bind protein ( $\approx -200$  RU). The positive response indicates protein is covalently immobilized to the SAM.

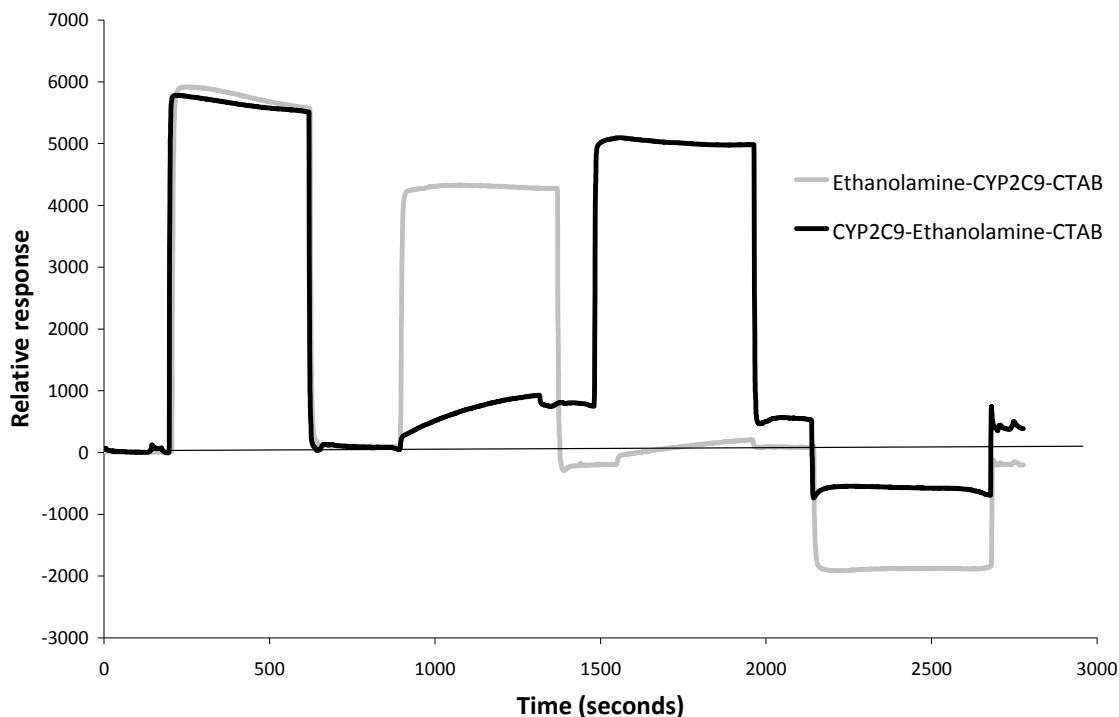
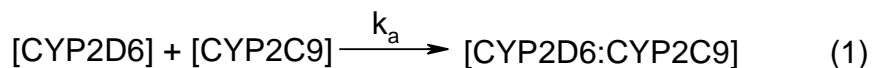


**Figure 4.1.** Real time immobilization of CYP2C9 using SPR. The active flow cell (FC2) containing CYP2C9 was treated with CYP2C9 before ethanolamine to promote covalent bonding of CYP2C9 to the SAM. Negative control experiment used to generate the blank flow cell is treated with ethanolamine before CYP2C9 to block covalent binding of CYP2C9 to the surface.

#### 4.3.2. Binding of CYP2D6 to immobilized CYP2C9

The preparation of both sample and reference flow cells in the SPR, as described above, allows for measurement of the binding between the immobilized CYP2C9 and solution CYP2D6 (Figure 4.2). Solutions of varying concentrations of CYP2D6 were flowed over both the sample flow cell, containing immobilized CYP2C9 as well as the reference flow cell to correct for non-specific interaction. The data in Figure 4.2 is shown as the corrected response, where ‘corrected’

means that the response of the reference flow cell is subtracted from that of the active flow cell (Fc2-Fc1). Initially, the solution CYP2D6 is injected on to the surface at a time point indicated by arrow 1 (Figure 4.2) and continued for 180 seconds. The subtracted data can be fit using a simple 1:1 kinetic model to arrive at an association rate constant ( $k_a$ ) ( $2.78 \times 10^4 \text{ M}^{-1} \text{ s}^{-1}$ ). This rate constant is the rate at which a complex of CYP2C9:CYP2D6 forms per second if CYP2C9 and CYP2D6 were present in solutions at 1 M. A simple equation for this process is seen in equation 1.

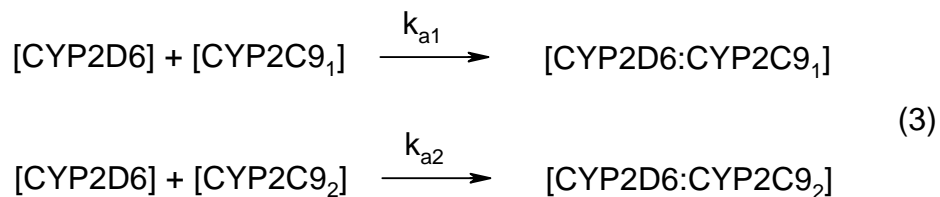


At time point 2 (indicated by the arrow labeled “2” in Figure 4.2) the CYP2D6 addition was terminated and from the resulting trace (180-1100 sec) is used to calculate the dissociation rate constant ( $k_d$ ). The dissociation rate constant ( $k_d$ ) ( $3.067 \times 10^{-5} \text{ s}^{-1}$ ) is the rate at which the CYP2C9:CYP2D6 complex separates into its individual components, CYP2C9 and CYP2D6 per second. A simple equation of this process can be seen below, in equation 2.

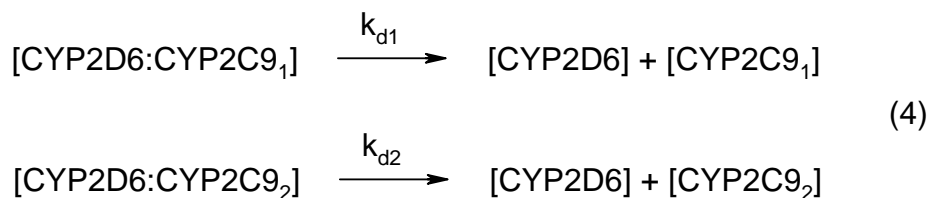


In addition to fitting the SPR binding curve to a model for 1:1 binding, we have also fit the data to a model for a heterogeneous ligand. In this model, it is assumed that because of the random bonding of the protein to the surface, that two binding sites may exist on the surface of CYP2C9. Using the binding curve shown in Figure 4.2, we have measured the association rate of

CYP2D6 to two theoretical binding sites ( $k_{a1}$ ) ( $4.068 \times 10^4 \text{ M}^{-1} \text{ s}^{-1}$ ) and ( $k_{a2}$ ) ( $4.447 \times 10^3 \text{ M}^{-1} \text{ s}^{-1}$ ). This model can be seen below, in equation 3.



Moreover, we can also model the dissociation rate of CYP2D6 from the two different theoretical binding sites on the immobilized CYP2C9. Using this model, we have measured the dissociation rate of CYP2D6 to two theoretical binding sites ( $k_{d1}$ ) ( $1.477 \times 10^{-5} \text{ s}^{-1}$ ) and ( $k_{d2}$ ) ( $1.735 \times 10^{-5} \text{ s}^{-1}$ ). A model for this process is shown below, in equation 4.



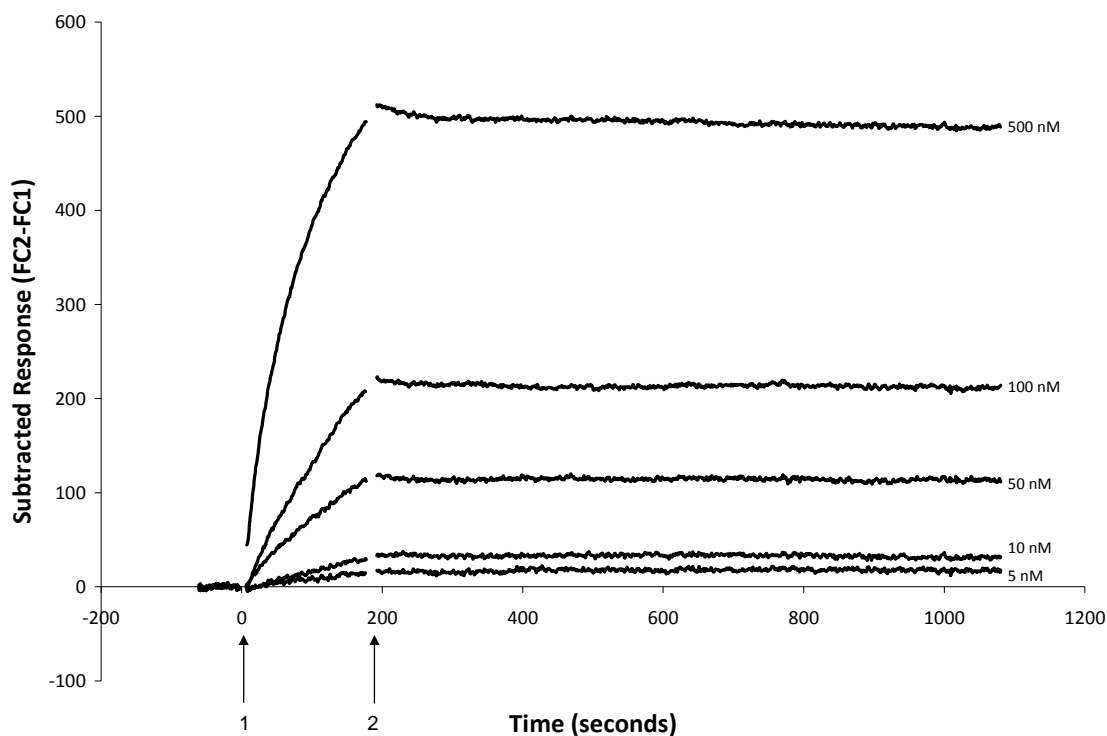


**Figure 4.2.** SPR data obtained from a solution of CYP2D6 interacting with immobilized CYP2C9 (see Figure 1 for set-up). Concentrations, from lower trace upward, of CYP2D6 are 0 nM, 5 nM, 10 nM, 50 nM, 100 nM and 500 nM. Sensorgrams are presented as a subtracted response, where the response in the active flow cell (FC2) is subtracted from the blank flow cell (FC1). Sensorgram corresponding to 0 nM is used to correct the sensorgrams for changes in refractive index associated to the sample buffer.

### 4.3.3. SPR Model Fitting

As described above, SPR binding curves can be fit to several different models of ligand/analyte binding. A kinetic model is generated based on experimental data, and the level of “fitness” of the curve is determined by a residual plot, shown in Figure 4.3. In Figure 4.3, the data from the experimental traces (black triangles, gray squares) is compared to a computer generated kinetic model (solid black line). As the experimental data deviates from the model at a given point, the response is measured to give a value for the change in response ( $\Delta$  response =

model response - experimental response). Models that acceptably fit the computer generated model have deviations of less than  $\pm 25$  RU (black boxes). Models which do not acceptably fit the experimental data generally have deviations fo greater than  $\pm 25$  RU (gray triangles), and may give poor results regarding kinetic modeling.

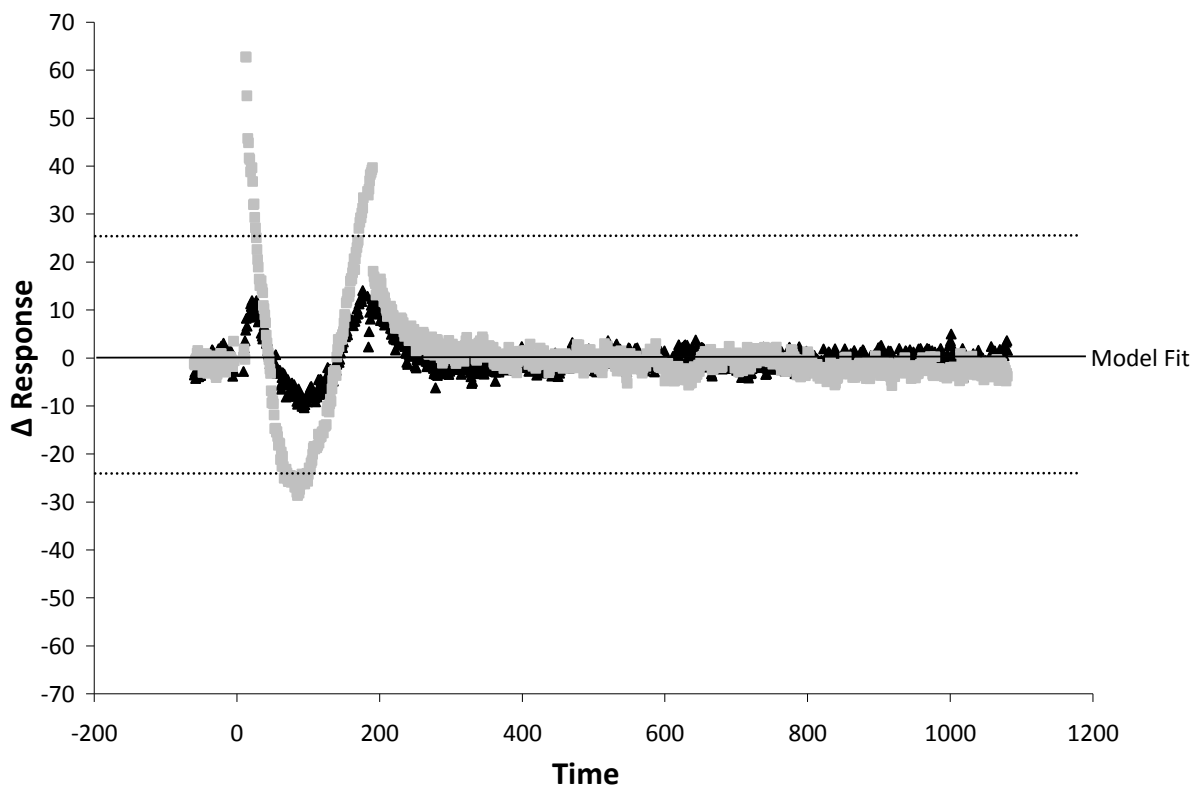


**Figure 4.3.** Residual plot of kinetic fit models. An example of a poorly fit model is shown (gray squares), as well kinetic model which is well fit to the data (black triangles). The horizontal line at the y-axis origin (Model Fit) represents the computer generated model response to which SPR binding curves are fit.

#### 4.3.4. Metabolism of Flurbiprofen with Immobilized CYP2C9

The ability of immobilized CYP2C9 constructs to metabolize flurbiprofen, a non-steroidal inflammatory drug, has been studied. In Figure 4.4 is shown the amount of metabolite formed from Au-SAM-CYP2C9 under various conditions. Here it can be seen that the

metabolism of flurbiprofen requires both NADPH and cytochrome b<sub>5</sub> (black bar) ( $18.37 \pm 2.33$  ng), and that the presence of both of these components produces significantly more metabolite than if either component is missing from the incubation. Incubations which have omitted NADPH (grey bar) produce very little metabolite ( $1.32 \pm 0.13$  ng). While, incubations containing NADPH but no cytochrome b<sub>5</sub> yield very little metabolite produced (white bar) ( $1.50 \pm 0.49$  ng), indicating that cytochrome b<sub>5</sub> is necessary to shuttle a second electron to the heme center of immobilized CYP2C9.

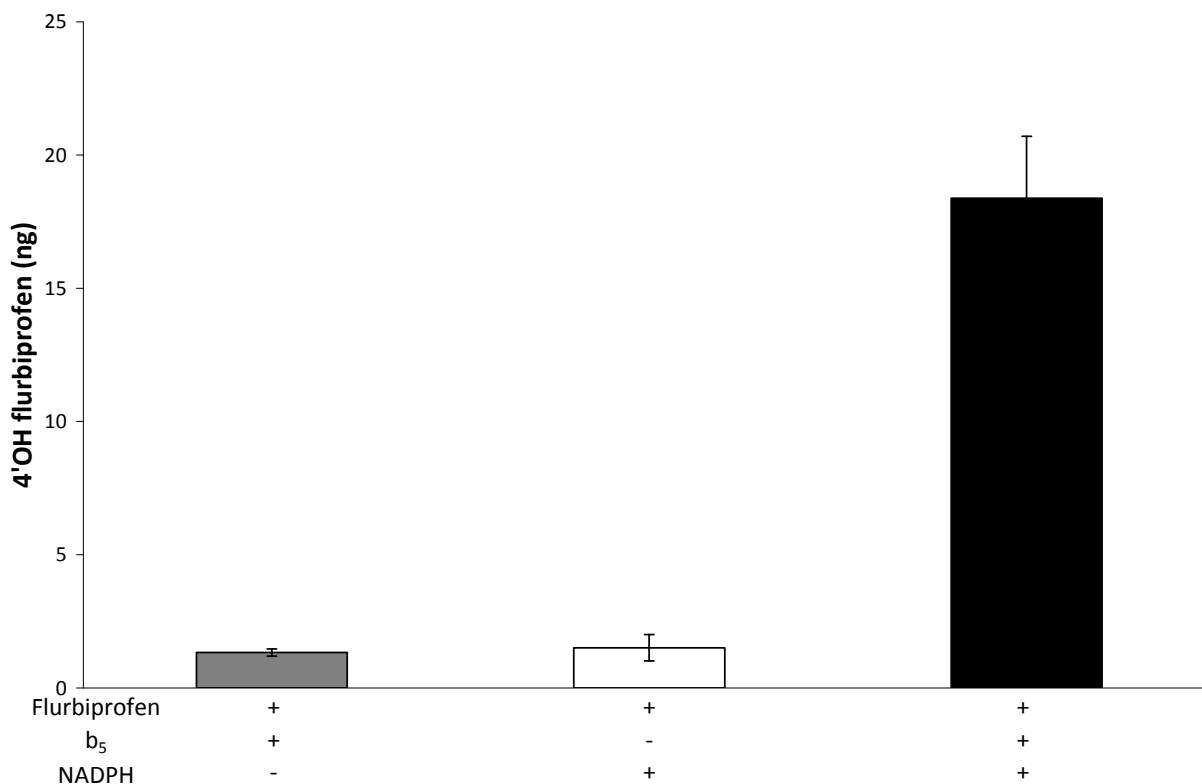


**Figure 4.4.** Effect of b<sub>5</sub> composition on metabolic activity of CYP2C9. All chip incubations contained CYP2C9, CPR, and flurbiprofen. Chip immobilized mixture were comprised of gold chips with the indicated SAM, bound (OT and EG3) or bonded ((3:1) OT:MUA) CYP2C9, flurbiprofen, CPR and NADPH.

#### **4.3.5. Effect of Increasing Concentrations of CYP2D6 on the Metabolism of Flurbiprofen by Immobilized CYP2C9.**

Several different concentrations of CYP2D6 were added to incubations containing immobilized CYP2C9 bearing gold chips, Figure 4.5. The calculated concentration of CYP2C9 present on a chip using an identical method of preparation is approximately  $0.5 \text{ pmol}^{71}$ , and serves as a reference point for the treatment of CYP2D6. CYP2C9 chips containing no CYP2D6 produced approximately  $18.37 \pm 2.32 \text{ ng}$  4'OH-flurbiprofen. Subsequent incubations where the ratio of (CYP2D6:CYP2C9) was increased produced  $16.15 \pm 1.05 \text{ ng}$  (0.3:1),  $20.51 \pm 1.53 \text{ ng}$ (0.5:1),  $18.55 \pm 1.53 \text{ ng}$  (1:1) and  $17.10 \pm 1.53 \text{ ng}$  (2:1) and show no significant difference from the control which contains no CYP2D6.

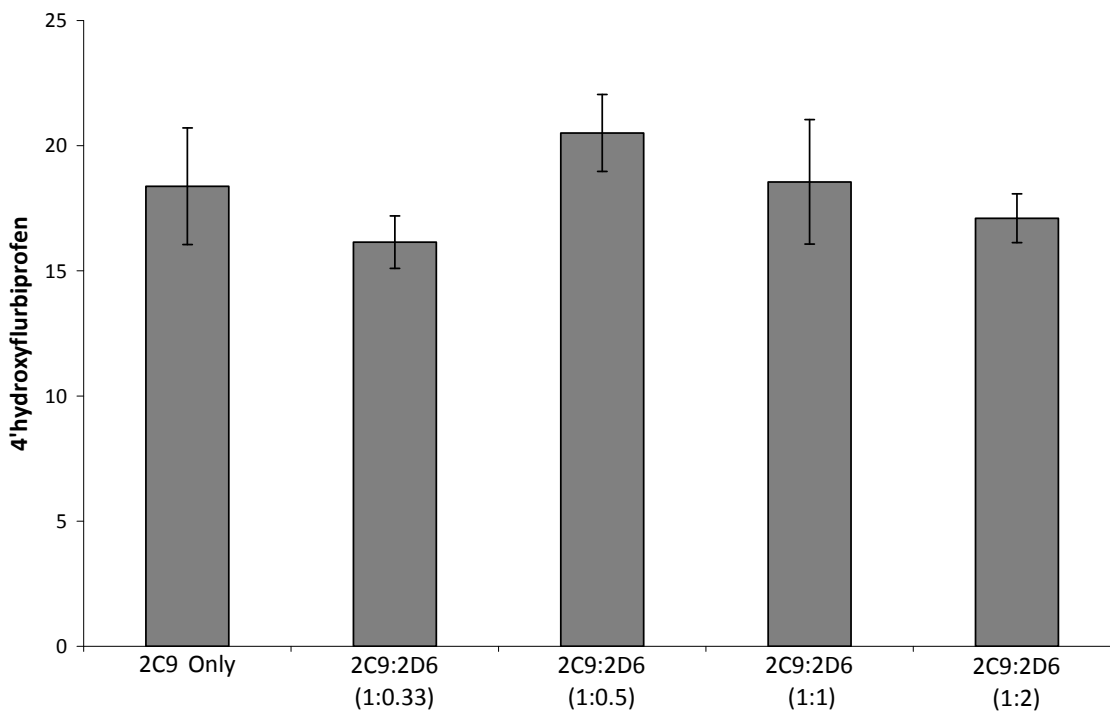


**Figure 4.5.** Effect of solution CYP2D6 on the metabolism of flurbiprofen by CYP2C9. Chip incubations contained CYP2C9, CPR, cytochrome B<sub>5</sub> and flurbiprofen. Incubations containing solution CYP2D6 contain (.75 nM (0.3:1)), (1.25 nM (0.5:1)), (2.5 nM (1:1)) and (5 nM (2:1)) respectively.

#### 4.4. Discussion

Cytochrome P450 enzymes have been characterized as an essential class of heme-containing enzymes responsible for the metabolism of a large number of pharmaceuticals. Typically, within the liver, cytochrome P450 enzymes are bound to the endoplasmic reticulum of hepatocyte cells and several different isoforms are expressed within these cells. As a result, protein-protein interactions between isoforms of P450 enzymes may play a role on the catalytic



activity of a given P450 enzyme. The exact nature of how protein-protein interactions occur, and the effect of the interaction on the catalytic activity both *in-vitro* and *in-vivo* is still unclear.

Several different *in-vitro* models have been utilized in an attempt to characterize P450 protein-protein interaction *in-vivo*. A commonly used method to study these interactions is to use reconstituted incubations, which combine recombinant P450s, CPR, phospholipids and NADPH to generate a “simulated” microsomal system, capable of metabolism. These systems have been used to conduct mixed enzyme incubations which contain at least two different P450 enzymes. Interaction between P450 enzymes is often determined by an effect on the catalytic activity of one or more of the P450’s which are present in the system.

The use of gold immobilized CYP2C9 also provides a platform to characterize biophysical interaction using SPR spectroscopy. Typically, SPR experiments are carried out on CM5 chips, which contain a carboxy-methyl dextran gel on the surface of a thin (50 nm) gold film. Imaging of a CM5 surface with an immobilized P450 to characterize the state of aggregation may prove to be difficult. The “soft” and inconsistent nature of the commercially available CM5<sup>192</sup>, could make it extremely difficult to characterize monomeric P450 structures on a surface. In contrast, by using a similar method to immobilize CYP2C9 to an OT/MUA SAM<sup>70</sup>, it is likely that P450 enzymes immobilized on the surface as described in the SPR immobilization experiment, exist in monomeric form, which can be determined by other methods (e.g., AFM).

SPR spectra in Figure 4.1 suggests the formation of an OT-MUA-CYP2C9 construct analogous to the construct presented in the literature<sup>70,71</sup>. Moreover, this data indicates that the OT-MUA SAM is capable of covalently bonding CYP2C9. Prior to this, evidence suggesting

the formation of a covalent bond between CYP2C9 and the SAM had been presented using x-ray photoelectron spectroscopy (XPS). XPS can characterize the type of bonds present on a surface and it was suggested that the disappearance of a peak at ~289 eV corresponding to electrons from a carboxylic carbon and would be replaced by an amide bond after linking CYP2C9 to the SAM, suggest the protein is covalently bonded<sup>71</sup>. However, the enzyme would contain identical carboxylic carbons, thus it would be difficult to conclusively determine if the disappearance of the electron peak associated with the carboxylic carbon from MUA-NHS esters truly disappeared, or if the peak obscured by the signal produced in the XPS spectrum of covalently bonded CYP2C9.

Additionally, the use of SPR has allowed for the determination of biophysical interaction constants between immobilized CYP2C9 and solution CYP2D6. After thorough searches of the literature, this is believed to be the first use of SPR based biosensors to characterize the interaction between two different P450 enzymes. Furthermore, these SPR based experiments can be tailored to observe interaction between virtually any P450 and can also be used to describe interactions that are heteromeric in nature but homomeric as well. Characterization of homomeric interactions may prove to be useful in elucidating the effects of aggregation in P450 enzyme incubations containing single P450 enzymes.

Kinetic evaluation of protein-protein interactions using SPR spectroscopy has recently become an indispensable tool for biochemists. Initially, derivation of equations regarding kinetic rate constants characterizing protein-protein interaction was accomplished using antibody-antigen interactions. Using rate constants modeled from subtracted SPR spectra probing interaction CYP2C9 and CYP2D6, in a 1:1 binding model, the quotient of the dissociation rate

( $k_d$ ) ( $3.067 \times 10^{-5} \text{ s}^{-1}$ ) divided by the association rate ( $k_a$ ) ( $2.78 \times 10^4 \text{ M}^{-1} \text{ s}^{-1}$ ) represents a dissociation constant ( $K_D$ ) of  $1.10 \times 10^{-9} \text{ M}$ . Additionally we have also fit the model to a ligand containing two theoretical binding sites, known as a heterogeneous ligand binding model. The dissociation constant of each individual binding site is calculated by taking the quotient of the dissociation rate ( $k_{d1}$ ) ( $1.477 \times 10^{-5} \text{ s}^{-1}$ ) and ( $k_{d2}$ ) ( $1.735 \times 10^{-5} \text{ s}^{-1}$ ) over the association rate ( $k_{a1}$ ) ( $4.068 \times 10^4 \text{ M}^{-1} \text{ s}^{-1}$ ) and ( $k_{a2}$ ) ( $4.447 \times 10^3 \text{ M}^{-1} \text{ s}^{-1}$ ). The dissociation of each binding site was calculated at ( $k_{D1}$ ) ( $3.631 \times 10^{-10} \text{ M}$ ) and ( $k_{D1}$ ) ( $3.9 \times 10^{-9} \text{ M}$ ). Fitting of both the 1:1 binding model and the heterogeneous ligand binding model to residual plots found that the experimental data, from both models, was inside the threshold of  $\pm 25 \text{ RU}$ . The poorly fit model in Figure 4.3 may be a result of the difference in refractive index of the solution being injected onto the surface, compared to the refractive index of the running buffer.

Interestingly, dissociation constants ( $K_D$ ) characterizing P450:CPR interactions<sup>193</sup> of P450 enzymes commonly utilized in drug metabolism (CYP3A4, CYP2D6, CYP2C19) ranges from 5-100 nM. The experimentally derived rate constant probing for interaction between CYP2C9 and CYP2D6 demonstrate a dissociation constant which is 5-100 times smaller than dissociation constants characterizing interaction between P450 and CPR, lending further credence to the idea that P450 based protein-protein interactions may be playing a key role in metabolism.

However, the SPR experiment described within the text is not without its limitations. SPR experiments can typically be used to describe dissociation constants from anywhere from  $10^{-5}$  to  $10^{-9} \text{ M}$ . P450 based protein-protein interactions have been shown to have sub nano-molar dissociation constants,<sup>65</sup> and, as a result, SPR may be incapable of characterizing some

interactions. Moreover, purified enzymes used in this experiment have exposed membrane-associated domains, which may artificially lower the dissociation constant measured. To counter this, SPR sensors can be made with a variety of different surface chemistries, capable of supporting artificial membrane bi-layers or liposomes. These approaches have the potential to provide some insight into the role of membrane or phospholipids on protein-protein interaction between P450 enzymes.

Reconstituted incubations provide the distinct advantage of being easy to modify to a variety of conditions and enzyme mixtures. The availability of different P450 isoforms has further been increased through the use of recombinant DNA technology. However, reconstituted incubations of P450 enzymes are prone to enzyme aggregation, and this aggregation often exhibits significant effects on the catalytic activity of an enzyme. Moreover, classical methods to reduce protein aggregation, including mutation of the enzyme and use of detergents to break up aggregates, may affect the activity of the enzyme. Ideally, it would be useful to design a system where the aggregation of P450 enzymes could be controlled and interactions could be observed using proteins interacting in a true 1:1 manner.

To solve this question, and to provide more insight into P450 based protein-protein interaction, gold-immobilized enzymes present a reasonable way to control and to observe protein-protein interactions of monomeric enzymes. By immobilizing the enzyme to a gold surface, it has been demonstrated that monomeric enzymes tend to form on the surface of interest<sup>70</sup>. Previous research has shown the interaction of solution CYP2D6 with gold-immobilized CYP2C9 suggests that higher concentrations of CYP2D6 may be inhibiting the metabolism of  $\Delta$ -9-tetrahydrocannabinol<sup>194</sup>. By using an analogous study design here, we present

data suggests that increasing concentrations of CYP2D6 in the presence of immobilized CYP2C9 does not significantly affect the metabolism of flurbiprofen by CYP2C9. This data may imply that the effect of protein-protein interactions on catalytic activity may be substrate dependent, further complicating the issue of P450 protein-protein interaction.

In contrast, solution experiments probing for interactions between CYP2C9 and CYP2D6 show that increasing concentrations of CYP2D6 (relative to CYP2C9), may serve to inhibit the metabolism of flurbiprofen by CYP2C9<sup>81</sup>. This is in disagreement with the data presented using gold-immobilized CYP2C9 (see Figure 4.5). It is conceivable that the effect observed with reconstituted solution incubations is an artifact of the conditions of the incubation. Aggregation in P450 enzymes may be occurring in solution, and the presence of a second P450 enzyme may be causing the formation of catalytically deficient mixed-enzyme aggregates. However when the enzyme is in monomeric form, the effect of CYP2D6 is not as pronounced and the formation of large aggregates of CYP2C9 is inhibited. As a result, the catalytic activity of CYP2C9 remains largely unaffected.

Here we have described a method to characterize the activity of gold –immobilized P450 enzymes using a well characterized preparation method designed to keep P450 enzymes in monomeric form. This gold-immobilized platform may be useful in elucidation of protein-protein interaction as it occurs with monomeric P450 enzymes. Moreover, the method of preparation for the formation of gold immobilized P450 enzymes can be analogously applied to SPR experiments to elucidate biophysical rate constants to better describe the interaction between different P450 enzymes. In turn, we believe that the model presented here may prove to provide better insight in predicting *in-vivo* drug metabolism using *in-vitro* models.

# **Chapter 5**

## **Summary and Future Directions**

## **5.1. Summary and Future Directions**

### **5.1.1. Summary**

In Chapter 2 the use of immobilized Cytochrome P450 (CYP2C9) in PMMA based bioreactors was described. Several parameters using 4 mm x 6 mm PMMA chips were optimized, including the concentration of enzyme used during attachment, enzyme attachment time, and the attachment method used for enzyme immobilization. In exploratory studies, it was found that treating PMMA chips with 100 nM CYP2C9 for 24 hours resulted in the highest levels of metabolite. Immobilization of CYP2C9 by coordination to nickel cations chelated by 1-acetato-4-benzyl-triazacyclononane (Acbztaen)(carboxy-terminus), was found to produce higher levels of metabolism as compared to N-hydroxysulfosuccinimide (NHS) and N-(3-dimethylaminopropyl)-N'-ethyl-carbodiimide hydrochloride (EDC) covalently bonded CYP2C9 (amino-terminus).

Once the optimal parameters were determined with PMMA chips, a plug-flow bioreactor was fabricated from PMMA in which a serpentine channel was milled. The optimized parameters from the exploratory were used for CYP2C9 attachment to the channel, NADPH, CPR and substrate were then pumped through the channel and fractions collected. Studies designed to optimize the production of metabolite found that static application of CYP2C9, following EDC-NHS activation of the PMMA channel produced the highest levels of metabolite. However, overall production of 4'-hydroxydiclofenac was considerably lower than the amount of compound needed to be able to conduct metabolite toxicity experiments.

As an alternative to the plug-flow bioreactor, an electrochemical based system was studied. In this system an EDC-NHS immobilized CYP2C9 electrode was used as the working electrode and when current is supplied to this electrode in the presence of a CYP2C9 substrate, metabolite may form. This system was used to generate a CYP2C9-mediated metabolite of warfarin, 7-hydroxywarfarin. At the scale used, this bioreactor produced only nanogram quantities of metabolite. However, based on the amount of enzyme present on the surface of the electrode, the system is very efficient. Moreover, the electrochemically based system requires no CPR or NADPH, reagents which are expensive and can become cost prohibitive, as in the case of the plug-flow PMMA bioreactor. Furthermore, several parameters could be optimized for the electrochemical batch bioreactor, including electrolysis running time, CYP2C9 electrode surface area and parameters to improve mass-transfer at the electrode interface could be easily modified to generate more metabolite, thus providing an efficient method to produce large quantities of metabolites for toxicity studies.

Chapter 3 described the fabrication of a device designed to reduce aggregation of Cytochrome P450 enzymes. It has been well established in the literature that P450 enzymes have a strong tendency to aggregate together, and this aggregation may affect the catalytic activity of a P450 enzyme, ultimately altering the kinetics of P450 metabolism. As fabricated, this device contained small (100 nm) “nano-beakers” designed to bind P450 enzymes in them at a discrete point on the surface of interest. Areas surrounding the nano-beaker were covered with poly-ethylene glycol (PEG) moieties that resist the adsorption of the protein to the areas between the nano-beakers.



The interaction of CYP2C with several self assembled monolayers (SAM) has been studied including octanethiol and (11-Mercaptoundecyl)tri(ethylene glycol) on gold and N-octyltrimethoxysilane and 2-[Methoxy(polyethyleneoxy)propyl] trimethoxysilane on silicon dioxide. The interaction between CYP2C9 and these surfaces has been monitored, in real time, with surface plasmon resonance spectroscopy. The results show a strong tendency for PEG SAMs (2-[Methoxy(polyethyleneoxy)propyl] trimethoxysilane and (11-Mercaptoundecyl)tri(ethylene glycol)) to resist CYP2C9 adsorption, while hydrophobic SAMs (octanethiol and N-octyltrimethoxysilane) tend to non-specifically adsorb CYP2C9. Moreover, we have also demonstrated similar interaction between CYP2C9 and our SAMs of interest using x-ray photoelectron spectroscopy (XPS). This differential adsorption was used to support the claim that CYP2C9 was bound in the nano-beaker and not the surrounding surface.

Ultimately, it would be ideal to further optimize the fabrication of the nanostructure device to form discrete binding points which are similar in size to a Cytochrome P450: Cytochrome P450 Reductase (CPR) redox complex (15-20 nm). This will allow for unequivocal control of the dispersal of P450 enzymes from large aggregates to monomeric structures. This will require advances in the fabrication techniques used to make the nano-beakers so that the dimensions can be reduced from 50-100 nm to 15-20 nm. In turn, a device with appropriate sized nano-beaker may provide results that will lead to better predictions of *in-vivo* drug metabolism based on *in-vitro* measurements.

In Chapter 5, surface plasmon resonance spectroscopy was utilized to measure on- and off-rate kinetics of binding between CYP2C9 and CYP2D6, by using a construct similar to one presented in the literature. SPR based biosensors provide the means to measure protein-protein

interactions in label free systems, and here we report one of the earliest instances of using SPR to measure protein-protein interactions between two P450 enzymes. Interestingly, we found a dissociation constant for a 1:1 complex of CYP2C9-CYP2D6 to be approximately 1.10 nM. The measurement of dissociation constants for CYP2C9-CPR is approximately  $2.3 \pm 1.0$  nM, indicating a propensity for protein-protein interactions between P450 enzymes and may be playing a key role in the catalytic activity of a given enzyme.

In addition to looking at protein-protein interaction on an octanethiol mercaptoundecanoic acid self-assembled monolayer, we also looked at the effect on metabolic activity of an immobilized CYP2C9 by solution CYP2D6. Previous reports suggested that increasing concentrations of CYP2D6 in the presence of immobilized CYP2C9 causes an increase in the metabolism of  $\Delta$ -9-tetrahydrocannabinol. Interestingly, repeating an identical experiment but with flurbiprofen as the substrate suggests that CYP2D6 does not modulate CYP2C9 activity, as increasing CYP2D6 concentrations produce no significant change in metabolite production. Moreover, this finding also suggests that protein-protein interaction may be substrate dependent, further complicating the issue of elucidating the effects of these protein-protein interactions.

In contrast, solution studies using mixed-enzyme reconstituted incubations containing CYP2C9-CYP2D6 suggest the presence of increasing concentrations of CYP2D6 causes a decrease in flurbiprofen metabolism<sup>81</sup>. It is hypothesized that aggregation in P450 enzymes can often modulate the catalytic activity of a given P450, and, in solution, incubations containing enzyme mixtures of CYP2C9 and CYP2D6 may produce catalytically deficient mixed-enzyme aggregates. This implies that solution experiments may poorly model protein-protein

interactions *in-vivo*. In contrast, experiments containing immobilized enzymes significantly reduce the aggregation state of CYP2C9. As a result, the formation of mixed enzyme aggregates is reduced, and the inhibitory effect of CYP2D6 is no longer observed.

### **5.1.2. Future Directions**

In future experiments, it would be interesting to further characterize the interaction of several different P450 enzymes with each other, using a similar approach to the one described in chapter 4. The use of SPR based sensors will allow for the elucidation of association constants for P450s. Additionally, SPR provides a reasonable model to elucidate the effect of incubation conditions (enzyme mutation or increased detergent concentrations) on protein-protein interactions. Furthermore, the use of immobilized monomeric enzymes can be tailored to study protein-protein interactions between virtually any pair of P450 enzymes, to determine if aggregation may be playing a role in protein-protein interactions in mixed enzyme reconstituted incubations. In particular we would like to elucidate interactions between immobilized CYP2D6 and solution CYP2C9, which in solution demonstrate no effect in the metabolism of dextromethorphan in the presence of increasing concentrations of CYP2C9. Preliminary results suggest that previously reported solution effects are different from the corresponding immobilized system.

In addition to elucidating effects of protein-protein interaction in mixed enzyme incubations, it would be interesting to further characterize the effect of P450 enzymes using nanostructure devices similar to the one presented here. Ideally, the dimensions of the nanowell would be reduced to the point where we could selectively bind monomeric P450 enzymes. This provides a potential approach to unequivocally control of P450 aggregation.

The construction of the nanowell device has also lead to the potential to use the nanostructure device in SPR experiments. As designed the nanostructure device contains a silicon dioxide layer on top of 100 nm thin films of gold. By producing microscope cover slides with 50 nm of gold layers and then covering them with the patterned silicon dioxide film, one could use this to measure binding kinetics of monomeric P450 enzymes to clarify P450 based protein-protein interactions. Moreover, the nanostructure device could be used to prepare a membrane bilayer<sup>195</sup> on top the gold-thiol well described in Chapter 3, creating a solid state Nanodisc®-like structure with which one could measure not only protein-protein interactions, but protein-membrane association as well.

Applications analogous to this idea extend beyond just P450 enzymes, as the formation of discoidal structures on SPR films may provide insight into monitoring protein-protein interactions and ligand screening for membrane bound receptors. These receptor types include G-protein coupled receptors, which have demonstrated a high propensity to be targets for pharmaceutical compounds.

## **5.2. Conclusions**

The platforms described here serve to provide some insight into issues related to solution P450 incubations. Typically, solution-based P450 assays are used in the early drug development process to predict *in-vivo* drug metabolism using *in-vitro* models. However many of these models ignore issues of enzyme aggregation or protein-protein interaction between P450 enzymes. This may result in poor predictions of *in-vivo* drug metabolism which may lead to failed investigational compounds. Presented within the text are models of P450 metabolism

which will address the affects of aggregation of P450 as well as protein-protein interactions in reconstituted P450 systems, and may serve to make improved predictions regarding *in-vivo* drug metabolism in the future.

# **Chapter 6 – Bibliography**

## 6.1. Reference List

1. Mueller, G. C.; Miller, J. A. The metabolism of 4-dimethylaminoazobenzene by rat liver homogenates. *Journal of Biological Chemistry* **1948**, *176*, 535-544.
2. Omura, T.; Sato, R. A new cytochrome in liver microsomes. *Journal of Biological Chemistry* **1962**, *237*, 1375-1376.
3. Lu, A. Y. H.; Coon, M. J. Role of hemoprotein P-450 in fatty acid omega-hydroxylation in a soluble enzyme system from liver microsomes. *Journal of Biological Chemistry* **1962**, *237*, 1331-1332.
4. Distlerath, L. M.; Reilly, P. E. B.; Martin, M. V.; Davis, G. G.; Wilkinson, G. R.; Guengerich, F. P. Purification and Characterization of the Human-Liver Cytochromes-P-450 Involved in Debrisoquine 4-Hydroxylation and Phenacetin O-Deethylation, 2 Prototypes for Genetic-Polymorphism in Oxidative Drug-Metabolism. *Journal of Biological Chemistry* **1985**, *260* (15), 9057-9067.
5. Barnes, H. J.; Arlotto, M. P.; Waterman, M. R. Expression and Enzymatic-Activity of Recombinant Cytochrome-P450 17-Alpha-Hydroxylase in Escherichia-Coli. *Proceedings of the National Academy of Sciences of the United States of America* **1991**, *88* (13), 5597-5601.
6. Wester, M. R.; Yano, J. K.; Schoch, G. A.; Yang, C.; Griffin, K. J.; Stout, C. D.; Johnson, E. F. The structure of human cytochrome P4502C9 complexed with flurbiprofen at 2.0-angstrom resolution. *Journal of Biological Chemistry* **2004**, *279* (34), 35630-35637.
7. Nebert, D. W.; Adesnik, M.; Coon, M. J.; Estabrook, R. W.; Gonzalez, F. J.; Guengerich, F. P.; Gunsalus, I. C.; Johnson, E. F.; Kemper, B.; Levin, W.; Phillips, I. R.; Sato, R.; Waterman, M. R. The P450 Gene Superfamily - Recommended Nomenclature. *Dna-A Journal of Molecular & Cellular Biology* **1987**, *6* (1), 1-11.
8. Nelson, D. R.; Kamataki, T.; Waxman, D. J.; Guengerich, F. P.; Estabrook, R. W.; Feyereisen, R.; Gonzalez, F. J.; Coon, M. J.; Gunsalus, I. C.; Gotoh, O.; Okuda, K.; Nebert, D. W. The P450 Superfamily - Update on New Sequences, Gene-Mapping, Accession Numbers, Early Trivial Names of Enzymes, and Nomenclature. *Dna and Cell Biology* **1993**, *12* (1), 1-51.
9. Sullivan-Klose, T. H.; Ghanayem, B. I.; Bell, D. A.; Zhang, Z. Y.; Kaminsky, L. S.; Shenfield, G. M.; Miners, J. O.; Birkett, D. J.; Goldstein, J. A. The role of the CYP2C9-Leu 359 allelic variant in the tolbutamide polymorphism. *Pharmacogenetics and Genomics* **1996**, *6* (4).

10. Nelson, D. R.; Strobel, H. W. On the Membrane Topology of Vertebrate Cytochrome-P-450 Proteins. *Journal of Biological Chemistry* **1988**, *263* (13), 6038-6050.
11. Szczesna-Skorupa, E.; Ahn, K. S.; Chen, C. D.; Doray, B.; Kemper, B. The Cytoplasmic and N-Terminal Transmembrane Domains of Cytochrome-P450 Contain Independent Signals for Retention in the Endoplasmic-Reticulum. *Journal of Biological Chemistry* **1995**, *270* (41), 24327-24333.
12. Gutierrez, A.; Grunau, A.; Paine, M.; Munro, A. W.; Wolf, C. R.; Roberts, G. C. K.; Scrutton, N. S. Electron transfer in human cytochrome P450 reductase. *Biochemical Society Transactions* **2003**, *31*, 497-501.
13. Shet, M. S.; Fisher, C. W.; Holmans, P. L.; Estabrook, R. W. Human Cytochrome-P450-3A4 - Enzymatic-Properties of A Purified Recombinant Fusion Protein Containing Nadph-P450 Reductase. *Proceedings of the National Academy of Sciences of the United States of America* **1993**, *90* (24), 11748-11752.
14. Griffin, B. W.; Peterson, J. A. Camphor binding of *Pseudomonas putida* cytochrome P-450. Kinetics and thermodynamics of the reaction. *Biochemistry* **1972**, *11* (25), 4740-4746.
15. Sevrioukova, I. F.; Li, H. Y.; Zhang, H.; Peterson, J. A.; Poulos, T. L. Structure of a cytochrome P450-redox partner electron-transfer complex. *Proceedings of the National Academy of Sciences of the United States of America* **1999**, *96* (5), 1863-1868.
16. Egawa, T.; Ogura, T.; Makino, R.; Ishimura, Y.; Kitagawa, T. Observation of the O-O stretching Raman band for cytochrome P-450cam under catalytic conditions. *Journal of Biological Chemistry* **1991**, *266* (16), 10246-10248.
17. Benson, D. E.; Suslick, K. S.; Sligar, S. G. Reduced oxy intermediate observed in D251N cytochrome P450(cam). *Biochemistry* **1997**, *36* (17), 5104-5107.
18. Vidakovic, M.; Sligar, S. G.; Li, H. Y.; Poulos, T. L. Understanding the role of the essential Asp251 in cytochrome P450cam using site-directed mutagenesis, crystallography, and kinetic solvent isotope effect. *Biochemistry* **1998**, *37* (26), 9211-9219.
19. Auclair, K.; Moenne-Loccoz, P.; de Montellano, P. R. O. Roles of the proximal heme thiolate ligand in cytochrome P450(cam). *Journal of the American Chemical Society* **2001**, *123* (21), 4877-4885.
20. Davydov, R.; Makris, T. M.; Kofman, V.; Werst, D. E.; Sligar, S. G.; Hoffman, B. M. Hydroxylation of camphor by-reduced oxy-cytochrome P450cam: Mechanistic implications of EPR and ENDOR studies of catalytic intermediates in native and



- mutant enzymes. *Journal of the American Chemical Society* **2001**, *123* (7), 1403-1415.
21. Gorsky, L. D.; Koop, D. R.; Coon, M. J. On the Stoichiometry of the Oxidase and Monooxygenase Reactions Catalyzed by Liver Microsomal Cytochrome-P-450 - Products of Oxygen Reduction. *Journal of Biological Chemistry* **1984**, *259* (11), 6812-6817.
  22. Stiles, A. R.; McDonald, J. G.; Bauman, D. R.; Russell, D. W. CYP7B1: One Cytochrome P450, Two Human Genetic Diseases, and Multiple Physiological Functions. *Journal of Biological Chemistry* **2009**, *284* (42), 28485-28489.
  23. McGiff, J. C. Cytochrome-P-450 Metabolism of Arachidonic-Acid. *Annual Review of Pharmacology and Toxicology* **1991**, *31*, 339-369.
  24. King, A. N.; Beer, D. G.; Christensen, P. J.; Simpson, R. U.; Ramnath, N. The Vitamin D/CYP24A1 Story in Cancer. *Anti-Cancer Agents in Medicinal Chemistry* **2010**, *10* (3), 213-224.
  25. Wikvall, K. Cytochrome P450 enzymes in the bioactivation of vitamin D to its hormonal form (Review). *International Journal of Molecular Medicine* **2001**, *7* (2), 201-209.
  26. Stierlin, H.; Faigle, J. W.; Sallmann, A.; Kung, W.; Richter, W. J.; Kriemler, H. P.; Alt, K. O.; Winkler, T. Biotransformation of Diclofenac Sodium (Voltaren) in Animals and in Man .1. Isolation and Identification of Principal Metabolites. *Xenobiotica* **1979**, *9* (10), 601-610.
  27. Atkinson, J. K.; Ingold, K. U. Cytochrome-P450 Hydroxylation of Hydrocarbons - Variation in the Rate of Oxygen Rebound Using Cyclopropyl Radical Clocks Including 2 New Ultrafast Probes. *Biochemistry* **1993**, *32* (35), 9209-9214.
  28. Sato, H.; Guengerich, F. P. Oxidation of 1,2,4,5-tetramethoxybenzene to a cation radical by cytochrome P450. *Journal of the American Chemical Society* **2000**, *122* (33), 8099-8100.
  29. Hollenberg, P. F.; Dwyer, L. A.; Rickert, D. E.; Kedderis, G. L. Source of the Oxygen Atom in the Product of Cytochrome-P-450-Catalyzed N-Demethylation Reactions. *Federation Proceedings* **1983**, *42* (4), 910.
  30. Guengerich, F. P.; Yun, C. H.; Macdonald, T. L. Evidence for a 1-electron oxidation mechanism in N-dealkylation of N,N-dialkylanilines by cytochrome P450 2B1 - Kinetic hydrogen isotope effects, linear free energy relationships, comparisons with horseradish peroxidase, and studies with oxygen surrogates. *Journal of Biological Chemistry* **1996**, *271* (44), 27321-27329.

31. Coleman, T.; Ellis, S. W.; Martin, I. J.; Lennard, M. S.; Tucker, G. T. 1-methyl-4-phenyl-1,2,3,6-tetrahydropyridine (MPTP) is n-demethylated by cytochromes P450 2D6, 1A2 and 3A4 - Implications for susceptibility to Parkinson's disease. *Journal of Pharmacology and Experimental Therapeutics* **1996**, *277* (2), 685-690.
32. Demontellano, P. R. O.; Stearns, R. A.; Langry, K. C. The Allylisopropylacetamide and Novonal Prosthetic Heme Adducts. *Molecular Pharmacology* **1984**, *25* (2), 310-317.
33. Vaz, A. D. N.; Roberts, E. S.; Coon, M. J. Olefin Formation in the Oxidative Deformylation of Aldehydes by Cytochrome-P-450 - Mechanistic Implications for Catalysis by Oxygen-Derived Peroxide. *Journal of the American Chemical Society* **1991**, *113* (15), 5886-5887.
34. Guengerich, F. P. Oxidation of Halogenated Compounds by Cytochrome-P-450, Peroxidases, and Model Metalloporphyrins. *Journal of Biological Chemistry* **1989**, *264* (29), 17198-17205.
35. Seto, Y.; Guengerich, F. P. Partitioning Between N-Dealkylation and N-Oxygenation in the Oxidation of N,N-Dialkylarylamines Catalyzed by Cytochrome-P450-2B1. *Journal of Biological Chemistry* **1993**, *268* (14), 9986-9997.
36. Guengerich, F. P. Cytochrome P450: Structure, Mechanism, and Biochemistry. 3rd ed.; Demontellano, P. R. O., Ed.; Kluwer Academic/Plenum Press: New York, NY, 2005; pp 377-531.
37. Guengerich, F. P. Cytochrome P450s and other enzymes in drug metabolism and toxicity. *Aaps Journal* **2006**, *8* (1), E101-E111.
38. Guengerich, F. P.; , W. Z.-L.; , B. C. J. Function of human cytochrome P450s: characterization of the remaining orphans. *Biochemical and Biophysical Research Communications* **2005**, (338), 465-469.
39. Wienkers, L. C.; Heath, T. G. Predicting in vivo drug interactions from in vitro drug discovery data. *Nature Reviews Drug Discovery* **2005**, *4* (10), 825-833.
40. Williams, J. A.; Hyland, R.; Jones, B. C.; Smith, D. A.; Hurst, S.; Goosen, T. C.; Peterkin, V.; Koup, J. R.; Ball, S. E. Drug-drug interactions for UDP-glucuronosyltransferase substrates: A pharmacokinetic explanation for typically observed low exposure (AUC(i)/AUC) ratios. *Drug Metabolism and Disposition* **2004**, *32* (11), 1201-1208.
41. Manyike, P. T.; Kharasch, E. D.; Kalhorn, T. F.; Slattery, J. T. Contribution of CYP2E1 and CYP3A to acetaminophen reactive metabolite formation. *Clinical Pharmacology & Therapeutics* **2000**, *67* (3), 275-282.

42. Cuttle, L.; Munns, A. J.; Hogg, N. A.; Scott, J. R.; Hooper, W. D.; Dickinson, R. G.; Gillam, E. M. J. Phenytoin metabolism by human cytochrome P450: Involvement of P450 3A and 2C forms in secondary metabolism and drug-protein adduct formation. *Drug Metabolism and Disposition* **2000**, *28* (8), 945-950.
43. Arlt, V. M.; Hewer, A.; Sorg, B. L.; Schmeiser, H. H.; Phillips, D. H.; Stiborova, M. 3-aminobenzanthrone, a human metabolite of the environmental pollutant 3-nitrobenzanthrone, forms DNA adducts after metabolic activation by human and rat liver microsomes: Evidence for activation by cytochrome P450 1A1 and P450 1A2. *Chemical Research in Toxicology* **2004**, *17* (8), 1092-1101.
44. Isley, W. L.; Oki, J. C. Hepatotoxicity of thiazolidinediones. *Diabetes, Obesity and Metabolism* **2001**, *3* (6), 389-392.
45. Shimada, T.; Gillam, E. M. J.; Oda, Y.; Tsumura, F.; Sutter, TR.; Guengerich, F. P.; Inoue, K. Metabolism of Benzo[a]pyrene to trans-7,8-Dihydroxy-7,8-dihydrobenzo[a]pyrene by Recombinant Human Cytochrome P450 1B1 and Purified Liver Epoxide Hydrolase. *Chemical Research in Toxicology* **1999**, *12* (7), 623-629.
46. Sanderson, J.; Naisbitt, D.; Park, B. Role Of Bioactivation in Drug-Induced Hypersensitivity Reactions. 8 ed.; 2006; p E55-E64.
47. Lee, S. S. T.; Buters, J. T. M.; Pineau, T.; FernandezSalguero, P.; Gonzalez, F. J. Role of CYP2E1 in the hepatotoxicity of acetaminophen. *Journal of Biological Chemistry* **1996**, *271* (20), 12063-12067.
48. Hoffmann, K.-J.; Streeter, A. J.; Axworthy, D. B.; Baillie, T. A. Structural characterization of the major covalent adduct formed in vitro between acetaminophen and bovine serum albumin. *Chemico-Biological Interactions* **1985**, *53*, 155-172.
49. Rogers, L. K.; Moorthy, B.; Smith, C. V. Acetaminophen binds to mouse hepatic and renal DNA at human therapeutic doses. *Chemical Research in Toxicology* **1997**, *10* (4), 470-476.
50. Meschter, C. L.; Mico, B. A.; Mortillo, M.; Feldman, D.; Garland, W. A.; Riley, J. A.; Kaufman, L. S. A 13-Week Toxicologic and Pathologic Evaluation of Prolonged Cytochromes P450 Inhibition by 1-Aminobenzotriazole in Male Rats. *Fundamental and Applied Toxicology* **1994**, *22* (3), 369-381.
51. Ernest, C. S.; Hall, S. D.; Jones, D. R. Mechanism-Based Inactivation of CYP3A by HIV Protease Inhibitors. *Journal of Pharmacology and Experimental Therapeutics* **2005**, *312* (2), 583-591.

52. Ahn, T.; Guengerich, F. P.; Yun, C. H. Membrane insertion of cytochrome P450 1A2 promoted by anionic phospholipids. *Biochemistry* **1998**, *37* (37), 12860-12866.
53. Imaoka, S.; Imai, Y.; Shimada, T.; Funae, Y. Role of Phospholipids in Reconstituted Cytochrome-P4503A Form and Mechanism of Their Activation of Catalytic Activity. *Biochemistry* **1992**, *31* (26), 6063-6069.
54. French, J. S.; Guengerich, F. P.; Coon, M. J. Interactions of Cytochrome-P-450, NADPH-Cytochrome P-450 Reductase, Phospholipid, and Substrate in the Reconstituted Liver Microsomal-Enzyme System. *Journal of Biological Chemistry* **1980**, *255* (9), 4112-4119.
55. Kelley, R. W.; Cheng, D. M.; Backes, W. L. Heteromeric complex formation between CYP2E1 and CYP1A2: Evidence for the involvement of electrostatic interactions. *Biochemistry* **2006**, *45* (51), 15807-15816.
56. Hollenberg, P. F. Characteristics and common properties of inhibitors, inducers, and activators of CYP enzymes. *Drug Metabolism Reviews* **2002**, *34* (1-2), 17-35.
57. Hutzler, M. J.; Wienkers, L. C.; Wahlstrom, J. L.; Carlson, T. J.; Tracy, T. S. Activation of cytochrome P450 2C9-mediated metabolism: mechanistic evidence in support of kinetic observations. *Archives of Biochemistry and Biophysics* **2003**, *410* (1), 16-24.
58. Hendrychova, T.; Anzenbacherova, E.; Hudecek, J.; Skopalik, J.; Lange, R.; Hildebrandt, P.; Otyepka, M.; Anzenbacher, P. Flexibility of human cytochrome P450 enzymes: Molecular dynamics and spectroscopy reveal important function-related variations. *Biochimica et Biophysica Acta-Proteins and Proteomics* **2011**, *1814* (1), 58-68.
59. Dean, W. L.; Gray, R. D. Relationship between state of aggregation and catalytic activity for cytochrome P-450LM2 and NADPH-cytochrome P-450 reductase. *Journal of Biological Chemistry* **1982**, *257* (24), 14679-14685.
60. Pernecky, S. J.; Larson, J. R.; Philpot, R. M.; Coon, M. J. Expression of Truncated Forms of Liver Microsomal P450 Cytochromes 2B4 and 2E1 in Escherichia-Coli - Influence of Nh2-Terminal Region on Localization in Cytosol and Membranes. *Proceedings of the National Academy of Sciences of the United States of America* **1993**, *90* (7), 2651-2655.
61. Pernecky, S. J.; Olken, N. M.; Bestervelt, L. L.; Coon, M. J. Subcellular-Localization, Aggregation State, and Catalytic Activity of Microsomal P450 Cytochromes Modified in the Nh2-Terminal Region and Expressed in Escherichia-Coli. *Archives of Biochemistry and Biophysics* **1995**, *318* (2), 446-456.

62. Dong, M. S.; Yamazaki, H.; Guo, Z. Y.; Guengerich, F. P. Recombinant human cytochrome P450 1A2 and an N-terminal-truncated form: Construction, purification, aggregation properties, and interactions with Flavodoxin, Ferredoxin, and NADPH-cytochrome P450 reductase. *Archives of Biochemistry and Biophysics* **1996**, *327* (1), 11-19.
63. Cosme, J.; Johnson, E. F. Engineering microsomal cytochrome P450 2C5 to be a soluble, monomeric enzyme - Mutations that alter aggregation, phospholipid dependence of catalysis, and membrane binding. *Journal of Biological Chemistry* **2000**, *275* (4), 2545-2553.
64. Von Wachenfeldt, C.; Richardson, T. H.; Cosme, J.; Johnson, E. F. Microsomal P450 2C3 Is Expressed as a Soluble Dimer in Escherichia coli Following Modifications of Its N-terminus. *Archives of Biochemistry and Biophysics* **1997**, *339* (1), 107-114.
65. Sevrioukova, I. F.; Kanaeva, I. P.; Koen, Y. M.; Samenkova, N. F.; Bachmanova, G. I.; Archakov, A. I. Catalytic Activity of Cytochrome P450 1A2 in Reconstituted System with Emulgen 913. *Archives of Biochemistry and Biophysics* **1994**, *311* (1), 133-143.
66. Wagner, S. L.; Dean, W. L.; Gray, R. D. Effect of A Zwitterionic Detergent on the State of Aggregation and Catalytic Activity of Cytochrome-P-450Lm2 and Nadph-Cytochrome P-450 Reductase. *Journal of Biological Chemistry* **1984**, *259* (4), 2390-2395.
67. Leitz, A. J.; Bayburt, T. H.; Barnakov, A. N.; Springer, B. A.; Sligar, S. G. Functional reconstitution of beta(2)-adrenergic receptors utilizing self-assembling Nanodisc technology. *Biotechniques* **2006**, *40* (5), 601-+.
68. Davydov, D. R.; Fernando, H.; Baas, B. J.; Sligar, S. G.; Halpert, J. R. Kinetics of dithionite-dependent reduction of cytochrome P450 3A4: Heterogeneity of the enzyme caused by its oligomerization. *Biochemistry* **2005**, *44* (42), 13902-13913.
69. Bayburt, T. H.; Sligar, S. G. Single-molecule height measurements on microsomal cytochrome P450 in nanometer-scale phospholipid bilayer disks. *Proceedings of the National Academy of Sciences of the United States of America* **2002**, *99* (10), 6725-6730.
70. Gannett, P. M.; Kabulski, J. L.; Perez, F. A.; Liu, Z.; Lederman, D.; Locuson, C. W.; Ayscue, R. A.; Thomsen, N.; Tracy, T. S. Preparation, Characterization, and Substrate Metabolism of Gold-Immobilized Cytochrome P450 2C9. *Journal of the American Chemical Society* **2006**, *128* (26), 8374-8375.

71. Yang, M. L.; Kabulski, J. L.; Wollenberg, L.; Chen, X. Q.; Subramanian, M.; Tracy, T. S.; Lederman, D.; Gannett, P. M.; Wu, N. Q. Electrocatalytic Drug Metabolism by CYP2C9 Bonded to A Self-Assembled Monolayer-Modified Electrode. *Drug Metabolism and Disposition* **2009**, *37* (4), 892-899.
72. Sakai-Kato, K.; Kato, M.; Homma, H.; Toyo'oka, T.; Utsunomiya-Tate, N. Creation of a P450 array toward high-throughput analysis. *Analytical Chemistry* **2005**, *77* (21), 7080-7083.
73. Fantuzzi, A.; Fairhead, M.; Gilardi, G. Direct electrochemistry of immobilized human cytochrome P450 2E1. *Journal of the American Chemical Society* **2004**, *126* (16), 5040-5041.
74. Krishnan, S.; Wasalathanthri, D.; Zhao, L. L.; Schenkman, J. B.; Rusling, J. F. Efficient Bioelectronic Actuation of the Natural Catalytic Pathway of Human Metabolic Cytochrome P450s. *Journal of the American Chemical Society* **2011**, *133* (5), 1459-1465.
75. Krishnan, S.; Wasalathanthri, D.; Zhao, L. L.; Schenkman, J. B.; Rusling, J. F. Efficient Bioelectronic Actuation of the Natural Catalytic Pathway of Human Metabolic Cytochrome P450s. *Journal of the American Chemical Society* **2011**, *133* (5), 1459-1465.
76. Peterson, J. A.; Ebel, R. E.; O'Keeffe, D. H.; Matsubara, T.; Estabrook, R. W. Temperature dependence of cytochrome P-450 reduction. A model for NADPH-cytochrome P-450 reductase:cytochrome P-450 interaction. *Journal of Biological Chemistry* **1976**, *251* (13), 4010-4016.
77. Miwa, G. T.; West, S. B.; Huang, M. T.; Lu, A. Y. Studies on the association of cytochrome P-450 and NADPH-cytochrome c reductase during catalysis in a reconstituted hydroxylating system. *Journal of Biological Chemistry* **1979**, *254* (13), 5695-5700.
78. Backes, W. L.; Batie, C. J.; Cawley, G. F. Interactions among P450 Enzymes When Combined in Reconstituted Systems: Formation of a 2B4E1A2 Complex with a High Affinity for NADPH-Cytochrome P450 Reductase. *Biochemistry* **1998**, *37* (37), 12852-12859.
79. Hazai, E.; Kupfer, D. INTERACTIONS BETWEEN CYP2C9 AND CYP2C19 IN RECONSTITUTED BINARY SYSTEMS INFLUENCE THEIR CATALYTIC ACTIVITY: POSSIBLE RATIONALE FOR THE INABILITY OF CYP2C19 TO CATALYZE METHOXYCHLOR DEMETHYLATION IN HUMAN LIVER MICROSOMES. *Drug Metabolism and Disposition* **2005**, *33* (1), 157-164.

80. Alston, K.; Robinson, R. C.; Park, S. S.; Gelboin, H. V.; Friedman, F. K. Interactions among cytochromes P-450 in the endoplasmic reticulum. Detection of chemically cross-linked complexes with monoclonal antibodies. *Journal of Biological Chemistry* **1991**, *266* (2), 735-739.
81. Subramanian, M.; Low, M.; Locuson, C. W.; Tracy, T. S. CYP2D6-CYP2C9 Protein-Protein Interactions and Isoform-Selective Effects on Substrate Binding and Catalysis. *Drug Metabolism and Disposition* **2009**, *37* (8), 1682-1689.
82. Kelley, R. W.; Reed, J. R.; Backes, W. L. Effects of Ionic Strength on the Functional Interactions between CYP2B4 and CYP1A2. *Biochemistry* **2005**, *44* (7), 2632-2641.
83. Luk, Y. Y.; Kato, M.; Mrksich, M. Self-assembled monolayers of alkanethiolates presenting mannitol groups are inert to protein adsorption and cell attachment. *Langmuir* **2000**, *16* (24), 9604-9608.
84. Chaki, N. K.; Vijayamohan, K. Self-assembled monolayers as a tunable platform for biosensor applications. *Biosensors & Bioelectronics* **2002**, *17* (1-2), 1-12.
85. Nuzzo, R. G.; Allara, D. L. Adsorption of bifunctional organic disulfides on gold surfaces. *Journal of the American Chemical Society* **1983**, *105* (13), 4481-4483.
86. de la Llave, E.; Scherlis, D. A. Selenium-Based Self-Assembled Monolayers: The Nature of Adsorbate-Surface Interactions. *Langmuir* **2009**, *26* (1), 173-178.
87. Caprioli, F.; Decker, F.; Marrani, A. G.; Beccari, M.; Castro, V. D. Copper protection by self-assembled monolayers of aromatic thiols in alkaline solutions. *Phys. Chem. Chem. Phys.* **2010**, *12* (32), 9230-9238.
88. Li, W.; Virtanen, J. A.; Penner, R. M. Self-Assembly of n-Alkanethiolate Monolayers on Silver Nanostructures: Protective Encapsulation. *Langmuir* **1995**, *11* (11), 4361-4365.
89. Love, J. C.; Wolfe, D. B.; Chabinyc, M. L.; Paul, K. E.; Whitesides, G. M. Self-Assembled Monolayers of Alkanethiolates on Palladium Are Good Etch Resists. *Journal of the American Chemical Society* **2002**, *124* (8), 1576-1577.
90. Stranick, S. J.; Parikh, A. N.; Tao, Y. T.; Allara, D. L.; Weiss, P. S. Phase-Separation of Mixed-Composition Self-Assembled Monolayers Into Nanometer-Scale Molecular Domains. *Journal of Physical Chemistry* **1994**, *98* (31), 7636-7646.
91. Wasserman, S. R.; Whitesides, G. M.; Tidswell, I. M.; Ocko, B. M.; Pershan, P. S.; Axe, J. D. The Structure of Self-Assembled Monolayers of Alkylsiloxanes on Silicon - A Comparison of Results from Ellipsometry and Low-Angle X-Ray Reflectivity. *Journal of the American Chemical Society* **1989**, *111* (15), 5852-5861.

92. Sagiv, J. Organized monolayers by adsorption. Formation and structure of oleophobic mixed monolayers on solid surfaces. *Journal of the American Chemical Society* **1980**, *102* (1), 92-98.
93. Gun, J.; Iscovici, R.; Sagiv, J. On the Formation and Structure of Self-Assembling Monolayers .2. A Comparative-Study of Langmuir-Blodgett and Adsorbed Films Using Ellipsometry and Ir Reflection Absorption-Spectroscopy. *Journal of Colloid and Interface Science* **1984**, *101* (1), 201-213.
94. Gun, J.; Sagiv, J. On the Formation and Structure of Self-Assembling Monolayers .3. Time of Formation, Solvent Retention, and Release. *Journal of Colloid and Interface Science* **1986**, *112* (2), 457-472.
95. Luscombe, C. K.; Li, H. W.; Huck, W. T. S.; Holmes, A. B. Fluorinated silane self-assembled monolayers as resists for patterning indium tin oxide. *Langmuir* **2003**, *19* (13), 5273-5278.
96. MCGovern, M. E.; Kallury, K. M. R.; Thompson, M. Role of Solvent on the Silanization of Glass with Octadecyltrichlorosilane. *Langmuir* **1994**, *10* (10), 3607-3614.
97. Krishnan, A.; Liu, Y. H.; Cha, P.; Woodward, R.; Allara, D.; Vogler, E. A. An evaluation of methods for contact angle measurement. *Colloids and Surfaces B-Biointerfaces* **2005**, *43* (2), 95-98.
98. Offord, D. A.; John, C. M.; Griffin, J. H. Contact-Angle Goniometry, Ellipsometry, Xps, and ToF-Sims Analysis of Gold-Supported, Mixed Self-Assembled Monolayers Formed from Mixed Dialkyl Disulfides. *Langmuir* **1994**, *10* (3), 761-766.
99. Palma, R.; Laureyn, W.; Frederix, F.; Bonroy, K.; Pireaux, J. J.; Borghs, G.; Maes, G. Formation of dense self-assembled monolayers of (n-decyl)trichlorosilanes on Ta/Ta<sub>2</sub>O<sub>5</sub>. *Langmuir* **2007**, *23* (2), 443-451.
100. Lee, J. K.; Chi, Y. S.; Choi, I. S. Reactivity of acetylenyl-terminated self-assembled monolayers on gold: Triazole formation. *Langmuir* **2004**, *20* (10), 3844-3847.
101. Lander, L. M.; Siewierski, L. M.; Brittain, W. J.; Vogler, E. A. A Systematic Comparison of Contact-Angle Methods. *Langmuir* **1993**, *9* (8), 2237-2239.
102. Krishnan, A.; Liu, Y. H.; Cha, P.; Allara, D.; Vogler, E. A. Interfacial energetics of globular-blood protein adsorption to a hydrophobic interface from aqueous-buffer solution. *Journal of the Royal Society Interface* **2006**, *3* (7), 283-301.
103. Hagstrom, S.; Nordling, C.; Siegbahn, K. Electron spectroscopic determination of the chemical valence state. *Zeitschrift f++r Physik A Hadrons and Nuclei* **1964**, *178* (5), 439-444.



104. Hollander, J. M.; Jolly, W. L. X-ray photoelectron spectroscopy. *Accounts of Chemical Research* **1970**, *3* (6), 193-200.
105. Lubbers, D. W.; Opitz, N. Eine neue pCO<sub>2</sub>-bzw: pO<sub>2</sub>-Messsonde zur Messung des pCO<sub>2</sub> oder pO<sub>2</sub> von Gasen und Flüssigkeiten. *Zeitschrift Für Naturforschung C* **1975**, *30*, 532-533.
106. Pockrand, I.; Swalen, J. D.; Gordon, J. G.; Philpott, M. R. Surface-Plasmon Spectroscopy of Organic Monolayer Assemblies. *Surface Science* **1978**, *74* (1), 237-244.
107. Homola, J.; Yee, S. S.; Gauglitz, G. Surface plasmon resonance sensors: review. *Sensors and Actuators B-Chemical* **1999**, *54* (1-2), 3-15.
108. Chadwick, B.; Gal, M. Enhanced Optical-Detection of Hydrogen Using the Excitation of Surface-Plasmons in Palladium. *Applied Surface Science* **1993**, *68* (1), 135-138.
109. Agbor, N. E.; Cresswell, J. P.; Petty, M. C.; Monkman, A. P. An optical gas sensor based on polyaniline Langmuir-Blodgett films. *Sensors and Actuators B-Chemical* **1997**, *41* (1-3), 137-141.
110. Jung, C. C.; Saban, S. B.; Yee, S. S.; Darling, R. B. Chemical electrode surface plasmon resonance sensor. *Sensors and Actuators B-Chemical* **1996**, *32* (2), 143-147.
111. Miwa, S.; Arakawa, T. Selective gas detection by means of surface plasmon resonance sensors. *Thin Solid Films* **1996**, *282* (1-2), 466-468.
112. Regnault, V.; Arvieux, J.; Vallar, L.; Lecompte, T. Immunopurification of human beta(2)-glycoprotein I with a monoclonal antibody selected for its binding kinetics using surface plasmon resonance biosensor. *Journal of Immunological Methods* **1998**, *211* (1-2), 191-197.
113. He, L.; Musick, M. D.; Nicewarner, S. R.; Salinas, F. G.; Benkovic, S. J.; Natan, M. J.; Keating, C. D. Colloidal Au-enhanced surface plasmon resonance for ultrasensitive detection of DNA hybridization. *Journal of the American Chemical Society* **2000**, *122* (38), 9071-9077.
114. Nelson, B. P.; Liles, M. R.; Frederick, K. B.; Corn, R. M.; Goodman, R. M. Label-free detection of 16S ribosomal RNA hybridization on reusable DNA arrays using surface plasmon resonance imaging. *Environmental Microbiology* **2002**, *4* (11), 735-743.
115. Sexton, B. A.; Feltis, B. N.; Davis, T. J. Characterisation of gold surface plasmon resonance sensor substrates. *Sensors and Actuators A-Physical* **2008**, *141* (2), 471-475.

116. Thurmond, R. L.; Wadsworth, S. A.; Schafer, P. H.; Zivin, R. A.; Siekierka, J. J. Kinetics of small molecule inhibitor binding to p38 kinase. *European Journal of Biochemistry* **2001**, 268 (22), 5747-5754.
117. Karlsson, O. P.; Lofas, S. Flow-mediated on-surface reconstitution of G-protein coupled receptors for applications in surface plasmon resonance biosensors. *Analytical Biochemistry* **2002**, 300 (2), 132-138.
118. Patel, R.; Andrien, B. A. Kinetic analysis of a monoclonal therapeutic antibody and its single-chain homolog by surface plasmon resonance. *Analytical Biochemistry* **2010**, 396 (1), 59-68.
119. Binnig, G.; Quate, C. F.; Gerber, C. Atomic Force Microscope. *Phys. Rev. Lett.* **1986**, 56 (9), 930.
120. Muller, D. J.; Janovjak, H.; Lehto, T.; Kuerschner, L.; Anderson, K. Observing structure, function and assembly of single proteins by AFM. *Progress in Biophysics & Molecular Biology* **2002**, 79 (1-3), 1-43.
121. Puntheeranurak, T.; Wildling, L.; Gruber, H. J.; Kinne, R. K. H.; Hinterdorfer, P. Ligands on the string: single-molecule AFM studies on the interaction of antibodies and substrates with the Na<sup>+</sup>-glucose co-transporter SGLT1 in living cells. *Journal of Cell Science* **2006**, 119 (14), 2960-2967.
122. Kienberger, F.; Ebner, A.; Gruber, H. J.; Hinterdorfer, P. Molecular recognition imaging and force spectroscopy of single biomolecules. *Accounts of Chemical Research* **2006**, 39 (1), 29-36.
123. Archakov, A. I.; Ivanov, Y. D. Application of AFM and optical biosensor for investigation of complexes formed in P450-containing monooxygenase systems. *Biochimica et Biophysica Acta-Proteins and Proteomics* **2011**, 1814 (1), 102-110.
124. Kiselyova, O. I.; Yaminsky, I. V.; Ivanov, Y. D.; Kanaeva, I. P.; Kuznetsov, V. Y.; Archakov, A. I. AFM study of membrane proteins, cytochrome P450B4, and NADPH-cytochrome P450 reductase and their complex formation. *Archives of Biochemistry and Biophysics* **1999**, 371 (1), 1-7.
125. Nussio, M. R.; Voelcker, N. H.; Miners, J. O.; Lewis, B. C.; Sykes, M. J.; Shapter, J. G. AFM study of the interaction of cytochrome P450 2C9 with phospholipid bilayers. *Chemistry and Physics of Lipids* **2010**, 163 (2), 182-189.
126. Su, J.; Mrksich, M. Using mass spectrometry to characterize self-assembled monolayers presenting peptides, proteins, and carbohydrates. *Angewandte Chemie-International Edition* **2002**, 41 (24), 4715-4718.

127. Su, J.; Mrksich, M. Using MALDI-TOF mass spectrometry to characterize interfacial reactions on self-assembled monolayers. *Langmuir* **2003**, *19* (12), 4867-4870.
128. Yeo, W. S.; Min, D. H.; Hsieh, R. W.; Greene, G. L.; Mrksich, M. Label-free detection of protein-protein interactions on biochips. *Angewandte Chemie-International Edition* **2005**, *44* (34), 5480-5483.
129. Anker, J. N.; Hall, W. P.; Lambert, M. P.; Velasco, P. T.; Mrksich, M.; Klein, W. L.; Van Duyne, R. P. Detection and Identification of Bioanalytes with High Resolution LSPR Spectroscopy and MALDI Mass Spectrometry. *Journal of Physical Chemistry C* **2009**, *113* (15), 5891-5894.
130. Ha, T. K.; Bin Oh, H.; Chung, J. Y.; Lee, T. G.; Han, S. Y. Investigation of the MALDI Process Used to Characterize Self-Assembled Monolayers of Alkanethiolates on Gold. *Langmuir* **2009**, *25* (6), 3692-3697.
131. Schlenoff, J. B.; Li, M.; Ly, H. Stability and self-exchange in alkanethiol monolayers. *Journal of the American Chemical Society* **1995**, *117* (50), 12528-12536.
132. Guengerich, F. P. Reactions and Significance of Cytochrome-P-450 Enzymes. *Journal of Biological Chemistry* **1991**, *266* (16), 10019-10022.
133. Kumar, G. N.; Surapaneni, S. Role of drug metabolism in drug discovery and development. *Medicinal Research Reviews* **2001**, *21* (5), 397-411.
134. Manyike, P. T.; Kharasch, E. D.; Kalthorn, T. F.; Slattery, J. T. Contribution of CYP2E1 and CYP3A to acetaminophen reactive metabolite formation. *Clinical Pharmacology & Therapeutics* **2000**, *67* (3), 275-282.
135. Manyike, P. T.; Kharasch, E. D.; Kalthorn, T. F.; Slattery, J. T. Contribution of CYP2E1 and CYP3A to acetaminophen reactive metabolite formation. *Clinical Pharmacology & Therapeutics* **2000**, *67* (3), 275-282.
136. Iverson, S. L.; Uetrecht, J. P. Identification of a reactive metabolite of terbinafine: Insights into terbinafine-induced hepatotoxicity. *Chemical Research in Toxicology* **2001**, *14* (2), 175-181.
137. Obach, R. S.; Walsky, R. L.; Venkatakrishnan, K. Mechanism-based inactivation of human cytochrome P450 enzymes and the prediction of drug-drug interactions. *Drug Metabolism and Disposition* **2007**, *35* (2), 246-255.
138. Loida, P. J.; Sligar, S. G.; Paulsen, M. D.; Arnold, G. E.; Ornstein, R. L. Stereoselective Hydroxylation of Norcamphor by Cytochrome P450(Cam) - Experimental-Verification of Molecular-Dynamics Simulations. *Journal of Biological Chemistry* **1995**, *270* (10), 5326-5330.

139. Meunier, B.; de Visser, S. P.; Shaik, S. Mechanism of oxidation reactions catalyzed by cytochrome P450 enzymes. *Chemical Reviews* **2004**, *104* (9), 3947-3980.
140. Urlacher, V. B.; Eiben, S. Cytochrome P450 monooxygenases: perspectives for synthetic application. *Trends in Biotechnology* **2006**, *24* (7), 324-330.
141. Li, Q. S.; Ogawa, J.; Schmid, R. D.; Shimizu, S. Indole hydroxylation by bacterial cytochrome p450 BM-3 and modulation of activity by cumene hydroperoxide. *Bioscience Biotechnology and Biochemistry* **2005**, *69* (2), 293-300.
142. Nagel, B.; Dellweg, H.; Gierasch, L. M. Glossary for chemists of terms used in Biotechnology. *Pure and Applied Chemistry* **1992**, *64* (1), 143-168.
143. Singh, V. Disposable bioreactor for cell culture using wave-induced agitation. *Cytotechnology* **1999**, *30* (1-3), 149-158.
144. Facchini, P. J.; Dicosmo, F. Plant-Cell Bioreactor for the Production of Protoberberine Alkaloids from Immobilized *Thalictrum-Rugosum* Cultures. *Biotechnology and Bioengineering* **1991**, *37* (5), 397-403.
145. Suzuki, M.; Roy, R.; Zheng, H. Y.; Woychik, N.; Inouye, M. Bacterial Bioreactors for high yield production of recombinant protein. *Journal of Biological Chemistry* **2006**, *281* (49), 37559-37565.
146. Chen, J.; Yu, Z.; Zhang, L.; Chen, G. Microfluidic Bioreactors for Highly Efficient Proteolysis. *Current Chemical Biology* **2009**, *3* (3), 291-301.
147. Rao, K. J.; Panda, T. Effect of mode of operation of bioreactors on the biosynthesis of penicillin amidase in *Escherichia coli*. *Bioprocess Engineering* **1996**, *14* (6), 317-321.
148. Wang, M. D.; Yang, M.; Huzel, N.; Butler, M. Erythropoietin production from CHO cells grown by continuous culture in a fluidized-bed bioreactor. *Biotechnology and Bioengineering* **2002**, *77* (2), 194-203.
149. Hao, D. C.; Zhu, P. H.; Yang, S. L.; Yang, L. Optimization of recombinant cytochrome p450 2C9 protein production in *Escherichia coli* DH5 alpha by statistically-based experimental design. *World Journal of Microbiology & Biotechnology* **2006**, *22* (11), 1169-1176.
150. Zhang, D. L.; Zhang, H. Y.; Aranibar, N.; Hanson, R.; Huang, Y.; Cheng, P. T.; Wu, S.; Bonacorsi, S.; Zhu, M. S.; Swaminathan, A.; Humphreys, W. G. Structural elucidation of human oxidative metabolites of muraglitazar: Use of microbial bioreactors in the biosynthesis of metabolite standards. *Drug Metabolism and Disposition* **2006**, *34* (2), 267-280.

151. Rushmore, T.; Reider, P.; Slaughter D; Assang, C.; Shou, M. Bioreactory Systems in Drug Metabolism: Synthesis of Cytochrome P450-Generated Metabolites. 2 ed.; 2000; pp 115-125.
152. Bader, A.; Fruhauf, N.; Zech, K.; Haverich, A.; Borlak, J. T. Development of a small-scale bioreactor for drug metabolism studies maintaining hepatospecific functions. *Xenobiotica* **1998**, 28 (9), 815-825.
153. De Bartolo, L.; Salerno, S.; Curcio, E.; Piscioneri, A.; Rende, M.; Morelli, S.; Tasselli, F.; Bader, A.; Drioli, E. Human hepatocyte functions in a crossed hollow fiber membrane bioreactor. *Biomaterials* **2009**, 30 (13), 2531-2543.
154. van Liempd, S. M.; Kool, J.; Reinen, J.; Schenk, T.; Meerman, J. H. N.; Irth, H.; Vermeulen, N. P. E. Development and validation of a microsomal online cytochrome P450 bioreactor coupled to solid-phase extraction and reversed-phase liquid chromatography. *Journal of Chromatography A* **2005**, 1075 (1-2), 205-212.
155. van Liempd, S. M.; Kool, J.; Meerman, J. H.; Irth, H.; Vermeulen, N. P. Metabolic profiling of endocrine-disrupting compounds by on-line cytochrome P450 bioreaction coupled to on-line receptor affinity screening. *Chemical Research in Toxicology* **2007**, 20 (12), 1825-1832.
156. Osorio-Lozada, A.; Surapaneni, S.; Skiles, G. L.; Subramanian, R. Biosynthesis of drug metabolites using microbes in hollow fiber cartridge reactors: Case study of diclofenac metabolism by *Actinoplanes* species. *Drug Metabolism and Disposition* **2008**, 36 (2), 234-240.
157. Guengrich FP Cytochrome P450s and Other Enzymes in Drug Metabolism and Toxicity. 8 ed.; 2006; p E101-E111.
158. Backes, W. L.; Kelley, R. W. Organization of multiple cytochrome P450s with NADPH-cytochrome P450 reductase in membranes. *Pharmacology & Therapeutics* **2003**, 98 (2), 221-233.
159. Sevrukova, I. F.; Kanaeva, I. P.; Koen, Y. M.; Samenkova, N. F.; Bachmanova, G. I.; Archakov, A. I. Catalytic Activity of Cytochrome P4501A2 in Reconstituted System with Emulgen 913. *Archives of Biochemistry and Biophysics* **1994**, 311 (1), 133-143.
160. Fantuzzi, A.; Fairhead, M.; Gilardi, G. Direct electrochemistry of immobilized human cytochrome P450 2E1. *Journal of the American Chemical Society* **2004**, 126 (16), 5040-5041.
161. Sevrukova, I. F.; Kanaeva, I. P.; Koen, Y. M.; Samenkova, N. F.; Bachmanova, G. I.; Archakov, A. I. Catalytic Activity of Cytochrome P4501A2 in Reconstituted

System with Emulgen 913. *Archives of Biochemistry and Biophysics* **1994**, *311* (1), 133-143.

162. Glangchai, L. C.; Caldorera-Moore, M.; Shi, L.; Roy, K. Nanoimprint lithography based fabrication of shape-specific, enzymatically-triggered smart nanoparticles. *Journal of Controlled Release* **2008**, *125* (3), 263-272.
163. Dryakhlushin, V. F.; Klimov, A. Y.; Rogov, V. V.; Vostokov, N. V. Fabrication of the nanodimensional elements by the near-field optical lithography method. *Physics of Low-Dimensional Structures* **2003**, *3-4*, 263-268.
164. Piner, R. D.; Zhu, J.; Xu, F.; Hong, S. H.; Mirkin, C. A. "Dip-pen" nanolithography. *Science* **1999**, *283* (5402), 661-663.
165. Shirakashi, J. Scanning Probe Microscope Lithography at the Micro- and Nano-Scales. *Journal of Nanoscience and Nanotechnology* **2010**, *10* (7), 4486-4494.
166. Ryan, D.; Parviz, B. A.; Linder, V.; Semetey, V.; Sia, S. K.; Su, J.; Mrksich, M.; Whitesides, G. M. Patterning multiple aligned self-assembled monolayers using light. *Langmuir* **2004**, *20* (21), 9080-9088.
167. Deshmukh, R. D.; Buxton, G. A.; Clarke, N.; Composto, R. J. Nanoscale block copolymer templates decorated by nanoparticle arrays. *Macromolecules* **2007**, *40* (17), 6316-6324.
168. Li, H. Q.; Wu, N. Q. A large-area nanoscale gold hemisphere pattern as a nanoelectrode array. *Nanotechnology* **2008**, *19* (27).
169. Stenberg, E.; Persson, B.; Roos, H.; Urbaniczky, C. Quantitative-Determination of Surface Concentration of Protein with Surface-Plasmon Resonance Using Radiolabeled Proteins. *Journal of Colloid and Interface Science* **1991**, *143* (2), 513-526.
170. Mrksich, M.; Sigal, G. B.; Whitesides, G. M. Surface Plasmon Resonance Permits in Situ Measurement of Protein Adsorption on Self-Assembled Monolayers of Alkanethiolates on Gold. *Langmuir* **1995**, *11* (11), 4383-4385.
171. Ostuni, E.; Chapman, R. G.; Liang, M. N.; Meluleni, G.; Pier, G.; Ingber, D. E.; Whitesides, G. M. Self-assembled monolayers that resist the adsorption of proteins and the adhesion of bacterial and mammalian cells. *Langmuir* **2001**, *17* (20), 6336-6343.
172. Stenberg, E.; Persson, B.; Roos, H.; Urbaniczky, C. Quantitative-Determination of Surface Concentration of Protein with Surface-Plasmon Resonance Using Radiolabeled Proteins. *Journal of Colloid and Interface Science* **1991**, *143* (2), 513-526.

173. Benoit, R. XPS, AES, UPS and ESCA. <http://www.lasurface.com/accueil/index.php> **2011**.
174. Finklea, H. O.; Robinson, L. R.; Blackburn, A.; Richter, B.; Allara, D.; Bright, T. Formation of An Organized Monolayer by Solution Adsorption of Octadecyltrichlorosilane on Gold - Electrochemical Properties and Structural Characterization. *Langmuir* **1986**, 2 (2), 239-244.
175. Yan, C.; Zharnikov, M.; Golzhauser, A.; Grunze, M. Preparation and characterization of self-assembled monolayers on indium tin oxide. *Langmuir* **2000**, 16 (15), 6208-6215.
176. Fukuzaki, S.; Urano, H.; Nagata, K. Adsorption of bovine serum albumin onto metal oxide surfaces. *Journal of Fermentation and Bioengineering* **1996**, 81 (2), 163-167.
177. Brandriss, S.; Margel, S. Synthesis and Characterization of Self-Assembled Hydrophobic Monolayer Coatings on Silica Colloids. *Langmuir* **1993**, 9 (5), 1232-1240.
178. Sharma, S.; Johnson, R. W.; Desai, T. A. XPS and AFM analysis of antifouling PEG interfaces for microfabricated silicon biosensors. *Biosensors & Bioelectronics* **2004**, 20 (2), 227-239.
179. Specht, E. The best known packings of equal circles in a circle (complete up to N = 1100). <http://hydra.nat.uni-magdeburg.de/packing/cci/#Results> **2010**.
180. Guengrich FP Cytochrome P450s and Other Enzymes in Drug Metabolism and Toxicity. 8 ed.; 2006; p E101-E111.
181. Miwa, G. T.; Lu, A. Y. H. The Association of Cytochrome-P-450 and Nadph-Cytochrome-P-450 Reductase in Phospholipid-Membranes. *Archives of Biochemistry and Biophysics* **1984**, 234 (1), 161-166.
182. Estabrook, R. W.; Franklin, M. R.; Cohen, B.; Shigamatzu, A.; Hildebrandt, A. G. Influence of hepatic microsomal mixed function oxidation reactions on cellular metabolic control. *Metabolism* **1971**, 20 (2), 187-199.
183. Alston, K.; Robinson, R. C.; Park, S. S.; Gelboin, H. V.; Friedman, F. K. Interactions Among Cytochromes-P-450 in the Endoplasmic-Reticulum - Detection of Chemically Cross-Linked Complexes with Monoclonal-Antibodies. *Journal of Biological Chemistry* **1991**, 266 (2), 735-739.
184. Subramanian, M.; Tam, H.; Zheng, H.; Tracy, T. S. CYP2C9-CYP3A4 Protein-Protein Interactions: Role of the Hydrophobic N Terminus. *Drug Metabolism and Disposition* **2010**, 38 (6), 1003-1009.

185. Cawley, G. F.; Zhang, S. X.; Kelley, R. W.; Backes, W. L. Evidence supporting the interaction of CYP2B4 and CYP1A2 in microsomal preparations. *Drug Metabolism and Disposition* **2001**, *29* (12), 1529-1534.
186. Kenworthy, A. K. Imaging protein-protein interactions using fluorescence resonance energy transfer microscopy. *Methods* **2001**, *24* (3), 289-296.
187. Pierce, M. M.; Raman, C. S.; Nall, B. T. Isothermal titration calorimetry of protein-protein interactions. *Methods-A Companion to Methods in Enzymology* **1999**, *19* (2), 213-221.
188. Greenfield, N. J. Using circular dichroism collected as a function of temperature to determine the thermodynamics of protein unfolding and binding interactions. *Nature Protocols* **2006**, *1* (6), 2527-2535.
189. Karlsson, R.; Falt, A. Experimental design for kinetic analysis of protein-protein interactions with surface plasmon resonance biosensors. *Journal of Immunological Methods* **1997**, *200* (1-2), 121-133.
190. Karlsson, R.; Michaelsson, A.; Mattsson, L. Kinetic-Analysis of Monoclonal Antibody-Antigen Interactions with A New Biosensor Based Analytical System. *Journal of Immunological Methods* **1991**, *145* (1-2), 229-240.
191. Choi, E. J.; Foster, M. D. Surfactant displacement of human serum albumin adsorbed on loosely packed self-assembled monolayers: cetyltrimethylammonium bromide versus sodium dodecyl sulfate. *Journal of Colloid and Interface Science* **2003**, *261* (2), 273-282.
192. Jung, S. H.; Jung, J. W.; Suh, I. B.; Yuk, J. S.; Kim, W. J.; Choi, E. Y.; Kim, Y. M.; Ha, K. S. Analysis of C-reactive protein on amide-linked N-hydroxysuccinimide - Dextran arrays with a spectral surface plasmon resonance biosensor for serodiagnosis. *Analytical Chemistry* **2007**, *79* (15), 5703-5710.
193. Shimada, T.; Mernaugh, R. L.; Guengerich, F. P. Interactions of mammalian cytochrome P450, NADPH-cytochrome P450 reductase, and cytochrome b5 enzymes. *Archives of Biochemistry and Biophysics* **2005**, *435* (1), 207-216.
194. Kabulski, J. L. Development of Au-immobilized P450 platform for exploring the effect of oligomer formation on P450-mediated metabolism for In vitro to In vivo drug metabolism predictions. West Virginia University, Apr 2010.
195. Maynard, J. A.; Lindquist, N. C.; Sutherland, J. N.; Lesuffleur, A.; Warrington, A. E.; Rodriguez, M.; Oh, S. H. Surface plasmon resonance for high-throughput ligand screening of membrane-bound proteins. *Biotechnology Journal* **2009**, *4* (11), 1542-1558.



**This page is intentionally blank.**

# **Chapter 7**

## **Back Matter**

**Lance Wollenberg**  
[lwollenb@gmail.com](mailto:lwollenb@gmail.com)  
Phone: 970-581-5866

**Education:**

**August 2005 – June 2011**

**West Virginia University - Morgantown, West Virginia**

**Doctor Of Philosophy - Pharmaceutical & Pharmacological Sciences**

- Completed relevant graduate level coursework in Cellular Physiology, Molecular Genetics, Biochemistry, Advanced Organic Chemistry, Drug Metabolism, and Pharmacokinetics.

**August 2001-May 2005**

**Colorado State University - Fort Collins, Colorado**

**Bachelor of Science - Biological Science**

- Completed relevant course work in Cell Biology, Advanced Cell Biology, Biochemistry and Molecular Genetics.
- Completed an Independent Study research project in Plant Molecular Biology.

**Professional Experience:**

**July 2011 – Current**

**Research Fellow**

**University of Buffalo – Buffalo, New York**

**March 2006 – June 2011**

**Doctoral Student in the Laboratory of Dr. Peter Gannett**

**West Virginia University - Morgantown, West Virginia**

- Currently working on a project characterizing the interaction of Cytochrome P450 2C9 to a gold-nanostructure surface.
- Employed various analytical techniques including liquid chromatography (LC), mass spectrometry (MS), x-ray photoelectron spectroscopy (XPS) and surface plasmon resonance (SPR).

**June 2009 – August 2009**

**IRES Predoctoral Fellow in the Laboratory of Dr. Wu Lixin**

**Jilin University – Changchun, Jilin Province, P.R.China**

- Assisted in the development of polymer-nanoparticle honeycomb films containing single molecule Mn-12 magnets.
- Techniques utilized to characterized films include optical microscopy (OM), atomic force microscopy (AFM), magnetic force microscopy (MFM) and scanning electron microscopy (SEM).

**June 2007 – August 2007**

**Amgen Inc. - Summer Intern in the Laboratory of Loren M. Berry in the Department of Pharmacokinetics and Drug Metabolism – Cambridge, Massachusetts**

- Independently worked on a project utilizing Mass Spectrometry (LC-MS/MS) and Native PAGE staining to characterize esterase activities in several pharmaceutically relevant animal models and humans.
- Co-authored a manuscript for work completed during the internship

**January 2006 - March 2006**

**Doctoral Student Research Rotation in the Laboratory of Dr. William Petros  
West Virginia University - Morgantown, West Virginia**

- Contributed to a project involving the pharmacokinetics of Atrasentan, a drug in phase I trials.
- Utilized various techniques such as liquid chromatography (LC), WinNonLin and plasma sample prep.

**September 2005 - December 2005**

**Doctoral Student Research Rotation in the Laboratory of Dr. Yon Rojanasakul,  
West Virginia University - Morgantown, West Virginia**

- Assisted on a project involving the effects of cisplatin on free radical formation and effects of lipoic acid on radical scavenging.
- Employed various techniques such as cell culture and flow cytometry to measure free radical formation.

**May 2005 - August 2005**

**Vector Surveillance Technician,  
Tri-County Health Department - Aurora, Colorado**

- Monitored mosquito populations throughout Arapahoe County for the presence of West Nile Virus.
- Developed a map of prairie dog (*Cynomys ludovicianus*) colonies throughout the region to be used by the CDC in controlling potential plague outbreaks.

**August 2004 - May 2005**

**Undergraduate Research Assistant in the Laboratory of Dr. Marinus Pilon,  
Colorado State University – Fort Collins, Colorado**

- Characterized the role of the Nif-S gene on the formation of iron-sulfur clusters in *Arabidopsis thaliana*
- Employed various molecular biology techniques including DNA and Protein electrophoresis, Polymerase Chain Reaction (PCR), density gradient centrifugation and Si-RNA knockdown using Agrobacterium transfection.

**Professional Memberships:**

**2006 – Current** – American Chemical Society

**2010 – Current – American Association of Pharmaceutical Scientists – Vice Chairman**

- West Virginia University - Founding Chapter Member

**Fellowships and Awards:**

**West Virginia Graduate Student Fellowship in Science, Technology, Engineering and Mathematics (STEM)**

- Awarded 3 Consecutive Years - \$71,000 award total

**International Research Experience for Students (IRES) Predoctoral Fellow**

- Supramolecular Structure and Materials in Nanoscience at Jilin University

**31st National Medicinal Chemistry Symposium, Pittsburgh, PA, June 15-19, 2008**

- Travel Award

**Peer-Reviewed Publications:**

Gannett, PM, Kabulski J, **Wollenberg L**, Gu J, Li D, Lederman D, Tracy TS. **Cytochrome P450-Gold Nanobiochip Platform for Basic Science Research and Practical Applications**, *Proceedings of the 15th International Conference on Cytochromes P450*, Bled, Slovenia, June 17-21, 2007.

Kabulski JL, **Wollenberg L**, Yang M, Wu N, Tracy T, Lederman D, and Gannett P. **Cytochrome P450-Gold Immobilized Nanobio Chip: Enzyme Characterization at the Nano-bio Interface**. *Biomedical Concurrent Session (Proceeding)*. *WVEPSCor STaR Symposium*. Morgantown, WV September 17-18, 2007

Berry LM, **Wollenberg L** and Zhao Z. (2009) **Esterase Activities in the Blood, Liver and Intestine of Several Preclinical Species and Humans**. *Drug Metabolism Letters* 2009 Apr;3(2):70-7.

Yang M, Kabulski JL, **Wollenberg L**, Chen X, Subramanian M, Tracy TS, Lederman D, Gannett PM, Wu N. (2009). **Electrocatalytic Drug Metabolism by CYP2C9 Bonded To A Self-Assembled Monolayer Modified Electrode**. *Drug Metab Dispos*. 2009 Apr;37(4):892-9

Sun H, Li W, **Wollenberg L**, Li B, Wu L, Li F, Xu L, **Self-Organized Microporous Structures of Mn<sub>12</sub> Single-Molecule Magnets** *J. Phys. Chem. B*, 2009, 113 (44): 14674–14680

**L. Wollenberg**, J. Jett, T. Tracy, Y. Wu, J. Kabulski, N. Wu, P. Gannett **Immobilized Cytochrome P450 enzymes: A construct to better predict in-vivo in-vitro correlation** *The AAPS Journal*. 2010; 12(S2) M1389

**Poster Presentations:**

**Wollenberg L, Kabulski J, Gannett PM, Perez FA, Liu Z, Lederman D, Locuson CW, Ayscue RA, Thomsen NM, Tracy TS. Preparation, characterization and substrate metabolism of gold immobilized cytochrome p450 2C9.** *39th Annual Mid-Atlantic Graduate Student Symposium in Medicinal Chemistry*, Columbus, OH, June 18-20, 2006.

**Wollenberg L, Kabulski J, Tracy TS, Lederman D, Gannett PM. Analysis of substrate metabolism for an immobilized Cytochrome P450 construct: A potential bioreactor application.** *234th ACS National Meeting*, Boston, MA, August 19-23, 2007.

**Wollenberg L, Kabulski JL, Yang M, Wu N, Powell M, Martin L, Thomsen N, Tracy TS, Gannett PM, Immobilized Cytochrome P450 enzymes: A biosynthetic approach to production of anti-cancer drug metabolites.** *Translational Research in Cancer Center Consortium Annual Meeting*, Morgantown, WV, Feb 21-22, 2008.

**Wollenberg L, Kabulski JL, Tracy TS, Powell M, Martin L, Yang M, Wu N, Jett, J, Thomsen N, Gannett PM Immobilized Cytochrome P450 enzyme constructs: A potential bioreactor application** *Multifunctional Nanomaterials International Symposium*, Roanoke, WV Apr 11-12, 2008

**Wollenberg L, Kabulski JL, Tracy TS, Powell M, Martin L, Yang M, Wu N, Jett, J, Thomsen N, Gannett PM Immobilized Cytochrome P450 enzyme constructs: A potential bioreactor application.** *31st National Medicinal Chemistry Symposium*, Pittsburgh, PA, June 15-19, 2008

**Wollenberg L, Kabulski JL, Tracy TS, Powell M, Martin L, Yang M, Wu N, Jett, J, Thomsen N, Gannett PM Immobilized Cytochrome P450 enzyme constructs: A potential bioreactor application.** *236th ACS National Meeting*, Philadelphia, PA, August 17-21, 2008.

**Wollenberg L, Kabulski JL, Jett, J, Wu N, Tracy TS, Gannett PM Immobilized Cytochrome P450 enzymes: A construct to better predict in-vivo in-vitro correlation.** *240th ACS National Meeting*, Boston, MA, August 22-26.

**Wollenberg L, Kabulski JL, Jett, J, Wu N, Tracy TS, Gannett PM Immobilized Cytochrome P450 enzymes: A construct to better predict in-vivo in-vitro correlation.** *FIP Pharmaceutical Sciences 2010 World Congress*, New Orleans, LA, November 14-18, 2010

**Teaching/Mentoring Experience:**

- Teaching Assistant and School of Pharmacy Tutor - Pharmacokinetics and Biopharmaceutics (2009-2010)
- Laboratory Proctor – Physical Pharmacy Lab I (2006-2007)
- Undergraduate Research Mentor – 3 students (2008-2010)